Characteristics and biocompatibility of magnesium-strontium (Mg-Sr) based alloys

By Meltem Top

A Thesis Submitted to the Faculty of Graduate Studies and Research in Partial Fulfilment of the requirements for the Degree of Masters of Science



Faculty of Dentistry
McGill University
Montreal, Canada

April 2017

© Meltem Top

ABSTRACT

In this study, we investigated the characteristics, corrosion rate and the biocompatibility of four (4) different magnesium-strontium (Mg-Sr) based alloys with the goal of developing a biodegradable, biocompatible cardiovascular implant material. The alloy compositions studied were Mg-0.5Sr, Mg-0.3. Sr-0.3Ca, Mg-0.3. Sr-0.3Ca-0.1Zn, Mg-0.3. Sr-0.3Ca-0.3Zn, and as controls, we used pure magnesium, the WE43 (Mg-0.4Y-4 Nd) commercial alloy and stainless steel 316L.

The material characteristics and corrosion rate were evaluated using atomic force micsroscopy (AFM), scanning electron microscopy (SEM) and X-ray diffraction (XRD as well as in vitro immersion tests.

Surface roughness was found to be alloy dependent with Mg-0.5Sr showing the highest decrease in roughness with polishing while stainless steel 316L the lowest. SEM analysis revealed that all Mg alloys studied exhibited cast dendritic structure with intermetallic second phases occupying the interdentritic regions. It was observed that zinc has a refining effect on dendrite size.

In vitro corrosion experiments were evaluated using modified simulated-body fluid (m-SBF) which yielded slightly different ranking in corrosion resistance based on weight loss and hydrogen evolution. For weight loss measurements, the ranking was found to be WE43<Mg-0.3Ca-0.3Sr-0.1Zn<Mg-0.3Ca-0.3Sr-0.3Zn<Mg-0.3Ca-0.3Sr<Mg-0.5Sr. For hydrogen evolution, the ranking was WE43<Mg-0.3Ca-0.3Sr-0.1Zn<Mg-0.3Ca-0.3Ca-0.3Sr-0.1Zn<Mg-0.3Ca-0.3Sr-0.3Zn<Mg-0.5Sr<Mg-0.3Ca-0.3Sr. It was seen that the zinc addition to Mg-Ca-Sr alloy improved the corrosion resistance.

Indirect in-vitro cytotoxicity tests were conducted using human umbilical vein endothelial cells (HUVECs) and mouse osteoblast precursor cells (MC3T3) with % cell viability measurements (hereafter referred to as % viability) taken at day 1, day 4 and day 7. Results of these experiments showed differences between the cell types. Noting that day 1 is the first exposure time that reflects directly the %viability of the alloys, we observed for HUVECs that the %viability in day 1 was significantly lower for WE43

compared to the other alloys. On the other hand, for MC3T3 cells, the highest % viability was observed for WE43 and pure magnesium.

We observed that the cells recovered at day 4 and %viability increased for both HUVECs and MC3T3 cells. Noting that day 4 represents the values in % viability 4 days after the first exposure to the alloys, the highest increase in %viability observed for HUVECs was for the Mg-0.3Ca-0.3Sr alloy and for MC3T3 cells it was observed for pure magnesium and the WE43 alloy.

At day 7, we observed a decrease in viability for HUVECs for all alloys and controls while for MC3T3 cells, % viability continued to increase for most of the alloys and controls. Overall, we observed that the % viability for MC 3T3 cells were higher compared to the HUVECs.

Hemolysis results showed that all our newly developed alloys caused less hemolysis compared to the WE43 commercial alloy. The hemolysis rate increased with the increase in alloy weight for all alloys. We also observed that the pH increase does not have a considerable effect on hemolysis rate.

Platelet aggregation studies were initiated yet these have not been discussed in the results because sufficient number of repeats could not be made. Platelet aggregation has been briefly included in the Appendix. This may be an interesting future study on the effect of magnesium on platelet aggregation.

RESUME

Nous avons étudié ici les propriétés de surface, la vitesse de corrosion et la biocompatibilité de quatre (4) différents alliages à base de magnésium-strontium (Mg-Sr) afin de développer un matériau pour implant cardiovasculaire biodégradable et biocompatible. Les compositions d'alliage Mg-0,5Sr, Mg-0,3. Sr-0.3Ca, Mg-0.3. Sr-0.3Ca-0.1Zn, Mg-0.3. Sr-0.3Ca-0.3Zn ont été étudiées, et du magnésium pur ainsi que l'alliage commercial WE43 (Mg-0.4Y-4 Nd) et l'acier inoxydable 316L ont été utilisés comme témoin.

Les propriétés du matériau et la vitesse de corrosion ont été évaluées par microscopie à force atomique (AFM), microscopie électronique à balayage (MEB) et diffraction des rayons X (XRD) ainsi que par des tests d'immersion in vitro.

Il a été montré qu la rugosité de surface était directement liée au choix de l'alliage avec Mg-0.5Sr montrant la plus forte diminution de la rugosité suite au polissage et l'acier inoxydable 316L la plus faible. L'analyse SEM a révélé que tous les alliages de Mg étudiés présentaient une structure dendritique avec des secondes phases intermétalliques occupant les régions interdentritiques. Il a été observé que le zinc permettait de rafiner la taille de la structure dendritique.

Les expériences de corrosion in vitro ont été effectuées à l'aide d'un fluide de corps simulé modifié (m-SBF) et ont conduit à un classement légèrement différent de la résistance à la corrosion en fonction de la perte de poids et de l'évolution de l'hydrogène. Pour les mesures de perte de poids, l'ordre obtenu était WE43 <Mg-0.3Ca-0.3Sr-0.1Zn <Mg-0.3Ca-0.3Sr-0.3Zn <Mg-0.3Ca-0.3Sr <Mg-0.5Sr. Pour l'évolution de l'hydrogène, l'ordre était WE43 <Mg-0.3Ca-0.3Sr-0.1Zn <Mg-0.3Ca-0.3Sr-0.3Zn <Mg-0.5Sr <Mg-0.3Ca-0.3Sr. Il a été noté que l'addition de zinc à l'alliage de Mg-Ca-Sr améliorait sa résistance à la corrosion.

Des tests indirects de cytotoxicité in vitro ont été effectués en utilisant des cellules endothéliales de la veine ombilicale humaine (HUVEC) et des cellules précurseurs d'ostéoblastes de souris (MC3T3) avec des mesures de viabilité cellulaire (ci-après

définies par le % de viabilité) à J1, J4 et J7. Ces mesures ont montré des résultats différents en fonction du type de cellules.

Considérant que J1 est la première mesure qui traduit directement le % de viabilité au contact des alliages, nous avons observé pour les HUVEC que le % de viabilité à J1 était significativement plus faible pour WE43 par rapport aux autres alliages. D'autre part, pour les cellules MC3T3, le % de viability le plus élevé a été observé pour WE43 et le magnésium pur.

Nous avons observé un regain de viabilité à J4 avec une augmentation du % de viabilité pour les cellules HUVEC et MC3T3. Considérant que J4 représente la valeur du % de viabilité après 4 jours d'exposition aux alliages, la plus forte augmentation de % de viabilité observée pour les HUVEC concernait l'alliage Mg-0.3Ca-0.3Sr, et pour les cellules MC3T3, le magnésium pur et l'alliage WE43.

À J7, il a été noté une diminution de la viabilité pour les HUVEC pour tous les alliages et contrôles, tandis que pour les cellules MC3T3, le % de viabilité continuait d'augmenter pour la plupart des alliages et des contrôles. Dans l'ensemble, le % de viabilité pour les cellules MC3T3 était plus élevé que celui des HUVEC.

Les résultats de l'hémolyse ont montré que tous nos alliages récemment développés causaient moins d'hémolyse par rapport à l'alliage commercial WE43.

Le taux d'hémolyse augmentait avec le poids des alliages pour tous les groupes. Nous avons également relevé que l'augmentation du pH n'avait pas d'effet significatif sur le taux d'hémolyse. Des études d'agrégation de plaquettes ont été initiées, mais celles-ci n'ont pas été discutées dans les résultats car un nombre suffisant de réplicats n'a pas pu être réalisé. L'agrégation des plaquettes est brièvement mentionnée dans l'annexe. Elle pourrait faire l'objet d'une future étude de l'effet du magnésium sur l'agrégation plaquettaire.

ACKNOWLEDGEMENTS

I would like to sincerely thank to Prof. Maryam Tabrizian for giving me the opportunity to work under her supervision and for her constant support and guidance in these past two years. I was inspired not only by her scientific skills but also by her human qualities, which made this research journey a very enriching experience.

I would like to express my deepest gratitude to Prof. Mihriban Pekguleryuz for her mentoring and support during these years. I was inspired by her vast knowledge in materials science and metallurgy, her commitment to science and her kindness towards collaborators and students.

I would like to thank my research colleagues in Prof. Pekguleryuz's group: Dr. Amir Rezaei Farkoosh, Dr. Mario Ascencio Pinedo, Dr. Mandana Bournapour, Luis Angel Armenta, Konstantinos Korgiopoulos, Brian Cook, Ogeday Rodop for their useful inputs and valuable comments as well as for the assistance in the casting of Mg alloys and their support in any other experimental work.

I would like to thank my former and current colleagues in the Biomat'X Laboratory; Dr. Mina Mekhail, Dr. Amir Foudeh, Dr. Lamees Nayef, Dr. Samira Taherkhani, Dr. Sandrine Filion-Cote, Dr. Khalil Leon Heileman, Dr. Saber Ghadakzadeh, Rosey Rasoda, Dr. Laila Benameur, Dr. Feriel Melaine, Dr. Timothee Edouard Baudequin, Kaushar Jahan, Francisco Castiello Flores, Paresa Modarres, Sultan Aati, Nicholas Distasio, Selya Amrani and Saadia Shoaib for all their support and advice, for the stimulating discussions and for all the good times we shared during the past two years. I would like to acknowledge Prof. Yahye Merhi, Dr. Souhad El Akoum and Kevin Kojok at Montreal Heart Institute for having taken the time to train and help me with the necessary equipment, as well as for the assistance with all the biocompatibility assays. I will always be grateful for their help and support.

My appreciation is extended to the staff members in Materials Engineering Pierre Vermette and Dr. Yasser Zedan and in the Chemical Engineering Department: Andrew Golsztajn and Ranjan Roy for all their help and support.

I would like to express my gratitude to my dear family; Sarah Cooper, Carol Cooper, Richard Cooper and Celil Aliravci. Thank you for being my family in Montreal and for the unconditional support and motivation.

I would like to sincerely thank to my friends: Fulya Kasap, Ilke Incekara Olcay Hekimoglu and Soneth Chan for their support and for being an inspiration to pursue my dreams and not to give up.

My deepest gratitude goes to my parents Sabriye and Suleyman, my siblings Yasemin, Cihangir and Sinem and my dearest nephew Oguz, for their unconditional love and support over the years, for being my inspiration and my strength.

Lastly, I gratefully acknowledge the financial support from the Natural Science and Engineering Research Council of Canada (NSERC), McGill University Faculty of Dentistry and De Seve Foundation.

TABLE OF CONTENTS

Abstract	i
Résumé	iii
Acknowledgements	v
Table of contents	vii
List of figures	х
List of tables	xiv
List of abbreviations	xv
List of elements	XV
Chapter 1 Introduction	1
1.1 Introduction	1
1.2 References	2
Chapter 2 Background and literature review	3
2.1 Biodegradable cardiovascular implants	3
2.1.1 Cardiovascular diseases and applications	3
2.1.2 Development of biodegradable stents	5
2.1.2.1 Magnesium as a biodegradable and bio-compa	tible metallic
implant material	7
2.1.2.1.1 Magnesium in the human body	7
2.1.2.1.2 Magnesium as a Bio-material	8
2.2 Metallurgical factors	13
2.2.1 Alloying elements for bio-degradable Mg alloys	13
2.2.2 Phases and microstructure of the alloys	16
2.3 Bio-Corrosion of Mg and Mg alloys	17
2.3.3 In vitro methodology for the investigation of the corrosion	n behavior of
Mg alloys for biodegradable applications	17
2.3.3.1 Weight loss	18
2.3.3.2 Hydrogen evolution	19
2.3.3.3 ICP-OES	20
	Vii

2.4.1 Tests used to evaluate biocompatibility. 21 2.4.1.1 In vitro studies. 22 2.4.1.1.2 In vitro hemacompatibility tests. 22 2.4.1.2 In vivo studies. 25 2.5 References. 27 Chapter 3 Motivation and Objectives. 37 3.1 Motivation. 37 3.2 Objectives. 37 3.3 References. 38 Chapter 4 Materials and Methods. 38 4.1 Sample preparation. 39 4.1.1 Alloy Casting. 39 4.1.2 ICP-OES Analysis. 39 4.2 Characterization. 41 4.2.1 Surface Characterization. 41 4.2.1.1 Atomic Force Microscopy (AFM). 41 4.2.1.2 X-Ray Diffraction (XRD). 42 4.2.1.3 Scanning Electron Microscopy (SEM). 42 4.2.2 Hydrogen evolution. 43 4.2.2.1 In vitro immersion tests. 45 4.2.2.2 Hydrogen evolution. 45 4.2.2.3 Weight Loss. 45 4.2.2.4 Electrolyte analysis (ICP-OES). 46 4.3 Cytotoxicity. 47 4.3.2.1 lon extract preparation. 47	2.4 Biocompatibility	21
2.4.1.1.1 In direct cytotoxicity tests. 22 2.4.1.2.2 In vitro hemacompatibility tests. 25 2.5 References. 27 Chapter 3 Motivation and Objectives. 37 3.1 Motivation. 37 3.2 Objectives. 37 3.3 References. 38 Chapter 4 Materials and Methods. 39 4.1 Sample preparation. 39 4.1.1 Alloy Casting. 39 4.1.2 ICP-OES Analysis. 39 4.2 Characterization. 41 4.2.1 Surface Characterization. 41 4.2.1.1 Atomic Force Microscopy (AFM). 41 4.2.1.2 X-Ray Diffraction (XRD). 42 4.2.1.3 Scanning Electron Microscopy (SEM). 42 4.2.2.1 In vitro immersion tests. 43 4.2.2.2 Hydrogen evolution. 45 4.2.2.3 Weight Loss. 45 4.2.2.4 Electrolyte analysis (ICP-OES). 46 4.3 Cytotoxicity. 47 4.3.1 Cell cultures (HUVEC, MC3T3). 47 4.3.2.1 Ion extract preparation. 47	2.4.1 Tests used to evaluate biocompatibility	21
2.4.1.1.2 In vitro hemacompatibility tests. 22 2.4.1.2 In vivo studies. 25 2.5 References. 27 Chapter 3 Motivation and Objectives. 37 3.1 Motivation. 37 3.2 Objectives. 37 3.3 References. 38 Chapter 4 Materials and Methods. 39 4.1 Sample preparation. 39 4.1.1 Alloy Casting. 39 4.1.2 ICP-OES Analysis. 39 4.2 Characterization. 41 4.2.1 Surface Characterization. 41 4.2.1.1 Atomic Force Microscopy (AFM). 41 4.2.1.2 X-Ray Diffraction (XRD). 42 4.2.1.3 Scanning Electron Microscopy (SEM). 42 4.2.2 Corrosion. 43 4.2.2.1 In vitro immersion tests. 43 4.2.2.2 Hydrogen evolution. 45 4.2.2.3 Weight Loss. 45 4.2.2.4 Electrolyte analysis (ICP-OES) 46 4.3 Cytotoxicity. 47 4.3.1 Cell cultures (HUVEC, MC3T3). 47 4.3.2.1 lon extract preparation. 47	2.4.1.1 In vitro studies	22
2.4.1.2 In vivo studies. 25 2.5 References. 27 Chapter 3 Motivation and Objectives. 37 3.1 Motivation. 37 3.2 Objectives. 37 3.3 References. 38 Chapter 4 Materials and Methods. 38 4.1 Sample preparation. 39 4.1.1 Alloy Casting. 39 4.1.2 ICP-OES Analysis. 39 4.2 Characterization. 41 4.2.1 Surface Characterization. 41 4.2.1.1 Atomic Force Microscopy (AFM). 41 4.2.1.2 X-Ray Diffraction (XRD). 42 4.2.1.3 Scanning Electron Microscopy (SEM). 42 4.2.2 Corrosion. 43 4.2.2.1 In vitro immersion tests. 43 4.2.2.2 Hydrogen evolution. 45 4.2.2.3 Weight Loss. 45 4.2.2.4 Electrolyte analysis (ICP-OES) 46 4.3 Cytotoxicity. 47 4.3.1 Cell cultures (HUVEC, MC3T3). 47 4.3.2.1 Ion extract preparation. 47	2.4.1.1.1 In direct cytotoxicity tests	22
2.5 References 27 Chapter 3 Motivation and Objectives 37 3.1 Motivation 37 3.2 Objectives 37 3.3 References 38 Chapter 4 Materials and Methods 39 4.1 Sample preparation 39 4.1.1 Alloy Casting 39 4.1.2 ICP-OES Analysis 39 4.2 Characterization 41 4.2.1 Surface Characterization 41 4.2.1.1 Atomic Force Microscopy (AFM) 41 4.2.1.2 X-Ray Diffraction (XRD) 42 4.2.1.3 Scanning Electron Microscopy (SEM) 42 4.2.2 Corrosion 45 4.2.2.1 In vitro immersion tests 43 4.2.2.2 Hydrogen evolution 45 4.2.2.3 Weight Loss 45 4.2.2.4 Electrolyte analysis (ICP-OES) 46 4.3 Cytotoxicity 47 4.3.1 Cell cultures (HUVEC, MC3T3) 47 4.3.2.1 lon extract preparation 47	2.4.1.1.2 In vitro hemacompatibility tests	22
Chapter 3 Motivation and Objectives 37 3.1 Motivation 37 3.2 Objectives 37 3.3 References 38 Chapter 4 Materials and Methods 39 4.1 Sample preparation 39 4.1.1 Alloy Casting 39 4.1.2 ICP-OES Analysis 39 4.2 Characterization 41 4.2.1 Surface Characterization 41 4.2.1 Atomic Force Microscopy (AFM) 41 4.2.1.2 X-Ray Diffraction (XRD) 42 4.2.1.3 Scanning Electron Microscopy (SEM) 42 4.2.2 Corrosion 43 4.2.2.1 In vitro immersion tests 43 4.2.2.2 Hydrogen evolution 45 4.2.2.3 Weight Loss 45 4.2.2.4 Electrolyte analysis (ICP-OES) 46 4.3 Cytotoxicity 47 4.3.1 Cell cultures (HUVEC, MC3T3) 47 4.3.2.1 loi extract preparation 47	2.4.1.2 In vivo studies	25
3.1 Motivation 37 3.2 Objectives 37 3.3 References 38 Chapter 4 Materials and Methods 39 4.1 Sample preparation 39 4.1.1 Alloy Casting 39 4.1.2 ICP-OES Analysis 39 4.2 Characterization 41 4.2.1 Surface Characterization 41 4.2.1.1 Atomic Force Microscopy (AFM) 41 4.2.1.2 X-Ray Diffraction (XRD) 42 4.2.1.3 Scanning Electron Microscopy (SEM) 42 4.2.2 Corrosion 43 4.2.2.1 In vitro immersion tests 43 4.2.2.2 Hydrogen evolution 45 4.2.2.3 Weight Loss 45 4.2.2.4 Electrolyte analysis (ICP-OES) 46 4.3 Cytotoxicity 47 4.3.1 Cell cultures (HUVEC, MC3T3) 47 4.3.2.1 lon extract preparation 47	2.5 References	27
3.2 Objectives 37 3.3 References 38 Chapter 4 Materials and Methods 39 4.1 Sample preparation 39 4.1.1 Alloy Casting 39 4.1.2 ICP-OES Analysis 39 4.2 Characterization 41 4.2.1 Surface Characterization 41 4.2.1.1 Atomic Force Microscopy (AFM) 41 4.2.1.2 X-Ray Diffraction (XRD) 42 4.2.1.3 Scanning Electron Microscopy (SEM) 42 4.2.2 Corrosion 43 4.2.2.1 In vitro immersion tests 43 4.2.2.2 Hydrogen evolution 45 4.2.2.3 Weight Loss 45 4.2.2.4 Electrolyte analysis (ICP-OES) 46 4.3 Cytotoxicity 47 4.3.1 Cell cultures (HUVEC, MC3T3) 47 4.3.2.1 lon extract preparation 47	Chapter 3 Motivation and Objectives	37
3.3 References. 38 Chapter 4 Materials and Methods. 39 4.1 Sample preparation. 39 4.1.1 Alloy Casting. 39 4.1.2 ICP-OES Analysis. 39 4.2 Characterization. 41 4.2.1 Surface Characterization. 41 4.2.1.1 Atomic Force Microscopy (AFM). 41 4.2.1.2 X-Ray Diffraction (XRD). 42 4.2.1.3 Scanning Electron Microscopy (SEM). 42 4.2.2 Corrosion. 43 4.2.2.1 In vitro immersion tests. 43 4.2.2.2 Hydrogen evolution. 45 4.2.2.3 Weight Loss. 45 4.2.2.4 Electrolyte analysis (ICP-OES) 46 4.3 Cytotoxicity. 47 4.3.1 Cell cultures (HUVEC, MC3T3). 47 4.3.2.1 lon extract preparation. 47	3.1 Motivation	37
Chapter 4 Materials and Methods 38 4.1 Sample preparation 39 4.1.1 Alloy Casting 39 4.1.2 ICP-OES Analysis 39 4.2 Characterization 41 4.2.1 Surface Characterization 41 4.2.1.1 Atomic Force Microscopy (AFM) 41 4.2.1.2 X-Ray Diffraction (XRD) 42 4.2.1.3 Scanning Electron Microscopy (SEM) 42 4.2.2 Corrosion 43 4.2.2.1 In vitro immersion tests 43 4.2.2.2 Hydrogen evolution 45 4.2.2.3 Weight Loss 45 4.2.2.4 Electrolyte analysis (ICP-OES) 46 4.3 Cytotoxicity 47 4.3.1 Cell cultures (HUVEC, MC3T3) 47 4.3.2 Indirect cytotoxicity assays 47 4.3.2.1 Ion extract preparation 47	3.2 Objectives	37
4.1 Sample preparation 38 4.1.1 Alloy Casting 39 4.1.2 ICP-OES Analysis 39 4.2 Characterization 41 4.2 Surface Characterization 41 4.2.1 Atomic Force Microscopy (AFM) 41 4.2.1.2 X-Ray Diffraction (XRD) 42 4.2.1.3 Scanning Electron Microscopy (SEM) 42 4.2.2 Corrosion 43 4.2.2.1 In vitro immersion tests 43 4.2.2.2 Hydrogen evolution 45 4.2.2.3 Weight Loss 45 4 2.2.4 Electrolyte analysis (ICP-OES) 46 4.3 Cytotoxicity 47 4.3.1 Cell cultures (HUVEC, MC3T3) 47 4.3.2 Indirect cytotoxicity assays 47 4.3.2.1 lon extract preparation 47	3.3 References	38
4.1.1 Alloy Casting. 39 4.1.2 ICP-OES Analysis. 39 4.2 Characterization. 41 4.2.1 Surface Characterization. 41 4.2.1.1 Atomic Force Microscopy (AFM). 41 4.2.1.2 X-Ray Diffraction (XRD). 42 4.2.1.3 Scanning Electron Microscopy (SEM). 42 4.2.2 Corrosion. 43 4.2.2.1 In vitro immersion tests. 43 4.2.2.2 Hydrogen evolution. 45 4.2.2.3 Weight Loss. 45 4 2.2.4 Electrolyte analysis (ICP-OES) 46 4.3 Cytotoxicity. 47 4.3.1 Cell cultures (HUVEC, MC3T3). 47 4.3.2 Indirect cytotoxicity assays. 47 4.3.2.1 lon extract preparation. 47	Chapter 4 Materials and Methods	39
4.1.2 ICP-OES Analysis	4.1 Sample preparation	39
4.2 Characterization 41 4.2.1 Surface Characterization 41 4.2.1.1 Atomic Force Microscopy (AFM) 41 4.2.1.2 X-Ray Diffraction (XRD) 42 4.2.1.3 Scanning Electron Microscopy (SEM) 42 4.2.2 Corrosion 43 4.2.2.1 In vitro immersion tests 43 4.2.2.2 Hydrogen evolution 45 4.2.2.3 Weight Loss 45 4.2.2.4 Electrolyte analysis (ICP-OES) 46 4.3 Cytotoxicity 47 4.3.1 Cell cultures (HUVEC, MC3T3) 47 4.3.2 Indirect cytotoxicity assays 47 4.3.2.1 Ion extract preparation 47	4.1.1 Alloy Casting	39
4.2.1 Surface Characterization. 41 4.2.1.1 Atomic Force Microscopy (AFM). 41 4.2.1.2 X-Ray Diffraction (XRD). 42 4.2.1.3 Scanning Electron Microscopy (SEM). 42 4.2.2 Corrosion. 43 4.2.2.1 In vitro immersion tests. 43 4.2.2.2 Hydrogen evolution. 45 4.2.2.3 Weight Loss. 45 4 2.2.4 Electrolyte analysis (ICP-OES) 46 4.3 Cytotoxicity. 47 4.3.1 Cell cultures (HUVEC, MC3T3). 47 4.3.2 Indirect cytotoxicity assays. 47 4.3.2.1 lon extract preparation. 47	4.1.2 ICP-OES Analysis	39
4.2.1.1 Atomic Force Microscopy (AFM) 41 4.2.1.2 X-Ray Diffraction (XRD) 42 4.2.1.3 Scanning Electron Microscopy (SEM) 42 4.2.2 Corrosion 43 4.2.2.1 In vitro immersion tests 43 4.2.2.2 Hydrogen evolution 45 4.2.2.3 Weight Loss 45 4 2.2.4 Electrolyte analysis (ICP-OES) 46 4.3 Cytotoxicity 47 4.3.1 Cell cultures (HUVEC, MC3T3) 47 4.3.2 Indirect cytotoxicity assays 47 4.3.2.1 Ion extract preparation 47	4.2 Characterization	41
4.2.1.2 X-Ray Diffraction (XRD) 42 4.2.1.3 Scanning Electron Microscopy (SEM) 42 4.2.2 Corrosion 43 4.2.2.1 In vitro immersion tests 43 4.2.2.2 Hydrogen evolution 45 4.2.2.3 Weight Loss 45 4.2.2.4 Electrolyte analysis (ICP-OES) 46 4.3 Cytotoxicity 47 4.3.1 Cell cultures (HUVEC, MC3T3) 47 4.3.2 Indirect cytotoxicity assays 47 4.3.2.1 Ion extract preparation 47	4.2.1 Surface Characterization	41
4.2.1.3 Scanning Electron Microscopy (SEM) 42 4.2.2 Corrosion 43 4.2.2.1 In vitro immersion tests 43 4.2.2.2 Hydrogen evolution 45 4.2.2.3 Weight Loss 45 4 2.2.4 Electrolyte analysis (ICP-OES) 46 4.3 Cytotoxicity 47 4.3.1 Cell cultures (HUVEC, MC3T3) 47 4.3.2 Indirect cytotoxicity assays 47 4.3.2.1 Ion extract preparation 47	4.2.1.1 Atomic Force Microscopy (AFM)	41
4.2.2 Corrosion	4.2.1.2 X-Ray Diffraction (XRD)	42
4.2.2.1 In vitro immersion tests 43 4.2.2.2 Hydrogen evolution 45 4.2.2.3 Weight Loss 45 4 2.2.4 Electrolyte analysis (ICP-OES) 46 4.3 Cytotoxicity 47 4.3.1 Cell cultures (HUVEC, MC3T3) 47 4.3.2 Indirect cytotoxicity assays 47 4.3.2.1 Ion extract preparation 47	4.2.1.3 Scanning Electron Microscopy (SEM)	42
4.2.2.2 Hydrogen evolution	4.2.2 Corrosion	43
4.2.2.3 Weight Loss	4.2.2.1 In vitro immersion tests	43
4 2.2.4 Electrolyte analysis (ICP-OES)	4.2.2.2 Hydrogen evolution	45
4.3 Cytotoxicity	4.2.2.3 Weight Loss	45
4.3.1 Cell cultures (HUVEC, MC3T3)	4 2.2.4 Electrolyte analysis (ICP-OES)	46
4.3.2 Indirect cytotoxicity assays	4.3 Cytotoxicity	47
4.3.2.1 Ion extract preparation47	4.3.1 Cell cultures (HUVEC, MC3T3)	47
·	4.3.2 Indirect cytotoxicity assays	47
4.3.2.2 ICP-OES analysis for the ions in the extract48	4.3.2.1 Ion extract preparation	47
	4.3.2.2 ICP-OES analysis for the ions in the extract	48

4.3.2.3 MTT test	48
4.4 Blood compatibility	49
4.4.1 Hemolysis	49
4.4.2 Platelet Aggregation	51
4.5 Cell attachment	52
4.5.1 Sample preparation	52
4.5.2 Confocal imaging	53
4.6 Statistical analysis	53
4.7 References	54
Chapter 5 Results and discussion	55
5.1 Material characterization	55
5.1.1 Surface Characterization via Atomic Force Microscopy (AF	FM)55
5.1.2 X-Ray Diffraction (XRD)	58
5.1.3 Scanning Electron Microscopy (SEM) and Energy	Dispersive
Spectroscopy (EDS) analysis	61
5.2 Corrosion rate	66
5.3 Indirect cytotoxicity tests	69
5.3.1 MTT test	69
5.4 Blood compatibility	71
5.4.1 Hemolysis	71
5.5 Results Summary	75
5.6 References	76
Chapter 6 Discussion	77
6.1. References	82
Chapter 7 Contributions and future work	83
Appendix	85
A.1 Cell attachment	85
A 2 Platelet aggregation	86

LIST OF FIGURES

- **Fig. 2.1.1.1:** An illustration of a coronary stent implantation: (a) the stent is transferred to the site of blockage using a catheter, (b) balloon inflation opens the narrowed artery while deploying the stent, (c) the balloon is deflated and the catheter is removed. The stent remains inside the artery providing support and enabling the blood flow [6].
- **Fig. 2.1.2.1:** Illustration of a desired correlation between mechanical integrity and degradation of a biodegradable stent [7].
- Fig. 2.1.2.2: Extent of degradation in implanted wires. Clean iron wire before implantation (A) and wires retrieved from the arterial wall after 1.5 months (B) and 3 (C) months. Iron wires retrieved from the artery lumen after 9 months at central (D) or wall locations (E). Clean magnesium wire before implantation (F), magnesium wires implanted in the arterial wall after 3 weeks (G and H), where (G) shows the in situ image of implanted magnesium with localized pits on the surface (yellow arrow in G) and subsequence fragmentation after 3 weeks (green arrows in H), and magnesium wires implanted in artery lumen in contact with blood after 3 weeks (I). [22].
- **Fig. 2.1.2.1:** Real/possible applications of biodegradable magnesium implants (a) cardiovascular stents (BIOTRONIK, Berlin, Germany, under clinical trial), (b) MAGNEZIX screw (received CE mark in Europe), (c) microclip for laryngeal microsurgery (pure magnesium), (d) biodegradable orthopedic implants, (e) wound-closing devices (WZ21) [32].
- **Fig. 2.2.1.1:** The immersion test results in SBF at 37 °C, for Mg–Sr samples with different Sr content. The average corrosion rate (mg day⁻¹ cm⁻²) were calculated in terms of mass loss and hydrogen evolution [86].
- **Figure 2.3.3.2.1:** Schematic illustration of the immersion cell set-up to measure the volume of hydrogen evolution [75].

Fig.2.4.1.2.1: (a, b) Optical and histology images after H & E staining of vascular tissue surrounding of Mg-0.3Sr-0.3Ca alloy stent, (c, d) WE43 tubular stent samples implanted in right and left femoral artery for 5 weeks. The stented artery was distorted and compressed in pictures a and b during histological processing.

Fig. 4.1.1.1: Casting procedure: **(a)** melting in graphite crucible with induction furnace, **(b)** thin plate cast sample, **(c)** chip obtaining using the drill.

Fig. 4.2.1.3.1: (a) Samples embedded in epoxy resin, **(b)** samples prepared for SEM imaging.

Fig. 4.2.2.1.1: (a) Immersion test set up, (b) the funnels used for attaching the alloy samples, (c) assembly of the funnel and the cylinders.

Fig. 4.2.2.3.1: The removal of corrosion layer on the samples using chromic acid ((180 g CrO3/dm3)).

Fig. 4.3.2.3.1: (a) Day 1 Alamar blue test plate for MC3T3 cells, **(b)** Day 1 MTT test plate for MC3T3 cells.

Fig. 4.4.1.1: (a) The blood samples mixed with Mg alloy particles after incubation and centrifugation, **(b)** blood samples transferred to a reading plate for spectroscopy.

Fig. 4.4.2.1: The aggregation of three samples compared to the collagen (blue line).

Fig. 5.1.1.2: The surface roughness (Rms) for four Mg alloys and controls WE43 and SS316L.

Fig. 5.1.1.2 (a): AFM pictures of SS 316L

Fig. 5.1.1.2 (b): AFM pictures of WE43

Fig.5.1.1.2 (c): AFM pictures of Mg-0.5 Sr

Fig.5.1.1.2 (d): AFM pictures of Mg-0.3 Sr - 0.3 Ca

Fig. 5.1.1.2 (e): AFM pictures of Mg-0.3 Sr - 0.3 Ca - 0.1 Zn

Fig. 5.1.1.2 (f): AFM pictures of Mg-0.3 Sr - 0.3 Ca - 0.3 Zn

- Fig. 5.1.2.1 (a): XRD patterns of Mg- 0.5 Sr
- Fig. 5.1.2.1 (b): XRD patterns of Mg- 0.3 Sr- 0.3 Ca
- Fig. 5.1.2.1 (c): XRD patterns of Mg- 0.3 Sr- 0.3 Ca- 0.1 Zn
- Fig. 5.1.2.1 (d): XRD patterns of Mg- 0.3 Sr- 0.3 Ca- 0.3 Zn
- Fig. 5.1.2.1 (e): XRD patterns of WE43 commercial alloy.
- **Fig. 5.1.3.1 (a)**: Mg 0.5 Sr alloy; (a) SEM image (500 μ m), (b) SEM image (100 μ m), (c) EDS chemical point analysis results (10 μ m).
- **Fig. 5.1.3.1 (b)**: Mg- 0.3-Ca -0.3 Sr alloy (a) SEM image (500 μ m), (b) SEM image (100 μ m), (c) EDS chemical point analysis results (10 μ m.
- **Fig. 5.1.3.1 (c):** Mg- 0.3-Ca -0.3 Sr 0.1 Zn alloy (a) SEM image (500 μ m), (b) SEM image (100 μ m), (c) EDS chemical point analysis results (10 μ m).
- **Fig. 5.1.3.1 (d):** Mg- 0.3-Ca -0.3 Sr 0.3 Zn alloy (a) SEM image (500 μ m), (b) SEM image (100 μ m), (c) EDS chemical point analysis results (10 μ m).
- **Fig. 5.1.3.1 (e):** WE43 alloy (a) SEM image (400 μ m), (b) SEM image (100 μ m), (c) SEM image (10 μ m).
- **Fig. 5.2.1 (a):** The average corrosion rate (mm/year) in terms of weight loss after immersion in SBF at 37°C for five days.
- **Fig. 5.2.1 (b):** The average corrosion rate (mm/year) in terms of hydrogen evolution after immersion in m-SBF at 37°C for five days.
- **Fig. 5.2.1 (c):** The average pH change in m-SBF during the five days of static immersion experiments at 37°C.
- **Fig. 5.4.1.1:** The % hemolysis of the samples after 30 minutes of incubation in blood at 37°C.
- **Fig. 5.4.1.2:** The % hemolysis of the samples after 60 minutes of incubation in blood at 37°C.

- **Fig. 5.4.1.3:** The % hemolysis of the samples after 90 minutes of incubation in blood at 37°C. *The hemolysis rate for WE43 2,5 mg and 5 mg samples were significantly higher than the other alloys (p<0.05).
- Fig. 5.4.1.4: pH values after 90 min. of incubation in blood at 37°C.
- **Fig. A .1:** The HUVECs confocal microscope image after 24h incubation on Mg- 0.3 Sr –0.3 Ca- 0.1 Zn alloy (DAPI (Blue- DNA (Nucleus)) & Phalloidin (Red) staining (Actin).
- **Fig. A. 2:** The platelet aggregation results for three control materials (pure magnesium, Stainless steel SS316L and WE43) and four test compositions. 0.5 micrograms/ml of collagen was used as an aggregating reagent.

LIST OF TABLES

Table 2.1.2.1.1.1: Distribution and concentrations of Mg in the body of a healthy adult [29].

Table 2.1.2.1: Physical and mechanical properties of some biomaterials and natural bone [14].

Table 2.1.2.1.2.2: Reports on magnesium and its biomedical applications in historiological order [24].

Table 2.4.1.1.2.1: Effects of the metal ion concentration on the hemolysis rate [95].

Table 4.1.1.1: Nominal composition of WE43 Mg alloy.

Table 4.1.2.1: The chemical composition of the alloys.

Table 4.2.2.1.1: Comparison for the concentrations of m-SBF with blood plasma [81, 82].

Table 4.2.2.1.2: Amounts of reagents used to prepare 1000 ml of m-SBF [1].

LIST OF ABBREVIATIONS

AFM Atomic force microscopy

AMI Acute myocardial infarction

HUVEC Human Umblical Vein Endothelial Cells

ICP-OES Inductively coupled plasma optical emission spectroscopy

EDS Energy dispersive spectroscopy

OPC Osteoblast precursor cells

PBS Phosphate buffered saline

SBF Simulated body fluid

SEM Scanning electron microscopy

XRD X-Ray diffraction

LIST OF ELEMENTS

Al Aluminium

Ca Calcium

Co Cobalt

Cr Chromium

Mg Magnesium

Mn Manganese

REE Rare earth element

Zn Zinc

Zr Zirconium

Chapter 1: INTRODUCTION

The idea of using magnesium as a biomaterial originates from 1878, where magnesium wire ligatures were used for controlling bleeding. Later, during the first half of the 20th century, there were different studies which proposed the use of magnesium as a bone implant but the in vivo high corrosion-rate of magnesium was a major drawback. Later on, studies on different magnesium alloys also explored its use in implants yet cytotoxicity results were unsatisfactory (1, 2). In 1940s, other metallic materials were introduced to the market as implant material, namely different stainless steel alloys as well as titanium alloys. These materials highly accepted and considered as the gold standard. Consequently, magnesium biomaterial research became less attractive for researchers (3). In the last two decades, magnesium started to gain more interest due to its unique properties as a biomaterial (4). As the fourth common cation in the human body and an enzymatic cofactor, Mg plays a big role in the cellular functions such as DNA and RNA stabilization (5). Mg degrades in the body because of corrosion and the release of Mg²⁺ ions that do not cause any harm to the body. The presence of the ions may benefit new bone formation and strengthen bone-implant interfaces [3, 6]. Therefore, research on Mg as biodegradable implant material has gained impetus in the recent years. Initially the existing commercial alloys such as WE43 or AZ91D were investigated and even though they contained ions that could prove to be harmful to the body; nevertheless, research proved that the magnesium alloys are still viable candidates to be used as implant materials (7). Among the uses suggested are bone implants and cardiovascular stents. The bio-degradation of Mg here is an advantage. Permanent metallic stents lead to various complications related to physical irritation, infection, cell proliferation which in the case of cardiovascular stent increase the risk of thrombosis. Often a second intervention is needed to retrieve the implant causing patient discomfort, health risks and health costs. In the case of biodegradable Mg, repeat interventions and long-term complications related to permanent stents are reduced. Bio-degradable implants are especially important for pediatric patients where stent replacements are necessary. Biodegradable magnesium also offers advantages

over biodegradable polymeric implants because it is more easily detectable by CT scan and has higher strength.

However, despite their numerous advantages, the research on Mg alloys is still considered new and new Mg alloys with improved biodegradation and biocompatibility for different applications are proposed continually. Herein, this project investigates the physical characteristics, in-vitro corrosion rate and the biocompatibility of four new Mg alloy compositions to be used as biodegradable implant materials. The following sections will introduce the current research on biodegradable Mg alloys, later we will discuss the metallurgical factors, the bio-corrosion and biocompatibility of the newly developed Mg-Sr based alloys. Finally, we conclude with a summary and future considerations.

1.2. REFERENCES

- 1. Witte, F. The history of biodegradable magnesium implants: A review. Acta Biomater. 2010, 6, 1680-1692.
- 2. Staiger, M. P., A. M. Pietak, et al. (2006). "Magnesium and its Alloys as Orthopedic Biomaterials: A Review." Biomaterials 27: 1728-1734.
- 3. Witte, F, V. Kaese, H. Haferkamp, E. Switzer, A. Meyer-Lindenberg, C.J. Wirth and H. Windhagen, "In vivo corrosion of four magnesium alloys and the associated bone response," Biomaterials, vol. 26, no. 17, pp. 3557-3563, 2005.
- 4. Waksman R, Pakala R, Kuchulakanti PK, Baffour R, Hellinga D, Seabron R, et al. Safety and efficacy of bioabsorbable magnesium alloy stents in porcine coronary arteries. Catheterization and Cardiovascular Interventions. 2006;68:607-17.
- 5. Erne P, Schier M, Resink TJ. The road to bioabsorbable stents: Reaching clinical reality? Cardiovascular and Interventional Radiology. 2006;29:11-6.
- Kuhlmann J, Bartsch I, Willbold E, Schuchardt S, Holz O, Hort N, et al. Fast escape of hydrogen from gas cavities around corroding magnesium implants. Acta Biomaterialia. 2013;9:8714-21
- 7. Gu XN, Zhou WR, Zheng YF, Chengd Y, Wei SC, Zhong SP, et al. Corrosion behaviours of two biomedical Mg alloys-AZ91D and WE43 in simulated body fluid. Acta Biomaterialia 2010;6: 4605-13.

Chapter 2: BACKGROUND and LITERATURE REVIEW

2.1 BIODEGRADABLE CARDIOVASCULAR IMPLANTS

2.1.1 Cardiovascular diseases and stent applications

Cardiovascular diseases (CVDs) are the number one cause of death worldwide. In 2012, 17.5 million people died from CDVs with 7.4 million due to coronary heart disease and 6.7 million due to stroke [1]. US data (American Heart Association values) reveal that in 2013, 801,000 people in the U.S. died as a result of heart disease, stroke and other cardiovascular disease which represent one in every three deaths in the US. Currently approximately 85.6 million Americans are living with some form of cardiovascular disease or the after-effects of stroke [2]. The figures for Canada are also very high. More than 1.6 million Canadians are reported to have heart disease. In 2012, 48,000 people died from CDVs related causes in Canada [3]. The number of people who are diagnosed with CDVs are increasing rapidly and it is estimated that by 2030, 23.6 million people will be affected.

Among the deaths caused by coronary artery diseases, 70% is associated with the blockage of the artery by cholesterol build-up [4]. To address this problem and to remove the blockage and open the artery, balloon angioplasty is performed. Balloon angioplasty operations involve a stent placement in 60% of the cases [5]. During this process, a thin tube called a catheter that has a small balloon on its tip is used. This catheter carries the stent which is a wire metal mesh tube to the blocked area inside the artery. By inflating the balloon upon reaching the blockage site in the artery, the plaque is flattened and compressed against the artery wall. Inflation of the balloon enables the stent to expand and lock inside the artery to keep it open (Fig. 2.1.1.1).

Stents help keep the coronary arteries open after removing the blockage until the artery heals completely. Current stents are mainly made of stainless steel, titanium and cobalt-chromium alloys [4, 5, 7]. Their corrosion resistance is a big advantage in keeping the stability during the healing process yet their permanent presence in the body causes other complications. The toxic ions such as nickel, chrome, or molybdenum in these metals cause harm in the body in the long term. Research showed that these ions are

associated with cancer [8], inflammation and allergic reactions in the body. One of the other main problem caused by permanent stents is the in-stent restenosis. About 25% of the angiographies showed some level of restenosis after permanent stent applications. [9]. Presence of the permanent stents also causes hyperplasia, thrombosis in the stent in addition to other inflammation in the surrounding tissue. Furthermore, the arterial wall develops atypical mechanical behavior in the presence of the stent [10]. Another major problem is the use of permanent stents in pediatric patients. The applied stents are not compatible when the patient starts to grow and the stent might relocate inside the artery that leads to other problems such as irritation and all which may necessitate a secondary intervention to remove it [11]. In the case of another angioplasty or bypass graft surgery, the presence a previous permanent stent in the artery puts the operation at risk.

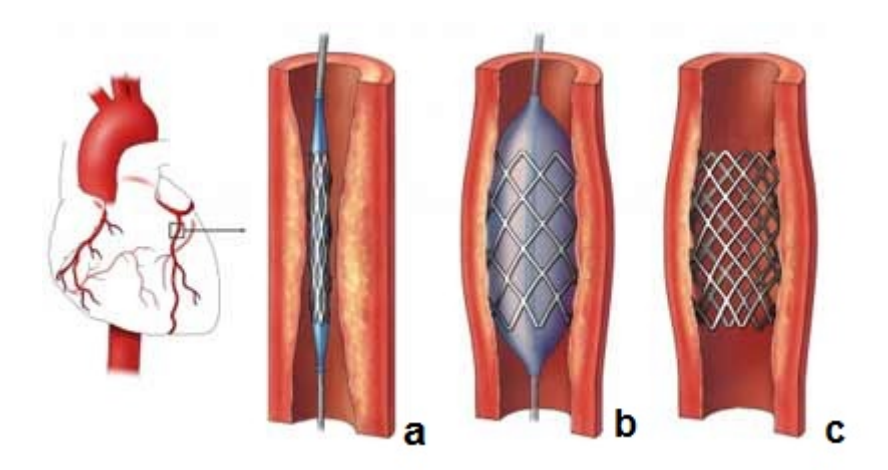


Fig. 2.1.1.1. An illustration of a coronary stent implantation: (a) the stent is transferred to the site of blockage using a catheter, (b) balloon inflation opens the narrowed artery while deploying the stent, (c) the balloon is deflated and the catheter is removed. The stent remains inside the artery providing support and enabling the blood flow [6].

When we consider how high the possibility is of another intervention on patients who have already suffered from a cardiovascular disease, the permanent stent becomes a risk factor. If any of the problems due to the presence of a permanent implant occurs, the patient is forced to undergo a secondary surgery to remove it. It is therefore important to find ways to avoid a secondary intervention as long as it is possible since it

puts the patient in danger; it is painful and also creates extra cost on health system [12, 13, 14]. The main role of the stent is to provide support to the artery during the healing process, which is finalized in about 6-12 months [7]. When the healing is completed, the stent serves no further purpose inside the body; in fact, it causes complications as restenosis or irritation. Consequently, a biodegradable stent, which will fade away after completing its purpose is ultimately the better option. [15, 16].

Economically, the stent market is growing rapidly, with the estimation of reaching 9.8 billion U.S. dollars by 2017 [4]. Thus, there is still a huge demand in developing biodegradable stents for specific purposes as pediatric use or for drug delivery applications.

2.1.2 Development of biodegradable stents

There are two main expectations from a potential biodegradable stent; (i) it must provide sufficient mechanical integrity until the healing of the artery is completed, and (ii) the corrosion rate of the stent needs to balance with the healing time (Fig. 2.1.2.1). During the arterial remodeling, the expectation is a slow degradation rate, which enables the degradation products to be removed from the area effectively while providing the adequate mechanical support [5, 10]. Ideally, considering the healing time of the arteries after the implementation of the stent, and depending on the material and the stenting area, we would expect the stent to degrade completely in 12-24 months. [7]. Polymers (eg. poly-l-lactic acid (PLLA)) and certain metals (Fe, Mg) are considered as the primary candidates in biodegradable stent development because of their high biocompatibility [17]. While the biocompatibility is good, the mechanical properties of the potential biodegradable polymer stents are limited [18]. In order for a polymer stent to provide required mechanical support to the arteries, the stent wall is maintained quite thick which however, would result in high weight. The metallic stents, on the other hand, can provide adequate mechanical performance in lower weights (15]. The two main candidates for biodegradable metallic stent research are iron and magnesium. In addition to their biocompatibility, both metals proved to have adequate mechanical capacity [19]. Iron is a main element in the body but at high levels can cause harm to the human body [20]. Recent animal studies on iron stents did not produce a negative inflammatory response or neointimal proliferation but proved that the stent failed to corrode completely in the required time [21].

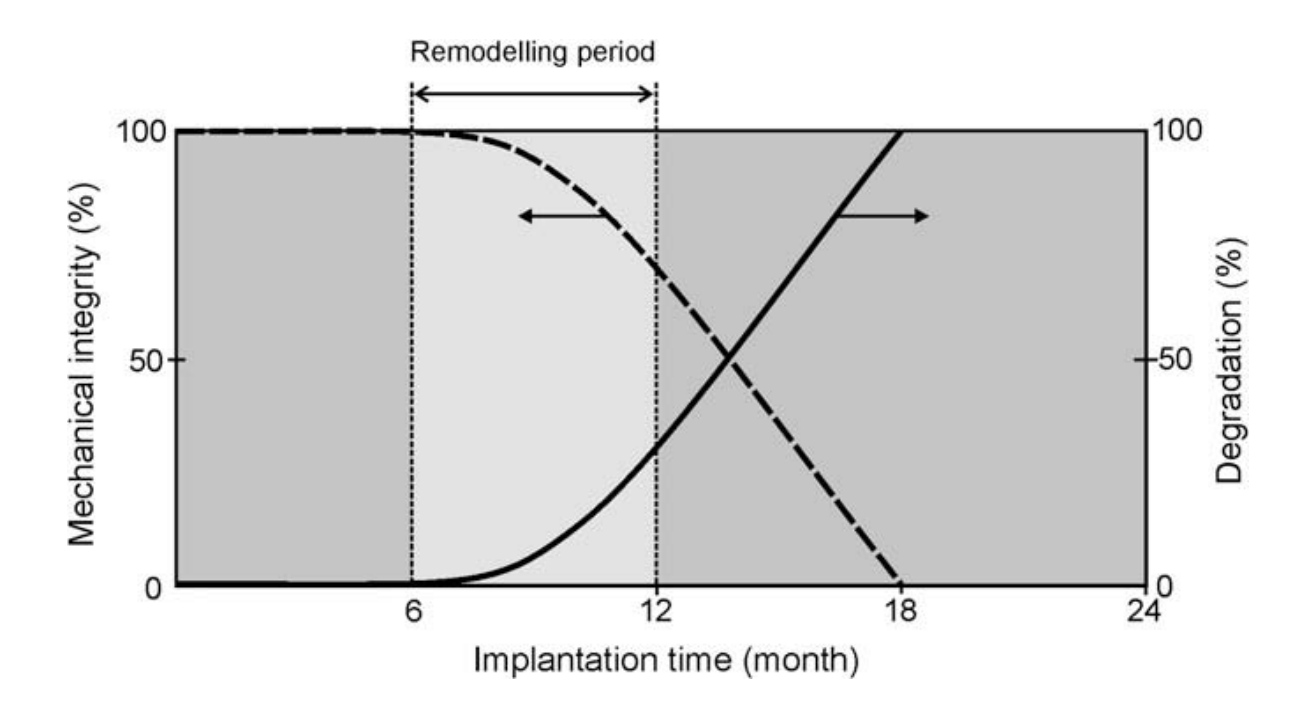


Fig. 2.1.2.1 Illustration of a desired correlation between mechanical integrity and degradation of a biodegradable stent [7].

Mg in comparison to the polymeric stents can provide the same mechanical performance in a weight range, which is ultimately lower [10, 16]. Another positive trait is that the mechanical properties of Mg are similar to the bone tissue, which is an advantage against the common metallic implants currently used for those applications [14]. As for another advantage Mg CT scanning provides better quality images.

In a study designed to compare the degradation behaviour in vivo for iron and magnesium, wires with the dimensions of 2 cm length × 0.25 mm diameter were implemented into the abdominal aorta of rats. Fig. 2.1.2.2 shows iron and magnesium wires implanted in the arterial wall and lumen after 1.5, 3 and 9 months. Wires were placed both in the artery and the wall. These two locations were chosen to investigate the stent-blood contact and stent-matrix contact [22]. After the removal of the wires, it

was observed that the wire placed in the arterial wall was still there and enlarged, even after 9 months.

The degradation products from the corroded iron wires were seemingly stable yet it was not clear if these residues might cause any harm to the integrity of the arterial wall after a long-term exposure. Whereas the corrosion rate seems to be higher for the artery wall implanted wires, the wires that were implanted inside the lumen showed very low degradation after 9 months. The results obtained on Mg wires showed that the corrosion rate was very fast inside the arterial wall. The corrosion was not homogenous on the surface and the corrosion related pit formation led to the wire fracture. Unlike the iron wires Mg wires did not show any retention of degradation products. After three weeks in contact with blood, the degradation of Mg wires was minimal.

2.1.2.1 Magnesium as a biodegradable and bio-compatible metallic implant material

2.1.2.1.1 Magnesium in the human body

Mg is one of the most common elements in the body, which plays important roles in several metabolic processes [9, 22]. Mg deficiency causes serious problems [29]. In the body, Mg is present and stored in different organs in different concentrations. It is known that a 70-kg adult body contains an average of 1 mol (24 g) of Mg [29, 30] (Table 2.1.2.1.1.1). A healthy diet provides 2–7.5 mg Mg/kg weight, consequently for a healthy individual 300–400 mg/day Mg is recommended [29]. Magnesium is absorbed from the gut, distributed to the cells and the excess amount is removed from the system through the kidneys [31].

Bone tissue holds most of the Mg inside the body. The second biggest location is muscles. The serum has only %1 of the total amount in the body. As expected bone tissue serves as a reserve for balancing the extracellular Mg levels in range. [29]

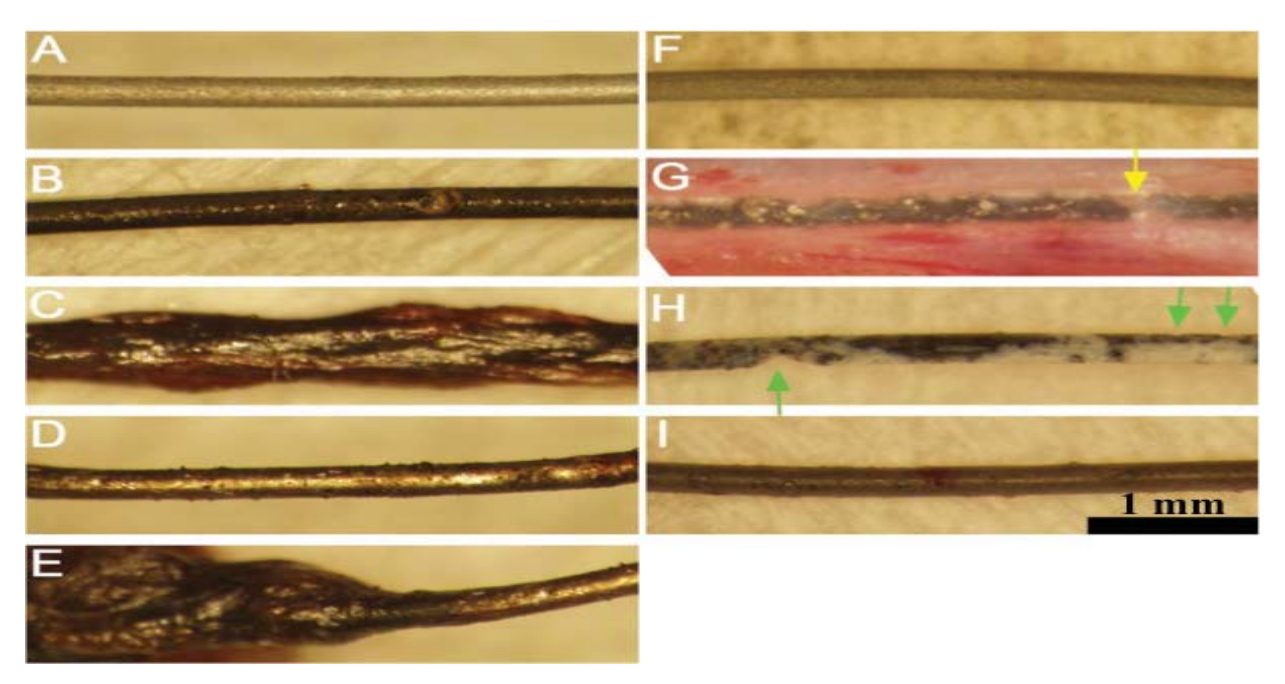


Fig. 2.1.2.2: Extent of degradation in implanted wires. Clean iron wire before implantation (A) and wires retrieved from the arterial wall after 1.5 months (B) and 3 (C) months. Iron wires retrieved from the artery lumen after 9 months at central (D) or wall locations (E). Clean magnesium wire before implantation (F), magnesium wires implanted in the arterial wall after 3 weeks (G and H), where (G) shows the in situ image of implanted magnesium with localized pits on the surface (yellow arrow in G) and subsequence fragmentation after 3 weeks (green arrows in H), and magnesium wires implanted in artery lumen in contact with blood after 3 weeks (I). [22].

2.1.2.1.2 Magnesium as a Bio-Material

J. Black first recognized magnesium as an element in 1707, and almost a century later identified in 1808 by Sir Humphrey Davy [23]. Mg is a unique metal, which makes it a desirable biomaterial. It is a very light metal with a density of 1.74 g/cm³. As a comparison, Mg is 1.6 and 4.5 times lighter than aluminum and steel [9]. The mechanical properties of magnesium are comparable to ceramics and other polymeric biomaterials and even better [17]. Mechanical properties of Mg compared to other biomaterials and natural bone are listed in Table 2.1.2.1.2.1.

The first use of magnesium as a biomaterial was as Mg wire ligatures for bleeding vessels in 1878 [24]. It wasn't until 20th century magnesium based materials were first

introduced in biomedical applications. All through the 20th century, it was used in different studies in the forms of wires, tubes, rods, vessels, plates, etc. [24].

In 1950s, with the introduction of more inert and stronger metals such as stainless steel and titanium alloys, the popularity of Mg faded. However, combined with its compatibility with the body, since Mg is a key element in many cellular functions (e.g. ion transportation, energy metabolism, cell signaling, cell proliferation, protein synthesis, etc) [26, 27], its non-toxic nature and positive effect on new bone formation [28], magnesium materials are attractive candidates for bio-implant applications. In addition, Mg has low thrombogenicity and it is entirely biocompatible which makes it also desirable in stent applications [28].

The corrosion rate was always a drawback for magnesium in implant applications due to the high hydrogen gas evolution [17, 25]. Magnesium corrodes faster under physiological conditions (pH= 7.4-7.6) and in the presence of chlorides. Fast corrosion rate leads to increased release of hydrogen gas that may damage the surrounding tissue or the loss of the mechanical properties of the alloy before the healing process is completed [17, 25]. Optimizing the corrosion rate is one of the big challenges in creating a non-toxic, biocompatible Mg alloy and this challenge is addressed by using different techniques as using different alloying elements, surface modification and mechanical preprocessing [14].

However, the major drawback of magnesium, which is its corrosion rate, has become an advantage with its high specific strength in recent years. For biodegradable implant applications, a biocompatible metal with the desirable corrosion rate is considered as a desirable candidate [5]. Permanent implants are associated with several side effects as physical irritation and chronic inflammation, and in some cases, calls for a secondary intervention to remove them. These problems would not occur if biodegradable biomaterials are used Mg and its alloys are being considered for applications in which the material does not need to stay inside the body after completing their purpose of providing mechanical integrity until the healing process is completed [14].

Table 2.1.2.1.1.1: Distribution and concentrations of Mg in the body of a healthy adult [29].

Percent distribution	Concentration
Bone (60–65%)	0.5% of bone ash
Muscle (27%)	6-10 mmol/kg wet weight
Other cells (6–7%)	6-10 mmol/kg wet weight
Erythrocytes	2.5 mmol/l
Serum	0.7–1.1 mol/l
Mononuclear blood cells	2.3–3.5 fmol/cell
Cerebrospinal fluid	1.25 mmol/l
Sweat	0.3 mmol/l (in hot environment)
Secretions	0.3–0.7 mmol/l
Total body May 20, 29 a	

Total body Mg: 20–28 g.

Table 2.1.2.1.2.1: Physical and mechanical properties of some biomaterials and natural bone [14].

			Compressive	Fracture
	Density	Elastic	yield strength	toughness
	(g/cm ³)	modulus (GPa)	(MPa)	(MPam1/2)
Natural bone	1.8-2.1	3.0-20	130-180	3.0-6.0
Magnesium	1.74-2.0	41-45	65-100	15-40
Ti alloy	4.4-4.5	110-117	758-1117	55-115
Co-Cr alloy	8.3-9.2	230	450-1000	N/A
Stainless steel	7.9-8.1	189-205	170-310	50-200
Synthetic hydroxyapatite	3.1	73-117	600	0.7

As in many implant applications, the main purpose of using a stent is to provide mechanical support for arteries [10] but in biodegradable stents, the mechanical support is needed until arterial healing is completed. For applications involving drug-delivery bio-degradability in a shorter time is more important.

Magnesium as a proven biocompatible, biodegradable and bio-resorbable metal is a perfect candidate for implant material [24]. In in vivo applications, Mg corrosion product is a soluble and non-toxic oxide that could be removed from the human body through urine without causing any harm [31]. There are many current or possible use of Mg implants in the research phase [32]. (Fig. 2.1.2.1.2.1.)

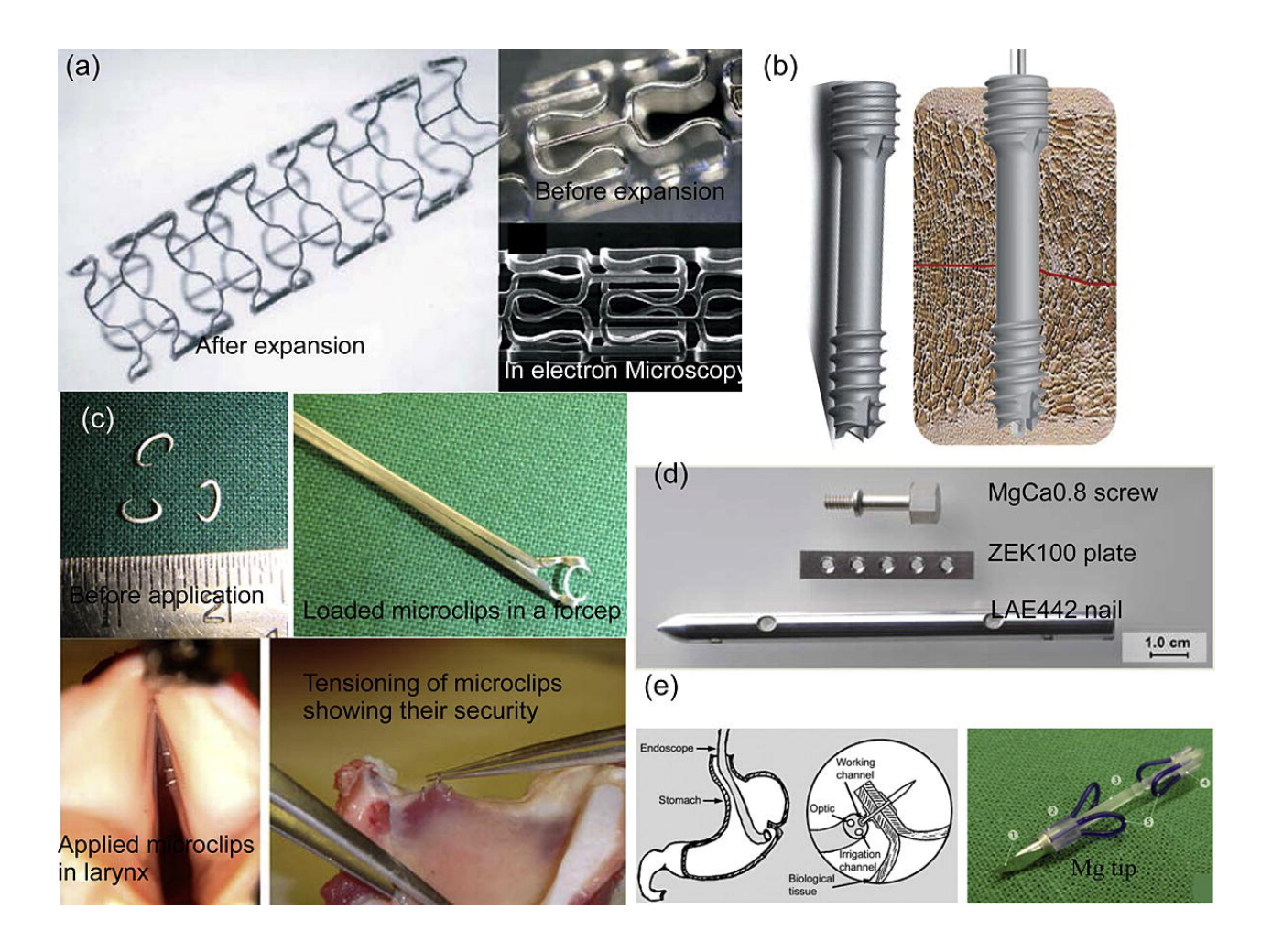


Fig. 2.1.2.1: Real/possible applications of biodegradable magnesium implants (a) cardiovascular stents (BIOTRONIK, Berlin, Germany, under clinical trial), (b) MAGNEZIX screw (received CE mark in Europe), (c) microclip for laryngeal microsurgery (pure magnesium), (d) biodegradable orthopedic implants, (e) wound-closing devices (WZ21). [32]

Table 2.1.2.1.2.2: Reports on magnesium and its biomedical applications in historiological order [24].

Author	Year	Magnesium (alley)	Cumplion	Application	Human/animal model
		Magnesium (alloy)	Supplier	Application	
Huse	1878	Pure magnesium	Not reported	Wires as ligature	Humans
	4000			Tubes (intestine,vessel,	
	1892		I. and C.W. Rohrbeck, Vienna,	nerve collector,	Humans, guinea
-	-		Austria, Al und Mg Fabrik	plates,arrows,wire,sheets,	pigs,rabbits, pigs,
Payr	1905	High-purity Mg	Hemelingen, Germany	rods	dogs
	4000		N	Magnesium cylinders as	
Höpfner	1903	Pure magnesium	Not reported	vessel connectors	Dogs
	1900		F: 1:1 W 1 0	Tubes, sheets and cylinder	
Obl	4005	Link water Man	Friedrich Wosch Company,	intestine connector,	Humans,
Chlumský	1905	High-purity Mg	Germany	arthoplastik	rabbits,dogs
	1906				Llumana rabbita
Lambotte	1022	Duro Ma (00.7%)	Not reported	Rada platas, aerowa	Humans,rabbits,
	1932	Pure Mg (99.7%)	Not reported	Rods,plates, screws	dogs
Lespinasse	1910	Metallic magnesium	Not reported	Ring-plates for anastomsis	Dogs
Groves	1913		Not reported	Intramedullar pegs in bone	Rabbits
		Pure Mg, mix. of eq. part:		Wires, clips as ligature,	
Andrews	1917	Mg/Al,Mg/Cd, Mg/Zn	Not reported	anastomosis	Dogs
		Pure Mg (99.99%), distilled in	American Mg Cooperation,		
Seelig	1924	vacuum	Niagra Falls, New York	Wires,strips, bands	Rabbits
			Al und Mg Fabrik,,		
Glass	1925	Pure Mg (99.8–99.9%)	Hemelingen,Germany	Magnesium arrows	Humans, rats, cats
Heinzhoff	1928	Pure magnesium	Not reported	Magnesium arrows	Rabbits
	1933	Dow Metal: Mg-Al6-Zn3-			
	-	Mn0.2%-wt. Elektron Mg–Al8%-	Dow Chemical Corp., USA		Humans,
Verbrugge	1937	wt.	Griesheim-Elektron, Germany	Plate,band, screws, pegs	dogs,rats, rabbits
		Mg-Mn3%-wt.,Mg-Al4-Mn0.3%-		Sheet, plate, band,	
McBride	1938	wt.	Not reported	screw,peg, wire	Humans,dogs
Nogara	1939	Elektron (alloy not specified)	Griesheim-Elektron, Germany	Rods	Rabbits
Troickin	1948	Mg-Cd	Not reported	Plate,screws, rod-plate	Humans
			I.G. Farben Industry AG,	Band, suture from woven	
Maier	1940	Magnesium	Bitterfeld, Germany	Mg wires, fusiform pins	Humans,rabbits
			Aluminium Company of		
Stone	1951	Mg–Al2%-wt. pure magnesium	America, OH, USA	Wires for clotting aneurysms	Dogs
		Indgrade purity: Domal Mg	, ,	0 ,	· ·
		(99.9%), T.L.H. Mg not reported			
		Lab-grade purity: "zone fondue"			
		Mg, R69 Mg MgMn1.5%-wt.,		Anodes for implantable	
Fontenier	1975	MgAI:GAZ8%,GAZ6%, GAZ3%	Not reported	batteries to feed pacemaker	Dogs
Wexler	1980	Mg-Al2%-wt.	McMaster Univ. Med., Canada	Wires intravascular	Rats
				Wires for hemangioma	
Hussl	1981	Pure Mg (99.8%)	Goodfellow Metals Ltd., GB	treatment	Rats, rabbits
	<u> </u>			Wires for hemangioma	
Wilflingseder	1981	Pure Mg (99.8%)	Goodfellow Metals Ltd, GB	treatment	Humans

However, using current Mg materials for bio-applications has not lead to immediate success. A German biomedical technology company Biotronik undertook a clinical study for potential biodegradable stent applications using Mg- 7RE alloy [33]. After the 4 months of the implantation on a baby's aortapulmonary collateral, they observed a serious restenosis [34, 35]. Following this first try with Mg- 7RE alloy, Biotronik continued their research using WE43 (Mg-4Y-3Nd) alloy as a potential biodegradable stent material. The animal study results for this alloy present better mechanical integrity yet the clinical study results were not as satisfactory where there was a thick neo-intima formation and thrombosis [36]. Nevertheless, the interest in using Mg is still very much alive and research in optimizing magnesium implant materials is still continuing to realize their application.

2.2 METALLURGICAL FACTORS

2.2.1 Alloying elements for bio-degradable Mg alloys

Many elements have been investigated as alloying elements for biodegradable Mg research. Main concern while choosing the elements was their biocompatibility and the contribution to improvement of the alloy's physical characteristics, such as improving the corrosion resistance. Most common elements tested were Al, Mn, Zn, Ca, Li, Zr, Y and rare earths [14-16, 37-39, 40-44]. These alloying elements contribute the mechanical, physical and corrosion properties of Mg alloys [42]. The effect of each alloying elements has been reviewed by Song and Witte and briefly been described below [42, 46].

- Al; the presence of Al increases the corrosion resistance by activating the precipitation of a corrosion resistant phase on the surface.
- Ca; Ca has an improving affect on solid solution strengthening.
- Mn; Mn lessen the harmful effect of the impurities in the alloy and by doing so contributed the corrosion resistance.

- RE; The RE metals strengthen the material by solid solution strengthening and precipitation strengthening [42]. Moreover, RE containing alloys has higher alloy surface stability as a result of RE derived formation of protective corrosion films, [71].
- Zn; Zn also reduces the effect of impurities. The tolerance limits are higher in the presence of Zn in the alloy.
- Zr; For Al- free Mg alloys, the addition of Zr results in grain refinement. Also, the corrosion resistance is increased by the precipitation of metallic impurities in Zr containing alloys.

However, not only the improvement in physical characteristics or corrosion resistance is sufficient in choosing the alloying elements for biodegradable applications. For example, (AI) and rare-earth elements (REEs) has shown to improve the alloys corrosion resistance and strength, yet AI has shown to be neurotoxic and the accumulation of some REEs causes toxicity in bone and liver [20, 47]. The elements with toxic nature should be avoided in designing new alloys. There is a limited number of elements that are fully tolerated in the human body as they are already present in the body, namely; Sr, Ca, Zn, Mn [48, 49].

Many elements were studied for the development of a new biocompatible and biodegradable Mg alloy such as Ca, Zn, Mn, Li, Sr etc. These elements were chosen because they were biocompatible and in case of corrosion, they would not cause any harm in the human body.

Calcium (Ca) (density of 1.55 g/cm³) belongs to the alkaline metal group as magnesium and is one of the widely used alloying elements in developing a biocompatible Mg alloy. It is a fundamental element of cell signaling processes and bones [50]. The presence of calcium improves the strength and creep resistance of magnesium while reducing the grain size. Calcium can only be added up to 0.3 wt% to magnesium and it has been shown to reduce melt oxidation and oxidation during heat treatment process for casting alloys [51]. One of the studies investigated the effect of Mg-xCa (x =1-3 wt.%) binary alloys that has a similar density to bone for biodegradable bone implants [52]. Results of the study reveal that Mg-1Ca system has the best mechanical properties, lower corrosion rate and good biocompatibility.

Studies on Mg - Ca alloys with different calcium content showed that alloys containing 0.6 wt.% calcium have the slowest corrosion rate, best mechanical properties, and low toxicity [53, 54]. Also, other researchers working on Mg alloys for bone related biomedical applications reported the optimum content of Mg-Ca binary alloys to be in the (0.6<Ca<1 wt.%) range [52, 55, 56]. The Ca content of the alloys for different applications might differ due to the required mechanical strength or biocompatibility.

Zinc (Zn) is an essential element in the body that has function in nucleic acid metabolism, gene expression and signal transduction. Many metallo enzymes and proteins contain zinc for structural reasons. Zinc also interacts with various organic ligands in the body [57]. Zinc increases the tensile strength of the magnesium without reducing its ductility and improves the alloy's corrosion resistance [51, 58, 59, 60].

In a biocompatibility study for coronary stent applications, four zinc wires were implanted in the abdominal aorta of rats for 1,5 to 6 months [61]. Result showed zinc to be biocompatible and is a good candidate for cardiovascular applications. In another study 0.6 wt.% Zn containing Mg alloys showed lower corrosion rate in SBF [60]. For the same alloy, biocompatibility study on rabbits resulted in 2.32 mm/yr degradation rate which doesn't cause any harm to the tissue around. 0.6 wt.% Zn containing Mg alloy was also tested on L-929 cells for their cytotoxicity and the rate was very low.

The benefits of strontium (Sr) on stimulation of osteoblasts and the reduction on bone resorption made it a valuable candidate for biomedical applications [62, 63]. Research showed that the presence of Sr with the hydroxyapatite (HA) advances bone formation [64,65]. The presence of Sr in the Mg alloys results in grain refinement and reduces the corrosion rate because of its surface-active character [66, 67].

For biodegradable implant applications, Mg-Sr alloys have been evaluated in several studies. In an in vivo and in vitro degradation study for 1-4 wt.% Sr containing alloy, the results showed that Mg-2Sr has the lowest corrosion rate and highest mechanical strength [68]. Its biocompatibility results for both in vitro and in vivo were also satisfactory. According to another study with heat-treated Mg-Sr and Mg-Sr-Zn alloys, the Mg-2Zn-0.5Sr alloy had the highest corrosion resistance [69].

Bornapour et al. investigated the corrosion rate of a series of Mg–Sr alloys, with Sr in the range of 0.3–2.5% [86]. The in vitro immersion tests in simulated body fluid (SBF)

results showed that the Mg–0.5 Sr alloy has the slowest corrosion rate compared to the other alloys. (Fig.2.2.1.1). They have also determined the formation of a Sr-modified hydroxi-apatite to from on the stent surface which improved its bio-corrosion and bio-compatibility in stent applications.

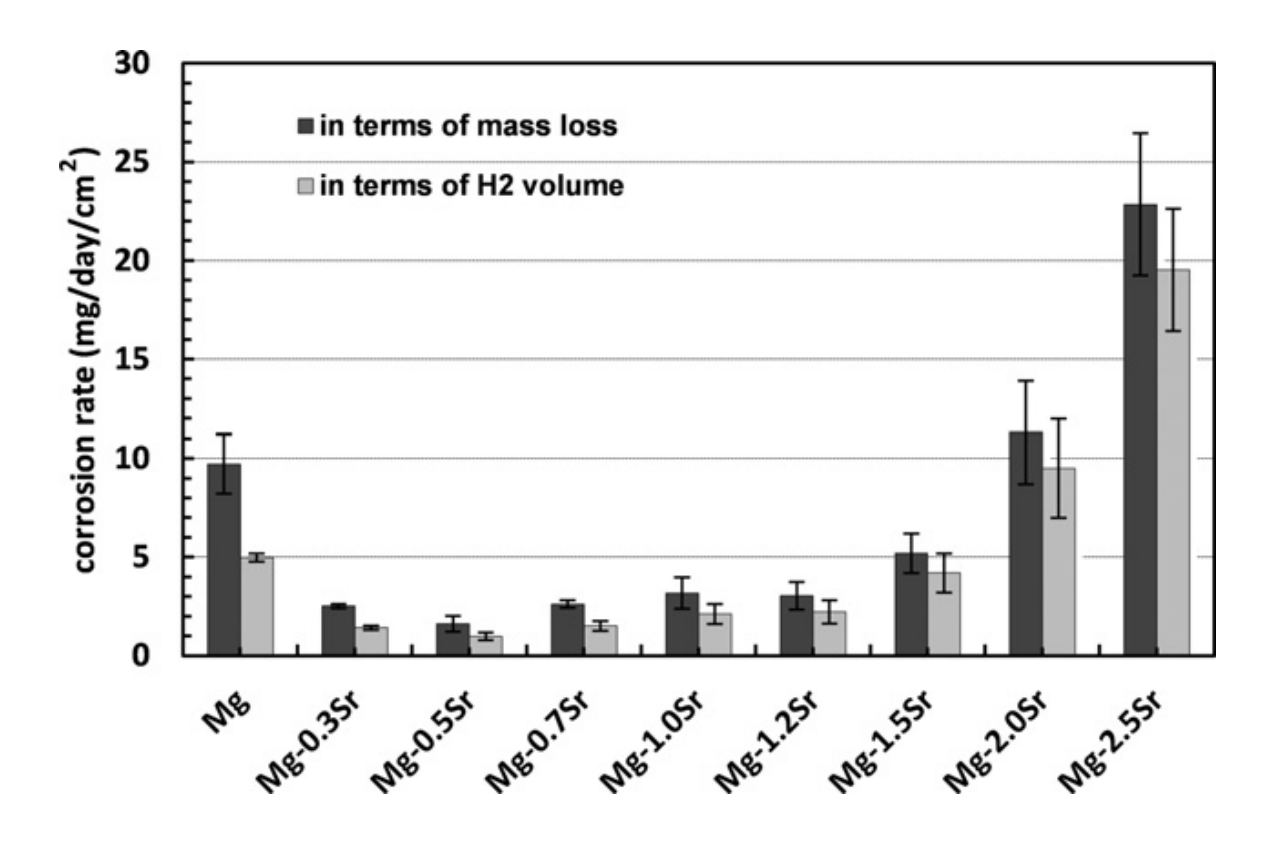


Fig. 2.2.1.1: The immersion test results in SBF at 37 °C, for Mg–Sr samples with different Sr content. The average corrosion rate (mg day⁻¹ cm⁻²) was calculated in terms of mass loss and hydrogen evolution [86].

2.2.2 Phases and microstructure of the alloys

The microstructure of an alloy plays an important role in their corrosion behaviour and it defines the phases present, their distribution throughout the alloy and the grain size [46, 70, 71].

Grain size and the phase distribution are two of the main reasons behind the corrosion rate differences in magnesium alloys [46, 71]. Different intermetallic phases in the alloys

or the presence of any of the alloying elements acts as a cathode since they are less active than magnesium [42]. Alloying elements tend to accumulate around grain boundaries which increase the cathodic behaviour around this area and in the presence of an efficient cathode, corrosion by a galvanic effect increases. Galvanic corrosion describes the process in which one metal corrodes preferentially to another when both metals are in electrical contact and immersed in an electrolyte. Yet, even though the grain boundaries are feeble areas, small grain size for magnesium alloys still favor the corrosion resistance since it results in a more homogeneous corrosion [42].

In the presence of the secondary phases, the corrosion rate can be faster. It is a result of less protective surface caused by the reduction of alloying elements in the matrix, or as they behave as cathodes causing an increase in corrosion in the α -matrix [72]. Different manufacturing processes such as heat treatment are used to improve the corrosion resistance for magnesium alloys [25, 42, 73, 74].

2.3 BIO-CORROSION of Mg and Mg ALLOYS

2.3.1 In vitro methodology for the investigation of the corrosion behaviour of Mg alloys for biodegradable applications

Mg has a low corrosion resistance because of its high electrochemical activity and micro galvanic corrosion. The standard reduction potential of pure magnesium is -2.37V vs standard hydrogen electrode [75].

A mixture of MgO and Mg(OH)₂ corrosion layer forms on the surface of the metal and this layer provides some corrosion protection but under the aqueous environment or in high humidity it becomes unstable [76]. In aqueous environments, corrosion of Mg produces magnesium hydroxide and hydrogen gas as shown in the equations below [46]. The presence of anions such as, chloride, nitrate or sulphate in the aqueous solution, accelerates the corrosion rate by either inhibiting the formation of the surface film or damaging the existing film [46, 77].

$$2H_2O + 2e^- \rightarrow H_2 + 2OH^-$$
 (cathodic reaction) (Reaction 2.1)

$$2Mg \rightarrow 2Mg^+ + 2e^-$$
 (anodic reaction) (Reaction 2.2)
 $2Mg^+ + 2H_2O \rightarrow 2Mg^{2+} + 2OH^- + H_2$ (chemical reaction) (Reaction 2.3)
 $2Mg + 4H_2O \rightarrow 2Mg^{2+} + 4OH^- + 2H_2$ (overall reaction) (Reaction 2.4)
 $Mg^{2+} + 2OH^- \rightarrow Mg(OH)_2$ (product formation) (Reaction 2.5)

The second phases and the impurities in the alloys acts as cathodes resulting dissolution of alloy matrix. The corrosion behaviour and corrosion rate calculations for metallic alloys for biomedical applications are commonly investigated by using electrochemical analysis and immersion tests. In these test systems, a simulated body fluid is used to mimic the physiological conditions. For the in vitro immersion test of Mg samples in SBF, the use of m-SBF that has the same ion concentrations with human blood was established by Oyane et al. [78].

2.3.3.1 Weight loss

Weight loss analysis is a long-established and widely used method of estimating corrosion rate. This method has many advantages: (i) The analysis does not require any sophisticated instruments; (ii) it allows the researchers to have direct measurement without any approximation; (iii) it could be applied in different corrosion set-ups; and (iv) it provides information for all forms of corrosion. A small sample from a material of interest is evaluated by exposing it to a process for a reasonable time and after the sample is cleaned of all the corrosion products and it is weighted again. The weight loss is converted to a corrosion rate by using the following formula;

$$R = \left(\frac{m}{t * A}\right) * 24$$

where: R: corrosion rate, m: mass loss, t: immersion time, A: surface area, 24h.

To obtain a healthy result from the experiments, attention in certain areas during the experiments is essential.

- a. The weight measurements needed to be performed accurately. Failure in the complete removal of the corrosion products would alter the results.
- b. Another factor, which may arise during the experiments, is the separation of big pieces from the samples. These big pieces might not be detached due to the corrosion but the physical structure of the samples. The cracks inside the casted alloys are a common occurrence, which can lead to this problem. This false weight loss results would affect the corrosion results.
- c. When it comes to the corrosion rate calculations, taking a precise surface area measurement is also crucial. To avoid the possible errors, samples need to be completely uniform with flat and parallel sides after the grinding process. One more point is also to ensure having an average of at least 5 points for each dimension to reduce the error in calculating the surface area.

2.3.3.2 Hydrogen evolution

There is a direct relationship between the corrosion of Mg and production of hydrogen by the dissolution of the metal according to the corrosion reaction of Mg. (Reaction 2.4). Based on this formula the production of 1 mole of hydrogen is a result of the oxidation of one mole of Mg. By using the formula, it is possible to calculate the corrosion rate values and the amount of the corroded Mg by using the amount of the hydrogen evolved during the immersion experiments.

Hydrogen gas evolution is an easy and low-cost way to determine the corrosion rate. The presence of the corrosion layer on the surface also has no effect on the hydrogen evolution during the corrosion experiments [19, 75]. In a standard immersion set up, the corrosion cell is structured to capture the evolving hydrogen using an inverted funnel attached to a burette or cylinder. (Figure 2.3.3.2.1) [75]. This closed system is susceptible to the local pH increase, which would affect the corrosion rate of the material. Also, the burettes might cause leaks that result in lower hydrogen evolution and inaccurate corrosion data [19]. Some publications reported a good correlation between weight loss and hydrogen evolution tests in determination of corrosion rate [75,

81] with a deviation in the stoichiometry ratio of 1:1 but also some reported a high variation between 0.22 and 1.31 [19, 74, 79, 80]. This difference can be attributed to the possible error in the collection of hydrogen gas effectively during the immersion experiments [19]. In our study, we used cylinders instead of burettes to avoid the leaking problem.

The observation of the hydrogen evolution data is especially important for Mg biodegradable alloy research since the fast production of hydrogen gas can result in excess gas accumulation *in vivo* and has been used vastly in the biodegradable Mg research [20, 74, 82, 83].

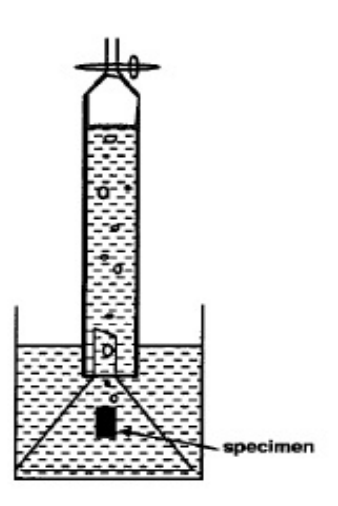


Fig. 2.3.3.2.1: Schematic illustration of the immersion cell set-up to measure the volume of hydrogen evolution [75].

2.3.3.3 ICP-OES

During the immersion tests, due to the corrosion, the ions in the metal sample are released into the electrolyte solution. By measuring the content of the electrolyte using inductively coupled plasma optical emission spectroscopy (ICP-OES), it is possible to determine the concentration of dissolved Mg and alloying elements in the electrolyte as a result of the corrosion process [20, 84, 85]. Corrosion rate values can be calculated from the concentration of dissolved magnesium. Yet, the corrosion rate results might not correlate directly with the actual corrosion, since the Mg in the Mg(OH)₂ corrosion layer

and insoluble magnesium phosphates and carbonates forming part of the corrosion layer or precipitated in the bulk electrolyte would not contribute to the detected Mg levels.

Recent Studies on Bio-corrosion of Mg alloys: In a recent study, the mechanism of WE43 bio-corrosion was investigated via electrochemical tests [105]. The corrosion mechanisms and kinetics of WE43 Mg alloy in m-SBF was investigated over a period of 5 days and our corrosion stages were identified. This study also presented an indirect evidence on the presence of a protective dehydrated inner MgO film and the formation of adsorbed Mg intermediates at the film-free regions. Ascencio et al. further investigated the effects of the electrolyte removal on the corrosion rate of WE43 alloy [106]. This study showed that the electrolyte renewal affects the corrosion mechanism by promoting partial dissolution of the corrosion layer and increasing mass transport. Due to these effects, the corrosion layer was not as protective against corrosion, resulting localized corrosion on the surface of the alloys.

The biocorrosion study done by Zhou et al. [07] on Mg-Li-Al-RE alloys for cardiovascular stent applications reported whether the addition of Al and RE elements increases the tensile strength of Mg-Li alloys, the corrosion resistance decreased due to the presence of intermetallic compounds distributed in the alloy matrix.

Another study on a new alloy developed by Mao et al. [108, 109] with the nominal composition Mg-2.5Nd-0.2Zn-0.4Zr showed a highly uniform degradation and reduced corrosion rate compared to commercial alloys WE43 and AZ31.

2.4 BIOCOMPATIBILITY

2.4.1 Tests used to evaluate biocompatibility

Biocompatibility refers to the compatibility of biomaterials with living tissue or a living system by not being toxic, injurious, or physiologically reactive and not causing immunological rejection. To determine the biocompatibility of a new material, in vitro and in vivo tests are essential. Researchers generally prefer the in vitro studies as the

first step of biocompatibility evaluation. These studies are much faster, economic, and easier to determine the biocompatibility of the material.

2.4.1.1 In vitro studies

2.4.1.1.1 Indirect cytotoxicity tests

The cytotoxicity of the materials is evaluated using different in vitro tests on cells, proteins, or tissues. For the cell viability testing, there are two methods; in direct or direct cell viability tests.

For direct cell viability tests, the cells are grown on the materials and the effect of the material is evaluated. For indirect cell viability tests, however, an extract, which is prepared by exposing the material to the cell medium, is used [86, 87]. Different cell types can be used depending on the application area of the potential implant material. For example, for bone applications, osteoblast-like cells such as MC3T3-E1, and for cardiovascular implants; vascular cells such as HUVEC are usually used [88, 89, 90]. In one of these studies, four different Mg-Zn-Y based alloys (ZW21, WZ21, ZQ30, and WE43) were evaluated using in vitro cell tests using human umbilical vein endothelial cells for the assessment of viability and growth of cells [88]. The findings showed that the viability and metabolic activity of the HUVECs in response to the SBF (T)-based eluates of ZW21, WZ21 and WE43 decreases with increasing eluate concentration. cytocompatibility the alloys' was follows: Thus. to eluates ranked as WE43 > WZ21 > ZW21.

Bornapour et al. reported that the %10 extract, which was used in indirect cytotoxicity assays on HUVECs, showed no toxicity effect. In fact, the presence of ions in the Mg-0.3Sr-0.3Ca extract proves to cause an increase in the viability of HUVECs after one week [90].

2.4.1.1.2 In vitro hemacompatibility tests

To evaluate the hemacompatibility of a potential implant, blood compatibility, thrombogenicity and platelet adhesion tests are used to determine the interaction between the material and the blood [12]. Certain implants, such as stents, are directly in

contact with the blood when they are placed inside the body. Evaluation of the effects of the implant materials on blood can provide us direct information to assess the compatibility with the physiological environment.

Hemolysis experiments are commonly used to evaluate the blood compatibility of a material. It is the lysis or the breaking of the erythrocytes (red blood cells which results in releasing of hemoglobin into the blood. Many factors cause hemolysis such as exposure to toxins or poison, certain immune reactions, change in temperature or bacterial hemolysins. The research on Mg and its alloys showed that the degradation of some magnesium alloys results in serious hemolysis. According to the ISO standard 10993-4, the recommended rate of the hemolysis is %5 [92]. The study by Gao et al, showed that the hemolysis rate for pure magnesium is varies between 30-65% [93]. In a recent study on the hemocompatibility of magnesium alloys, the hemolysis percentages were measured as 41.1 % for AZ31, 9.27 % for WE43 and 69% for Mg-Mn-Zn alloy [94]. These very high hemolysis rates can be attributed to either high metal ion concentration or the high pH since it is known that the fast degradation rate of Mg alloys causes an increase in pH value as high as 11.

In order to better understand the correlation between the ion concentration, pH value and the hemolysis rate, different ion concentration effects and pH on hemolysis are investigated [95]. Results showed that high metal ion release due to the degradation of magnesium alloys does not cause hemolysis (Table 2.4.1.1.2.1) but the hemolysis rate increases with the increase of pH value (Fig. 2.4.1.1.2.1).

Platelet activation is considered as one of the major factors in acute vascular thrombosis, and in the pathogenesis of acute myocardial infarction (AMI). It is also considered one of the responsible elements of the complications of coronary balloon angioplasty and stenting.

Table 2.4.1.1.2.1: Effects of the metal ion concentration on the hemolysis rate [95].

	Concentration	Hemolysis		Concentration	Hemolysis
lons	(mg/L)	(%)	lons	(mg/L)	(%)
Mg ²⁺	46.4	0	Zn ²⁺	2.7	0
	66.4	0		3.9	0
	86.4	0		5.1	0
	106.4	0.81		6.3	0
	186.4	0		11.1	0.91
	2000	0.25		121.5	0
Ca ²⁺	54.6	0	Mn ²⁺	0.4	0.37
	55.6	0		0.8	0.61
	56.6	0		1.2	1.5
	57.6	0		1.6	0.24
	61.6	0		3.2	0
	153.6	0.62		40	0.86
Y ³ -	0.8	0	Al ³⁻	1.8	0
	1.6	0		3.6	0.12
	2.4	0		5.4	0.12
	3.2	0		7.2	0
	6.4	0		14.4	0
	80	1.1		180	0

Research on magnesium showed that Mg suppresses platelet activation by inhibiting platelet-stimulating factors (eg. thromboxane A2), or by stimulating synthesis of platelet inhibitory factors (eg. prostacyclin PGI 2 [96-102]. Recent studies also showed that magnesium reduces platelet aggregation in healthy volunteers [96]. Also, the research proved that high magnesium levels inhibit blood coagulation [103] and thrombus formation in vivo [104] and results in reduce of platelet aggregation [97-99].

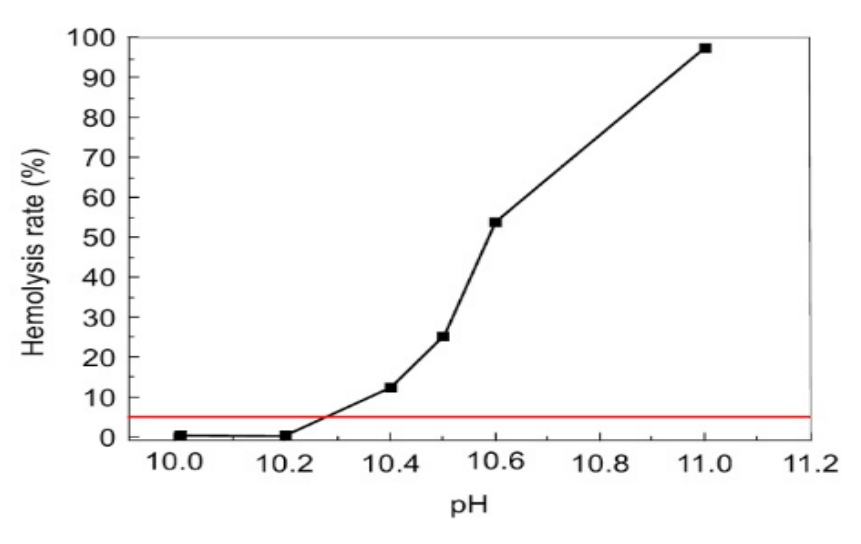


Fig. 2.4.1.1.2.1: Effect of pH value on the hemolysis rate [95].

2.4.1.2 In vivo studies

In vivo animal testing is the next level for evaluating the behaviour and the effects of the material inside the body. The type and the size of the material determine what type of animal studies will be needed. Animal testing, requires different steps to observe the behaviour and the effects of the material during its time inside the body; radiographic imaging, histological evaluation and microscopy are the most common methods to determine the behaviour of the material inside the body and its effects on the surrounding tissue and the cells.

Most commonly, the animal studies are conducted on mice, rats, rabbits, dogs, and pigs [87, 88, 89]. Mg implant research includes several in vivo studies on different animal models such as rabbits [44, 87] and dogs [24, 90] and guinea pigs [91].

Witte et al. implanted rods from four different magnesium alloys (two aluminium (A) and zinc (Z) containing magnesium alloys (AZ31, AZ91) and two rare earth (E) containing magnesium alloys (WE43, LAE442) and a degradable polymer as a control into the femora of guinea pigs [91]. After 6 and 18 weeks histomorphologic analysis showed that metallic implants made of magnesium alloys degraded in different amounts in vivo depending on the composition of the alloying elements. High mineral apposition rates and an increased bone mass around the magnesium rods supported that the high magnesium ion concentration could lead to bone cell activation.

In a following study LAE442 alloy was evaluated as a bone implant using a rabbit model [44]. Extruded cylinders from LAE442 were prepared. Half of them were coated additionally with MgF₂ and implanted into the medial femur condyle of adult rabbits. Results shows that the corrosion rates for magnesium alloy LAE442 were low and host response was satisfactory. The results also showed that the MgF₂ coating reduced in vivo corrosion rate.

In a recent in vivo study conducted by Bornapour et al. one of the compositions which we have also used in our study (Mg-0.3 Sr-0.3 Ca alloy) was used. A perforated stent with 2.4 mm diameter, 10 mm length and 0.25 mm wall thickness implanted into both right and left femoral arteries of a dog. A WE43 alloy was used as a control. After five weeks of implantation the histological analyses were conducted on the removed arteries. There was no thrombosis observed in the artery with Mg-0.3Sr-0.3Ca stent whereas the artery implanted with WE43 stent was extensively clogged and thrombosed [90]. (Figure 2.4.1.2.1).

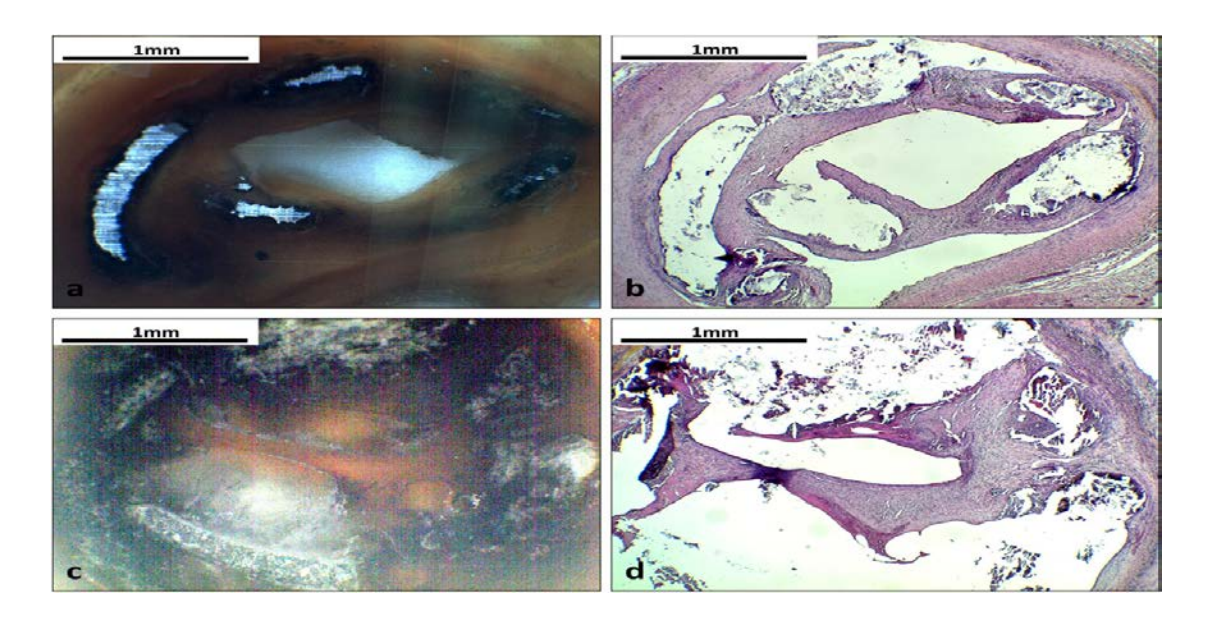


Fig. 2.4.1.2.1: (a, b) Optical and histology images after H & E staining of vascular tissue surrounding of Mg-0.3Sr-0.3Ca alloy stent, **(c, d)** WE43 tubular stent samples implanted in right and left femoral artery for 5 weeks. The stented artery was distorted and compressed in pictures a and b during histological processing.

2.5 REFERENCES

- 1. http://www.who.int/mediacentre/factsheets/fs317/en/
- 2. https://www.heart.org/idc/groups/ahamahpublic/@wcm/@sop/@smd/documents/downloadable/ucm 480086.pdf
- 3. http://healthycanadians.gc.ca/diseases-conditions-maladies-affections/disease-maladie/heart-disease-eng.php
- Fang G, Ai W-J, Leeflang S, Duszczyk J, Zhou J. Multipass cold drawing of magnesium alloy minitubes for biodegradable vascular stents. Materials science & engineering C, Materialsfor biological applications. 2013;33:3481-8.
- 5. Moravej M, Mantovani D. Biodegradable Metals for Cardiovascular Stent Application:Interests and New Opportunities. International Journal of Molecular Sciences. 2011;12:4250-70.
- 6. https://heart.uvahealth.com/services/ebsco_images/5013.jpg
- 7. Hermawan H, Dube D, Mantovani, D. Developments in metallic biodegradable stents. Acta Biomaterialia 2010;6:1693-7.
- 8. Boffetta P. Carcinogenicity of trace-elements with reference to evaluations made by the international-agency-for-research-on-cancer. Scandinavian Journal of Work Environment & Health. 1993;19:67-70.
- 9. Chan AW, Moliterno DJ. In-stent restenosis: Update on intracoronary radiotherapy. Cleveland Clinic Journal of Medicine. 2001;68:796-803.
- 10. Erne P, Schier M, Resink TJ. The road to bioabsorbable stents: Reaching clinical reality? Cardiovascular and Interventional Radiology. 2006;29:11-6.
- 11. Mirensky TL, Nelson GN, Brennan MP, Roh JD, Hibino N, Yi T, et al. Tissue-engineered arterial grafts: long-term results after implantation in a small animal model. Journal of Pediatric Surgery. 2009; 44:1127-33.
- 12. Ratner BD, Hoffman AS, Schoen FJ, Lemons JE. Biomaterials Science: An Introduction to Materials in Medicine: Elsevier Academic Press 2004.
- 13. Niinomi M. Recent metallic materials for biomedical applications. Metallurgical and Materials Transactions a-Physical Metallurgy and Materials Science. 2002;33:477-86.

- 14. Staiger MP, Pietak AM, Huadmai J, Dias G. Magnesium and its alloys as orthopedic biomaterials: A review. Biomaterials. 2006;27:1728-34.
- 15. Heublein B, Rohde R, Kaese V, Niemeyer M, Hartung W, Haverich A. Biocorrosion of magnesium alloys: a new principle in cardiovascular implant technology? Heart. 2003;89:651-6.
- 16. Waksman R, Pakala R, Kuchulakanti PK, Baffour R, Hellinga D, Seabron R, et al. Safety and efficacy of bioabsorbable magnesium alloy stents in porcine coronary arteries. Catheterization and Cardiovascular Interventions. 2006;68:607-17.
- 17. Tan LL, Yu XM, Wan P, Yang K. Biodegradable Materials for Bone Repairs: A Review. Journal of Materials Science & Technology. 2013;29:503-13.
- 18. Serruys PW, Ong ATL. Coronary-artery stents Reply. New England Journal of Medicine. 2006;354:2078.
- 19. Kirkland NT, Birbilis N, Staiger MP. Assessing the corrosion of biodegradable magnesium implants: A critical review of current methodologies and their limitations. Acta Biomaterialia. 2012;8:925-36.
- 20. Gu X, Zheng Y, Cheng Y, Zhong S, Xi T. In vitro corrosion and biocompatibility of binary magnesium alloys. Biomaterials. 2009;30:484-98.
- 21. Peuster M, Wohlsein P, Brugmann M, Ehlerding M, Seidler K, Fink C, et al. A novel approach to temporary stenting: degradable cardiovascular stents produced from corrodible metal results 6-18 months after implantation into New Zealand white rabbits. Heart. 2001;86:563-9.
- 22. Pierson D, Edick J, Tauscher A, Pokorney E, Bowen P, Gelbaugh J, et al. A simplified in vivo approach for evaluating the bioabsorbable behavior of candidate stent aterials. Journal of Biomedical Materials Research Part B-Applied Biomaterials. 2012;100B:58-67.
- 23. Durlach J. Overview of magnesium research: History and current trends. New Perspectives in Magnesium Research: Nutrition and Health. 2007:3-10.
- 24. Witte F. The history of biodegradable magnesium implants: A review. Acta Biomaterialia. 2010;6:1680-92.

- 25. Zeng R, Dietzel W, Witte F, Hort N, Blawert C. Progress and challenge for magnesium alloys as biomaterials. Advanced Engineering Materials. 2008;10:B3-B14.
- 26. Romani A, Scarpa A. Regulation of cell magnesium. Archives of Biochemistry and Biophysics. 1992;298:1-12.
- 27. Hartwig A. Role of magnesium in genomic stability. Mutation Research-Fundamental and Molecular Mechanisms of Mutagenesis. 2001;475:113-21.
- 28. Peuster M, Beerbaum P, Bach FW, Hauser H. Are resorbable implants about to become a reality? Cardiology in the Young. 2006;16:107-16.
- 29. Vormann J. Magnesium: nutrition and metabolism. Molecular aspects of medicine. 2003;24:27-37.
- 30. Brink EJ, Beynen AC. Nutrition and magnesium absorption a review. Progress in Food and Nutrition Science. 1992;16:125-62.
- 31. Saris NEL, Mervaala E, Karppanen H, Khawaja JA, Lewenstam A. Magnesium An update on physiological, clinical and analytical aspects. Clinica Chimica Acta. 2000;294:1-26.
- 32. Chen, Y,. et al., Recent advances on the development of magnesium alloys for biodegradable implants. Acta biomaterialia, 2014 Nov; 10(11): 4561-73
- 33. Ramcharitar S, Serruys PW. Fully Biodegradable Coronary Stents Progress to Date. American Journal of Cardiovascular Drugs. 2008;8:305-14.
- 34. McMahon CJ, Oslizlok P, Walsh KP. Early restenosis following biodegradable stent implantation in an aortopulmonary collateral of a patient with pulmonary atresia and hypoplastic pulmonary arteries. Catheterization and Cardiovascular Interventions. 2007;69:735-8.
- 35. Waksman R, Erbel R, Di Mario C, Bartunek J, de Bruyne B, Eberli FR, et al. Early- and Long-Term Intravascular Ultrasound and Angiographic Findings After Bioabsorbable Magnesium Stent Implantation in Human Coronary Arteries. Jacc-Cardiovascular Interventions. 2009;2:312-20.
- 36. Peuster M, Beerbaum P, Bach FW, Hauser H. Are resorbable implants about to become a reality? Cardiology in the Young. 2006;16:107-16.

- 37. Zartner, P, R. Cesnjevar, H. Singer, M. Weyand, First successful implantation of a biodegradable metal stent into the left pulmonary artery of a preterm baby, Catheterization and Cardiovascular Interventions, 66 (2005) 590-594.
- 38. Peeters, P., M. Bosiers, J. Verbist, K. Deloose, B. Heublein, Preliminary results after application of absorbable metal stents in patients with critical limb ischemia, Journal of Endovascular Therapy, 12 (2005) 1-5.
- 39. Erbel, R, C. Di Mario, J. Bartunek, J. Bonnier, B. de Bruyne, F.R. Eberli, P. Erne, M. Haude, B. Heublein, M. Horrigan, C. Ilsley, D. Böse, J. Koolen, T.F. Lüscher, N. Weissman, R. Waksman, Temporary scaffolding of coronary arteries with bioabsorbable magnesium stents: a prospective, non-randomised multicentre trial, Lancet, 369 (2007) 1869-1875.
- 40. Krause, A., N. Von Der Höh, D. Bormann, C. Krause, F.W. Bach, H. Windhagen, A. Meyer-Lindenberg, Degradation behaviour and mechanical properties of magnesium implants in rabbit tibiae, Journal of Materials Science, 45 (2010) 624-632.
- 41.F. Witte, V. Kaese, H. Haferkamp, E. Switzer, A. Meyer-Lindenberg, C.J. Wirth, H. Windhagen, In vivo corrosion of four magnesium alloys and the associated bone response, Biomaterials, 26 (2005) 3557-3563.
- 42. Witte F, N. Hort, C. Vogt, S. Cohen, K.U. Kainer, R. Willumeit, F. Feyerabend, Degradable biomaterials based on magnesium corrosion, Current Opinion in Solid State and Materials Science, 12 (2008) 63-72.
- 43. Xu L, E. Zhang, D. Yin, S. Zeng, K. Yang, In vitro corrosion behaviour of Mg alloys in a phosphate buffered solution for bone implant application, Journal of Materials Science: Materials in Medicine, 19 (2008) 1017-1025. 71.
- 44. Witte F, J. Fischer, J. Nellesen, C. Vogt, J. Vogt, T. Donath, F. Beckmann, In vivo corrosion and corrosion protection of magnesium alloy LAE442, Acta Biomaterialia, 6 (2010) 1792-1799.
- 45. Schranz D, P. Zartner, I. Michel-Behnke, H. Akintürk, Bioabsorbable metal stents for percutaneous treatment of critical recoarctation of the aorta in a newborn, Catheterization and Cardiovascular Interventions, 67 (2006) 671-673.

- 46. Song G, A. Atrens, Corrosion mechanisms of magnesium alloys. Advanced Engineering Materials, 1999. 1(1): p. 11-33.
- 47. Abd El-Rahman SS. Neuropathology of aluminum toxicity in rats (glutamate and GABA impairment). Pharmacological Research. 2003;47:189-94.
- 48. Song G, Control of biodegradation of biocompatable magnesium alloys, Corrosion Science, 49 (2007) 1696-1701.
- 49. Bornapour M, N. Muja, D. Shum-Tim, M. Cerruti, M. Pekguleryuz, Biocompatibility and biodegradability of Mg–Sr alloys: The formation of Sr-substituted hydroxyapatite, Acta Biomaterialia, 9 (2013) 5319-5330.
- 50. Aljarrah M, Medraj M. Thermodynamic modelling of the Mg-Ca, Mg-Sr, Ca-Sr and Mg- Ca-Sr systems using the modified quasichemical model. Calphad-Computer Coupling of Phase Diagrams and Thermochemistry. 2008;32:240-51.
- 51. Gupta, M. and Sharon, N.M.L. 2010. Magnesium, Magnesium alloys and Magnesium Composites. Wiley, ISBN-13: 978-0-470-49417-2.
- 52. Li Z, Gu X, Lou S, Zheng Y. The development of binary Mg-Ca alloys for use as biodegradable materials within bone. Biomaterials. 2008;29:1329-44.
- 53. Hassel T, Bach F-W, Golovko A, Krause C. Investigation of the mechanical properties and the corrosion behavior of low alloyed magnesium-calcium-alloys for use as absorbable biomaterial in the implant technique. In: Pekguleryuz M, Mackenzie L, editors. 45th Annual Conference of Metallurgists of CIM. Montreal: Magnesium Technology in the Global Age; 2006. p. 359.
- 54. Wan Y, Xiong G, Luo H, He F, Huang Y, Zhou X. Preparation and characterization of a new biomedical magnesium-calcium alloy. Materials & Design. 2008;29:2034-7.
- 55. Ilich JZ, Kerstetter JE. Nutrition in bone health revisited: A story beyond calcium. Journal of the American College of Nutrition. 2000;19.
- 56. Gu XN, Zheng W, Cheng Y, Zheng YF. A study on alkaline heat treated Mg-Ca alloy for the control of the biocorrosion rate. Acta Biomaterialia. 2009;5:2790-9.
- 57. Hambidge KM, Krebs NF. Zinc deficiency: A special challenge. Journal of Nutrition. 2007;137:1101-5.

- 58. Jia-Cheng, G., Sha, W., Li-Ying, Q. and Yong, W. 2008. Corrosion behavior of Mg and Mg-Zn alloys in simulated body fluid. Transactions of Nonferrous Metals Socciety China 18, pp.588-592.
- 59. Zhang, E., Yin, D., Xu, L., Yang, L. and Yang, K. 2009. Microstructure, mechanical and corrosion properties and biocompatibility of Mg-Zn-Mn alloys for biomedical application. Materials Science and Engineering C 29, pp.987-993.
- 60. Zhang, S., Zhang, X., Zhao, C., Li, J., Song, Y., Xie, C., Tao, H., Zhang, Y., He, Y., Jiang, Y. and Bian, Y. 2010. Research on an Mg-Zn alloy as a degradable biomaterial. Acta Biomaterialia 6, pp.626-640.
- 61. Bowen PK, Drelich J, Goldman J. Zinc exhibits ideal physiological corrosion behavior for bioabsorbable stents. Advanced materials (Deerfield Beach, Fla). 2013;25:2577-82.
- 62. Nielsen SP. The biological role of strontium. Bone. 2004;35:583-8.
- 63. Dahl SG, Allain P, Marie PJ, Mauras Y, Boivin G, Ammann P, et al. Incorporation and distribution of strontium in bone. Bone. 2001;28:446-53.
- 64. Zhang W, Shen Y, Pan H, Lin K, Liu X, Darvell BW, et al. Effects of strontium in modified biomaterials. Acta Biomaterialia. 2011;7:800-8.
- 65. Bigi A, Boanini E, Capuccini C, Gazzano M. Strontium-substituted hydroxyapatite nanocrystals. Inorganica Chimica Acta. 2007;360:1009-16.
- 66. Zeng XQ, Wang YX, Ding WJ, Luo AA, Sachdev AK. Effect of strontium on the microstructure, mechanical properties, and fracture behavior of AZ31 magnesium alloy. Metallurgical and Materials Transactions a-Physical Metallurgy and Materials Science. 2006;37A:1333-41.
- 67. Pekguleryuz M. An overview of the effects of Calcium and Strontium on the properties of Aluminum and Magnesium alloys. IMMC (15th International Metallurgy and Materials Congress). Istanbul, Turkey2010.
- 68. Gu XN, Xie XH, Li N, Zheng YF, Qin L. In vitro and in vivo studies on a Mg-Sr binary alloy system developed as a new kind of biodegradable metal. Acta Biomaterialia. 2012;8:14.
- 69. Brar HS, Wong J, Manuel MV. Investigation of the mechanical and degradation properties of Mg-Sr and Mg-Zn-Sr alloys for use as potential biodegradable

- implant materials. Journal of the mechanical behavior of biomedical materials. 2012;7:87-95.
- 70. Deng Y, Z. Yin, K. Zhao, J. Duan, J. Hu, Z. He, Effects of Sc and Zr microalloying additions and aging time at 120°C on the corrosion behaviour of an Al–Zn–Mg alloy, Corrosion Science, 65 (2012) 288-298.
- 71. Liu M, P. Schmutz, P.J. Uggowitzer, G. Song, A. Atrens, The influence of yttrium (Y) on the corrosion of Mg–Y binary alloys, Corrosion Science, 52 (2010) 3687-3701.
- 72. Coy A.E, F. Viejo, P. Skeldon, G.E. Thompson, Susceptibility of rare-earth-magnesium alloys to micro-galvanic corrosion, Corrosion Science, 52 (2010) 3896-3906.
- 73. Wang H, Y. Estrin, Z. Zúberová, Bio-corrosion of a magnesium alloy with different processing histories, Materials Letters, 62 (2008) 2476-2479.
- 74. Hort N, Y. Huang, D. Fechner, M. Störmer, C. Blawert, F. Witte, C. Vogt, H. Drücker, R. Willumeit, K.U. Kainer, F. Feyerabend, Magnesium alloys as implant materials Principles of property design for Mg-RE alloys, Acta Biomaterialia, (2009).
- 75. Song G, A. Atrens, Understanding magnesium corrosion. A framework for improved alloy performance, Advanced Engineering Materials, 5 (2003) 837-858.
- 76. Montemor, M.F. and M.G.S. Ferreira, Electrochemical study of modified bis-(triethoxysilylpropyl) tetrasulfide silane films applied on the AZ31 Mg alloy. Electrochimica Acta, 2007. 52 (27):p, 7486-7495.
- 77. Makar, G.L. and J, Kruger, Corrosion of Magnesium. International Materials Reviews, 1993. 38 (3): p. 138-153.
- 78.A. Oyane, H.M. Kim, T. Furuya, T. Kokubo, T. Miyazaki, T. Nakamura, Preparation and assessment of revised simulated body fluids, Journal of Biomedical Materials Research Part A, 65 (2003) 188-195.
- 79. Ren Y, J. Huang, B. Zhang, K. Yang, Preliminary study of biodegradation of AZ31B magnesium alloy, Frontiers of Materials Science in China, 1 (2007) 401-404.

- 80. Xin Y. C, Corrosion behavior of biomedical AZ91 magnesium alloy in simulated body fluids, Journal of Materials Research, 22 (2007) 2004-2011.
- 81. Shi Z, M. Liu, A. Atrens, Measurement of the corrosion rate of magnesium alloys using Tafel extrapolation, Corrosion Science, 52 (2010) 579-588.
- 82. Ghali E, W. Dietzel, K.U. Kainer, Testing of general and localized corrosion of magnesium alloys: A critical review, Journal of Materials Engineering and Performance, 13 (2004) 517-529.
- 83. Song G, S. Song, A possible biodegradable magnesium implant material, Advanced Engineering Materials, 9 (2007) 298-302.
- 84. Gu X, Y. Zheng, S. Zhong, T. Xi, J. Wang, W. Wang, Corrosion of, and cellular responses to Mg-Zn-Ca bulk metallic glasses, Biomaterials, 31 (2010) 1093-1103.
- 85. Zhang H.X, Q. Li, L.Q. Li, J.C. Zhou, S.Y. Wang, F. Liu, P. Zhang, In vitro studies of hydrothermally treated magnesium alloy in common simulated body fluid, Transactions of the IMF, 91 (2013) 141-149.
- 86. Bornapour M, Muja N, Shum-Tim P, Cerruti M, Pekguleryuz M. Biocompatibility and biodegradability of Mg-Sr alloys: The formation of Sr-substituted hydroxyapatite. Acta Biomaterialia. 2013;9:5319-30.
- 87. Li Y, Wen C, Mushahary D, Sravanthi R, Harishankar N, Pande G, et al. Mg-Zr-Sr alloys as biodegradable implant materials. Acta biomaterialia. 2012;8:3177-88.
- 88. Haenzi AC, Gerber I, Schinhammer M, Loeffler JF, Uggowitzer PJ. On the in vitro and in vivo degradation performance and biological response of new biodegradable Mg-Y-Zn alloys. Acta Biomaterialia. 2010;6.
- 89. Chou D-T, Hong D, Saha P, Ferrero J, Lee B, Tan Z, et al. In vitro and in vivo corrosion, cytocompatibility and mechanical properties of biodegradable Mg-Y-Ca-Zr alloys as implant materials. Acta Biomaterialia. 2013;9:8518-33.
- 90. Bornapour M, H Mahjoubi, H Vali, D Shum-Tim, M Cerruti, M Pekguleryuz Surface characterization, in vitro and in vivo biocompatibility of Mg-0.3 Sr-0.3 Ca for temporary cardiovascular implant. Materials Science and Engineering: C 67, 72-8.2016.

- 91. Witte F, Kaese V, Haferkamp H, Switzer E, Meyer-Lindenberg A, Wirth CJ, Windhagen H. In vivo corrosion of four magnesium alloys and the associated bone response. Biomaterials 2005 Jun;26 (17): 3557-63.
- 92.ISO 10993-4. Biological Evaluation of Medical Devices-Part 4: Selection of Tests for Interactions with Blood, Annex D, 1993.
- 93. Gao J, Qiao Li, Li L, Wang Y. J. Hemolysis effect and calcium-phosphate precipitation of heat-organic-film treated magnesium. Transactions of Nonferrous Metals Society of China, v16 n3 (200606): 539-544.
- 94.YE Cheng-hong; XI Ting-fei; ZHENG Yu-feng; WANG Shu-qin; Yang-de LI Affiliation: Dongguan EONTEC Co., Ltd., Dongguan 523000, China. In vitro corrosion and biocompatibility of phosphating modified WE43 magnesium alloy. Transactions of Nonferrous Metals Society of China, v23 n4 (April 2013): 996-1001.
- 95.T S N Sankara Narayanan, Il-Song Park; Min Ho Lee. Surface modification of magnesium and its alloys for biomedical applications. Volume 2, Modification and coating techniques. Cambridge, UK: Woodhead Publishing, [2015] ©2015.
- 96. Frandsen NJ, Winther K, Pedersen F, et al. Magnesium and platelet function: in vivo in fl uence on aggregation and alpha-granule release in healthy volunteers. Magnesium Bull. 1995;17:37–40.
- 97. Hwang DL, Yen CF, Nadler JL. Effect of extracellular magnesium on platelet activation and intracellular calcium mobilization. Am J Hypertens. 1992;5:700–6.
- 98.Born GVR, Cross GP. Effect of inorganic ions and plasma proteins on the aggregation of blood platelets by adenosine diphosphate. J Physiol. 1964;170:397–414.
- 99. Gawaz M, Ott I, Reininger AJ, et al. Effects of magnesium on platelet aggregation and adhesion. Magnesium modulates surface expression of glycoproteins on platelets in vitro and ex vivo. Thromb Haemost. 1994;72:912–8.
- 100.Nadler JL, Goodson S, Rude RK. Evidence that prostacyclin mediates the vascular action of magnesium in humans. Hypertension. 1987;9:379–83.

- 101. Gawaz M. Effects of intravenous magnesium on platelet function and platelet-leukocyte adhesion in symptomatic coronary heart disease. Thromb Res. 1996;83:341–9.
- 102. Badimon L, Badimon JJ, Galvez A, et al. Influence of arterial damage and wall shear rate on platelet formation: ex vivo study in a swine model. Arteriosclerosis. 1986;6:312–20.
- 103. Anstall HB, Huntsman RG, Lehmann H, et al. The effect of magnesium on blood coagulation in human subjects. Lancet. 1959;1:814–5.
- 104. Adams JH, Mitchel JRA. The effect of agents which modify platelet behavior and of magnesium ions on thrombus formation in vivo. Thromb Haemost. 1979;42:603– 10.
- 105. Ascencio, M, M Pekguleryuz; S Omanovic. An investigation of the corrosion mechanisms of WE43 Mg alloy in a modified simulated body fluid solution: The influence of immersion time. Corrosion Science, v87 (October 2014): 489-503.
- 106. Ascencio, M, M Pekguleryuz; S Omanovic. An investigation of the corrosion mechanisms of WE43 Mg alloy in a modified simulated body fluid solution: The effect of eletrolyte removal. Corrosion Science, v91 (February 2015): 297-310.
- 107. W.R. Zhou, Y.F. Zheng, M.A. Leeflang, J. Zhou, Mechanical property, biocorrosion and in vitro biocompatibility evaluations of Mg–Li–(Al)–(RE) alloys for future cardiovascular stent application, Acta Biomaterialia, 9 (2013) 8488-8498.
- 108. L. Mao, L. Shen, J. Niu, J. Zhang, W. Ding, Y. Wu, R. Fan, G. Yuan, Nanophasic biodegradation enhances the durability and biocompatibility of magnesium alloys for the next-generation vascular stents, Nanoscale, 5 (2013) 9517-9522.
- 109. L. Mao, G. Yuan, S. Wang, J. Niu, G. Wu, W. Ding, A novel biodegradable Mg–Nd–Zn–Zr alloy with uniform corrosion behavior in artificial plasma, Materials Letters, 88 (2012) 1-4.

Chapter 3: MOTIVATION and OBJECTIVES

3.1 Motivation

The development of biodegradable implant Mg alloys is an expanding field of research. Even though the history of Mg alloys in biomedical applications is new, a significant number of studies have been carried out and the shortcomings of Mg have been identified. Mg alloys corrode rapidly in the physiological environment and their useful life as temporary implants can be inadequate unless the bio-corrosion rate is decreased. Additionally, while Mg itself is bio-compatible, Mg alloys contain other alloying elements which can be toxic. One of the main problems in cardiovascular stents is that alloying elements such as rare earths which are not part of the body chemistry can lead to smooth cell proliferation in the stented area increasing the risk of thrombosis.

Previous research conducted by Prof. Pekguleryuz's team at McGill focused on Mg alloys containing Sr and Ca to be used as biodegradable cardiovascular implants (1). The developments in this research led the group to the idea of developing new alloys containing also Zn in their composition to improve the mechanical properties and the corrosion resistance of the alloy. Preliminary studies showed that the alloys perform better than control alloys in limited in vivo studies and have acceptable bio-corrosion rates. It was noted that further research needs to be conducted on the bio-compatibility and bio-degradation of these alloys. Thus, the purpose of this master thesis is to investigate the bio-degradation and biocompatibility Mg-Sr-Ca and Mg-Sr-Ca-Zn based alloys with the purpose of developing a viable Mg implant alloy for the human body.

3.2 Objectives

Four (4) different Mg alloys have been chosen for evaluation in this project. These alloy compositions are as follows;

- 1. Magnesium 0.5 % Strontium
- 2. Magnesium 0.3 % Strontium 0.3 Calcium
- 3. Magnesium 0.3 % Strontium 0.3 Calcium 0.1 Zinc
- 4. Magnesium 0.3 % Strontium 0.3 Calcium 0.3 Zinc

To ensure the understanding of the physical properties and biocompatibility of these alloys four main objectives are defined;

<u>Objective 1-</u> Characterization of the Mg alloys by defining the surface properties using SEM, XRD, AFM techniques and evaluation of biocorrosion.

<u>Objective 2-</u> Evaluation of cytotoxicity of the alloys on two different cell types by using indirect cytotoxicity tests.

<u>Objective 3</u>- Evaluation of blood compatibility by investigating the hemolysis effect of alloys and the effect on platelet aggregation.

Objective 4 - Evaluation of cell interactions with the surface of the Mg alloys.

3.3 References;

- Bornapour, M., Celikin, M. & Pekguleryuz, M. Thermal exposure effects on the in vitro degradation and mechanical properties of Mg-Sr and Mg-Ca-Sr 30 biodegradable implant alloys and the role of the microstructure. Mater Sci Eng C Mater Biol Appl 46, 16–24 (2015).
- 2. Bornapour, M. Celikin, M. Cerruti, M. Pekguleryuz, Magnesium implant alloy with with low levels of strontium and calcium: The third element effect and phase selection improve bio-corrosion resistance and mechanical performance, Materials Science and Engineering: C, 35 (2014) 267-282.
- Bornapour, M, H Mahjoubi, H Vali, D Shum-Tim, M Cerruti, M Pekguleryuz. Surface characterization, in vitro and in vivo biocompatibility of Mg-0.3 Sr 0.3 Ca for temporary cardiovascular implant. Materials Science and Engineering: C 67, 72-84.

Chapter 4: MATERIALS and METHODS

4.1 SAMPLE PREPARATION

4.1.1 Alloy Casting

Commercial grade pure Mg (99.9 wt.%), pure Sr (99.99 wt.%), Mg-30wt%Ca master alloy and pure Zn (99.99 wt.%), all supplied by Applied Magnesium (Formerly Timminco), were used to synthesize all the Mg alloys with various levels of strontium, calcium, and zinc content.

Pure Mg (99.9 wt.%) was melted in a graphite crucible using Lindberg/Blue M Crucible Furnace (Fig.4.1.1.1. a). The melt temperature was constantly monitored using a digital thermometer with a K-type (Chromel-Alumel) thermocouple. The melt was regularly stirred with a graphite rod to remove any oxide layer that formed. Ca, Zn and Sr were added to the melt at 700 °C; the melt was held at the specified temperature for 15 min to dissolve the additions. After 3 minutes of degassing with high purity argon gas, the alloys were cast from a melt temperature of 720 °C into a pre-heated (400 °C) permanent mold to obtain thin-plate castings 6mm in thickness (Fig.4.1.1.1. b). Recovery rates of 85%, 80% and 85% were used for Sr, Ca and Zn additions, respectively, based on previous experiments in the research team. CO₂ with 0.5% SF6 was used at a flow rate of 1.1 L/min as a protective gas to prevent burning during melting and casting.

WE43 Mg alloy supplied by Magnesium Elektron, USA was also cast into plates. The nominal composition of the WE43 Mg alloy is given in Table 4.1.1.1.

4.1.2 ICP-OES Analysis

Each sample cast was drilled to obtain ~5 g of specimen chips to be analyzed using ICP-OES (Fig 4.1.1.1.c). To determine the chemical compositions of the alloys, inductively coupled plasma optical emission spectroscopy (ICP -OES) (Thermo Jarrell Ash Trace Scan, USA), was used. The compositions of the alloys are presented in Table 4.1.2.1. All compositions are given in wt.%. For the digestion, 5 mg of the alloy chips were dissolved in 3 ml hydrochloric acid and 1 ml nitric acid mixture.

Table 4.1.1.1: Nominal composition of WE43 Mg alloy.

Element	Mass Fraction (wt. %)
Yttrium	3.7-4.3
Rare earths (mainly Nd)	2.4-4.4
Zirconium	Min. 0.4
Magnesium	Balance





Fig. 4.1.1.1: Casting procedure: **(a)** melting in graphite crucible with induction furnace, **(b)** thin plate cast sample, **(c)** chip obtaining using the drill.

Table 4.1.2.1: The chemical composition of the alloys.

Chemical composition (wt. %)

Alloy	Ca	Fe	Sr	Zn	Mg
Mg-%0.5 Sr - Plate 1	0	0.14	0.4	0	Balance
Mg-%0.5 Sr - Plate 2	0	0.13	0.34	0	Balance
Mg-%0.3 Sr- 0.3 Ca - Plate 1	0.39	0	0.31	0	Balance
Mg-%0.3 Sr- 0.3 Ca- 0.1 Zn - Plate 1	0.25	0.02	0.24	0.09	Balance
Mg-%0.3 Sr- 0.3 Ca- 0.1 Zn - Plate 2	0.28	0.02	0.21	0.09	Balance
Mg-%0.3 Sr- 0.3 Ca- 0.3 Zn - Plate 1	0.28	0.02	0.21	0.3	Balance
Mg-%0.3 Sr- 0.3 Ca- 0.3 Zn - Plate 2	0.25	0.02	0.23	0.28	Balance

4.2 CHARACTERIZATION

4.2.1 Surface Characterization

4.2.1.1 Atomic Force Microscopy (AFM)

The topography of the alloy samples was imaged via AFM in dry conditions using the Nanoscope III (Digital Instruments) system in the tapping mode. Before the analysis, all samples were cut using ISOMET low speed saw (Buehler) into 5×10×2 mm and later polished by using gradually 600-800-1200 grit SiC paper. As a last step, samples were polished using a Buehler Tex met cloth using 3 µm diamond suspension. Next, the samples were rinsed three times in reagent alcohol and sonicated for 5 min to ensure removal of the residues from the surface. Samples were air dried.

The images were acquired in air at ambient temperature using a silicon probe with a nominal spring constant of 40 N/m and a nominal radius of curvature of 35 μ m (model RTESP, Veeco). A 100 \times 100 μ m² area was scanned using the minimum amount of force required to obtain steady images. Root mean square (RMS) surface roughness was calculated using Nanoscope v 5.12r5 software. The AFM measurements were conducted on samples polished with 800 grit, 1200 grit respectively and after polishing with the diamond suspension.

4.2.1.2 X-Ray Diffraction (XRD)

XRD phase analysis was carried out using a Bruker D8 diffractometer (USA), equipped with a GADDS 2D detector and Cu K α radiation (λ = 0.15406 nm). A current of 40 mA and voltage of 40 kV were utilized. It is noted that XRD can detect phases that are in excess of ~5wt%.

4.2.1.3 Scanning Electron Microscopy (SEM)

Samples from the cast plates were cut using ISOMET Precision saw (Buehler), then, embedded in epoxy resin and kept overnight to allow curing. The samples were taken out of the molds (Fig.4.2.1.3.1) and polished using, in sequence, 600- 800 -1200 grit SiC paper. As a last step, they were polished on a Buehler Tex met cloth with 5 μ m and finally 3 μ m diamond suspension. The samples were later sonicated in ethanol for 5 min. They were than washed with ethanol and air dried.

Samples were inspected using a Hitachi S- 4700 field emission gun scanning electron microscope (FEG-SEM) equipped with an Oxford INCA energy dispersive spectroscopy (EDS) detector with a maximum resolution of 100nm was used to evaluate the second phases in as-cast alloys. Accelerating voltage was 5 kV and secondary electron mode was used for examination.

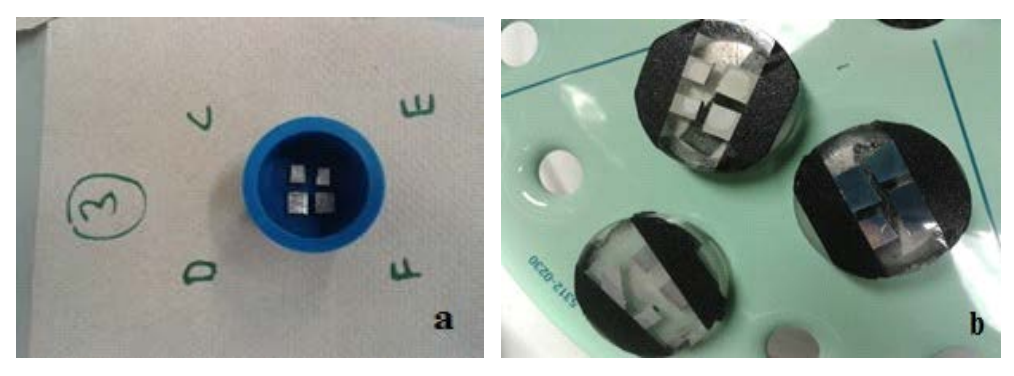


Fig. 4.2.1.3.1: (a) Samples embedded in epoxy resin, **(b)** samples prepared for SEM imaging.

4.2.2 Corrosion

4.2.2.1 In Vitro Immersion Tests

Thin plates castings were cut into sections (1 cm ×1 cm × 6 mm) and polished down to 1200 grit with silicon-carbide (SiC) paper and then fine polished with diamond paste. To remove polishing residue, samples were sonicated in ethanol for 5 minutes and air dried. The initial surface area and weight of each sample was measured before the immersion test.

A buffered modified simulated body fluid (m-SBF) was used as an electrolyte which was defined by Oyane et al. [1] with a pH of 7.4 to closely simulate the physiological environment – in our case the blood plasma (Table 4.2.2.1.1). The composition of m-SBF is given in the Table 4.2.2.1.2.

Table 4.2.2.1.1: Comparison for the concentrations of m-SBF with blood plasma [1].

Species	Blood plasma	m-SBF
Na ⁺ (mM)	142.00	142.00
K ⁺ (mM)	5.00	5.00
Ca ²⁺ (mM)	2.50	2.50
Mg^{2+} (mM)	1.50	1.50
HCO ₃ - (mM)	27.00	10.00
Cl ⁻ (mM)	103.00	103.00
HPO ₄ ²⁻ (mM)	1.00	1.00
SO ₄ ²⁻ (mM)	0.50	0.50
Hepes ^a (g L ⁻¹)	5.96	17.89

^aHEPES=2-(4-(2-hydroxyethyl)-1-piperazinyl) ethanesulfonic acid

The temperature was maintained at 37 °C using a water bath equipped with a thermostat during immersion testing. The water bath had a moving platform which ensured that the m-SBF mixed constantly. The ratio of m-SBF solution to the surface

area of the sample was kept at 100 ml/cm² and all the experiments were done in triplicates. All experiments were conducted for five days.

Each sample was hooked on to a wire through a mounting hole drilled on its surface and attached to a funnel covered by an inverted glass cylinder filled with m-SBF solution (Fig. 4.2.2.1.c). All the hydrogen bubbles released from the corroded samples were collected inside the cylinder. The experimental setup used for the in vitro immersion tests is shown in Fig. 4.2.2.1.a. The pH variation in m-SBF was measured every 24 hours and the volume of hydrogen gas evolved was monitored from the change of the solution level during the tests. The samples were removed from solution after five days, gently rinsed with distilled water and air dried for the later weight measurements.

Table 4.2.2.1.2: Amounts of reagents used to prepare 1000 ml of m-SBF [1].

Reagents ^a	Purity / %	Amount
NaCl	>99.5	5.4030 g
NaHCO ₃	>99.5	0.5040 g
Na ₂ CO ₃	>99	0.4260 g
KCI	>99	0.2250 g
K ₂ HPO ₄	>98	0.1756 g
$MgCl_2 \times 6H_2O$	>99.4	0.3110 g
HEPES ^b	>99.5	17.8920 g ^c
CaCl ₂ × 2H ₂ O	>99	0.3881 g
Na ₂ SO ₄	>99.2	0.0720 g
1.0 M NaOH		~15 ml

a Listed in sequence of dissolution

b HEPES, 2-(4-(2-hydroxyethyl)-1-piperazinyl) ethanesulfonic acid

c HEPES was previously dissolved in 100 ml of 0.2M NaOH







Fig. 4.2.2.1.1: (a) Immersion test set up, (b) the funnels used for attaching the alloy samples, (c) assembly of the funnel and the cylinders.

4.2.2.2 Hydrogen evolution

The average value of the corrosion rate in terms of hydrogen evolution was calculated as average values of the triplicate corrosion tests.

The following equation was used to calculate the corrosion rate for the samples from hydrogen evolution:

$$R = \left(\frac{V * \rho * MW_{alloy}}{t * A * MW_{H_2}}\right) * 24$$

where, R: corrosion rate, t: immersion time (h), A: surface area (cm²), V: volume of H₂ (cm³), ρ : density of H₂ (g/L), MW_{H2} : molar mass of H₂ (g/mol) and MW_{alloy} : molar mass (g/mol).

4.2.2.3 Weight Loss

After the immersion test was finalized, the corrosion layer on the samples was dissolved by immersing into chromic acid (180 g CrO³/dm³) for 5 minutes, rinsed in ethanol 3 times under the hood, air dried and weighed immediately.



Fig. 4.2.2.3.1: The removal of corrosion layer on the samples using chromic acid ((180 g CrO³/dm³)).

The weight change of the samples was measured for each sample. The following equation was used to calculate the corrosion rate from the weight loss:

$$R = \left(\frac{m}{t * A}\right) * 24$$

where, R: corrosion rate, m: mass loss, t: immersion time, A: surface area

4.2.2.4 Electrolyte analysis (ICP-OES)

Inductively coupled plasma optical emission spectroscopy (ICP-OES) was used to determine the concentration of dissolved Mg and alloying elements in the electrolyte as a result of corrosion [2, 3, 4]. Three samples were taken from the electrolyte every 24 hours during the course of the experiment and analysed to determine the ion level change inside the medium due to corrosion of the alloy samples. The change in the amount of different ions in the electrolyte could be correlated with the rate of the corrosion. In this experiment, we measured the daily accumulation of the ions, so it is limited to determining the rate of corrosion at 24-hour intervals.

4.3 CYTOTOXICITY

4.3.1 Cell cultures (HUVEC, MC3T3)

To evaluate the cytocompatibility of Mg alloy samples, two types of cells were used. These were human umbilical vascular endothelial cells (HUVECs) and Mouse osteoblast precursor cell line (MC3T3).

HUVEC cell culture (subclone 4-6) was maintained in M-200 medium supplemented with low serum growth supplement (LSGS) (Invitrogen, Carlsbad, CA) at 37°C in humidified atmosphere at of 5% CO2. Gelatin coated (0.2%) culture flasks were used for subcultures.

Mouse preosteoblast MC3T3 (subclone 22) cells (supplied by American Type Culture Collection (ATCC, Manassas, VA), and grown in a Alpha-MEM (Gibco, Invitrogen Corporation) media, supplemented with 10% FBS (Gibco, Invitrogen), 1% penicillin/streptomycin (Invitrogen), 0.2 mM L-ascorbic acid (Sigma), and 2 mM L-glutamine (Sigma) and incubated at 37°C in a humidified atmosphere of 5% CO₂. Culture flasks were used for subcultures.

4.3.2 Indirect Cytotoxicity assays

4.3.2.1 Ion extract preparation

lon extract was obtained from 1 × 1 × 0.6 cm of the sample by incubating in serum free m-200 cell culture media for HUVECs and serum free Alpha-MEM media for MC3T3s. The samples were polished down to 1200 grit with silicon-carbide (SiC) paper then fine polished with diamond paste. To remove polishing residue, samples were sonicated in ethanol for 5 minutes and air dried. Then the samples were placed under UV for 30 minutes for sterilization. The surface / media ratio was 1 cm 2 / 2.5 ml. The samples inside the medium were incubated for 72 hours in a humidified atmosphere containing 5% CO $_2$ and 95% air at 37 °C. After 72 hours, the alloy samples were removed from the media, rinsed with distilled water, air dried and stored. The extracted medium was used in 10% concentration. The media with serum supplements were used as a positive control for cell growth.

4.3.2.2 ICP-OES analysis for the ions in the extract

To determine the ion composition in the extracts, inductively coupled plasma optical emission spectroscopy (ICP -OES) (Thermo Jarrell Ash Trace Scan, USA), was used. 1 ml of the extract was dissolved in 4 ml nitric acid. All compositions are given in wt.%.

4.3.2.3 MTT test

For MTT tests HUVECs and MC3T3 cells were counted using a hemocytometer. For HUVECs, 96-well cell culture plates were coated with 100 μ l 0.1 % gelatin solution prior to the cell seeding. The coated plates were stored for 24 hrs in a humidified atmosphere containing 5% CO2 and 95% air at 37 °C. Both cell types were seeded onto at 5 × 10³ cells/ 200 μ l medium in each well and incubated overnight to ensure attachment to the well.

After 24 hours of incubation, the medium in each well was replaced with 100 µl of extraction medium and incubated in a humidified atmosphere with 5% CO2 at 37°C for 24h, 4 days and 7 days. During the experiment, the cells were treated every three days with a fresh extraction medium containing serum

At the end of each time point, indicator MTT (10% in M-200 medium for HUVECs and Alpha-MEM media for MC3T3 cells) was added to each well and further incubated at 37 °C for 4 hrs. After 4 hours, 300 μ L 0.04M HCl in isopropanol added to solubilise the crystals. Later we transferred 100 μ L to reading plate. Fluorescence emission of the solution was measured at 600nm for MTT assays. After background subtraction, fluorescence intensity was analyzed relative to the control medium. (Fig. 4.3.2.3.1).

Three wells were seeded for each alloy composition and each medium concentration for various assay time points. The average value was calculated and reported as the % viability of the cells at each specific condition.



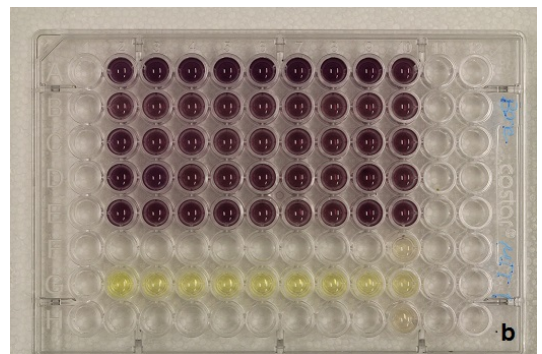


Fig. 4.3.2.3.1: (a) Day 7 MTT test plate for HUVECs, (b) Day 7 MTT test plate for MC3T3 cells.

4.4 BLOOD COMPATIBILITY

Blood compatibility assays were performed at the laboratory of Thrombosis and Hemostasis in the Research Center of the Montreal Heart Institute. This laboratory which is directed by Dr. Yahye Merhi, specializes in the study of blood reactions (platelets, endothelial progenitor cells, leukocytes, coagulation) in cardiovascular disease and coronary heart disease, in particular the acute coronary syndrome.

4.4.1 Hemolysis

Blood was obtained from healthy adult human volunteers, who had not taken any antiplatelet drugs for at least two weeks before sampling. Blood was anticoagulated with 13% tri-sodium citrate, nine parts blood to one part anticoagulant. A full blood count and platelet count were performed using a Coulter S Plus IV (Coulter Electronics Ltd, Luton, Beds).

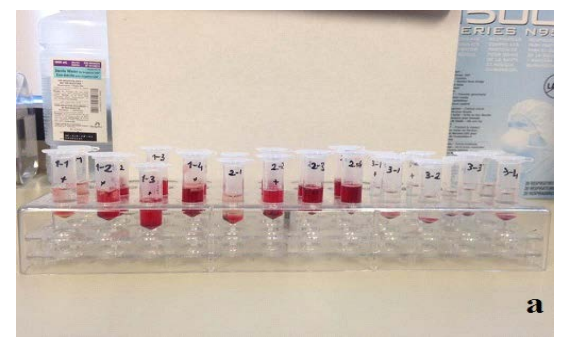
For hemolysis experiments, pure magnesium, stainless steel 316L and WE43 were used as controls to compare with four new alloy compositions.

The blood and the saline solution was placed in the water bath at 37° for 15 min for warming. Standard curve samples were prepared as follows;

- For 100% lysis, 900 μL of H₂O was added to 100μL of blood

- For 50% lysis, 400 μL of saline solution and 500 μL of H₂O was added to 100 μL of blood
- For 25% lysis, 650 μL of saline solution and 250 μL of H2O was added to 100 μL of blood
- For 0% lysis, 900 μL of saline solution was added to 100μL of blood

The whole blood was diluted 1:10 times in pre-warmed saline (e.g. $100\mu L$ of RBC + $900\mu L$ of saline). 1 ml of diluted blood was placed into each Eppendorf tubes with corresponding chip weight. We used, 1 mg, 2.5 mg, 5 mg and 10 mg chips from each alloy samples. The alloy samples with the diluted blood were gently mixed on the rotator at room temperature for 30 min, 60 min and 90 min (Fig. 4.4.1.1.a). After the rotation, the samples were centrifuged for 5 minutes at 950xg, and subsequently the supernatant of each sample in the amount of $100~\mu L$ was transferred twice in two different wells in the 96 well plate. The absorbance was measured at 541 nm. (Fig. 4.4.1.1 b)



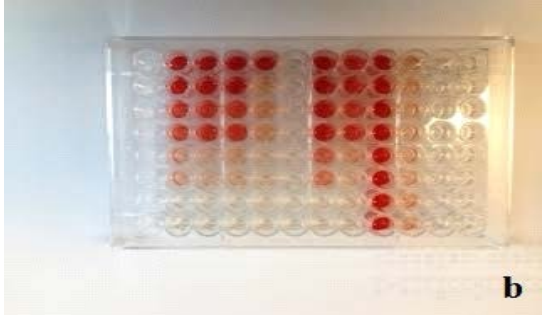


Fig. 4.4.1.1: (a) The blood samples mixed with Mg alloy particles after incubation and centrifugation, **(b)** blood samples transferred to a reading plate for spectroscopy.

For each alloy composition, experiments were done in triplicates. The absorbance values of the 100% lysis and the 0% lysis samples were used to obtain the percentage lysis the alloy samples.

4.4.2 Platelet Aggregation

Blood was obtained from healthy adult human volunteers, who had not taken any anti platelet drugs for at least two weeks before sampling between 08:00 h and 10:00 h am in order to avoid any diurnal influence. The sample was transferred into vacuum filled tubes containing 3.8% sodium citrate (1:9 volume). Whole blood platelet aggregation was performed in citrated blood using the Chronolog Model 540 whole blood aggregometer (Coulter Electronics Ltd, Luton, Beds).

For each alloy and controls, 5 mg of chips were incubated with a 1:1 dilution with 0.5 ml of physiological saline and the specimen of whole blood for 30 min. Later, 975 µl of the specimen of the whole blood sample was transferred in a non-siliconized glass cuvette 10 x 44 mm and placed in the device reaction well and then stirred with a Teflon coated stir bar after inserting the impedance electrode. The platelets in the blood sample adhere to two fine palladium wires on the electrode, resulting in a uniform monolayer of platelets coating the wires. By applying a small voltage difference across the two wires, it is possible to measure the impedance caused by the platelets coating the wires. As platelet coating on the palladium wires thickens over the course of the experiment there will be a corresponding increase in electrical impedance between the electrode wires. This change in impedance is directly proportional to the extent of platelet aggregation and is indicated on the digital display in ohms [5].

The calibration and gain controls were used to calibrate a Rikadenki R302 chart recorder in ohms. In order to obtain an aggregation trace, 0.5 micrograms/ml of aggregating reagent collagen (Hormon Chemie, Munchen) was added and the change in impedance (ohms) recorded at a paper speed of 2 cm/min. Aggregation was performed at stirrer speeds varying between 100 and 1200 rpm on the same sample of blood. For each alloy samples and controls the response curves were produced. After completion of impedance aggregation, the electrodes were carefully cleaned to remove all aggregated cells using isotonic saline solution and lightly cleaned with a tissue.

Rate of aggregation was assessed by measuring the angle between the base line and the linear portion of the aggregation curve; a higher aggregation rate is represented by an increase in the angle. Thus, the slope of the curve represents the aggregation rate. Extent of aggregation was measured as the maximum height of response in chart paper units. This could also be expressed in ohms, since 10 units equaled 5 ohms.

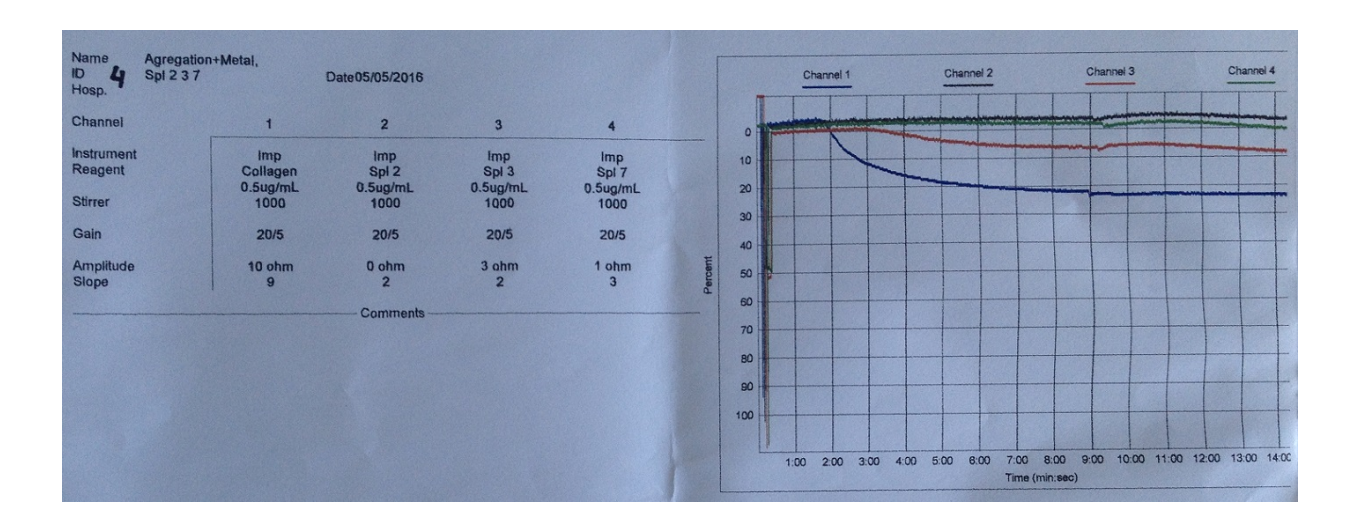


Fig. 4.4.2.1: The aggregation of three samples compared to the collagen (blue line).

4.5 CELL ATTACHMENT

4.5.1 Sample preparation

Thin cast plate samples were cut into sections (0.5 cm × 0.5 cm × 2 mm) and polished down to 1200 grit with silicon-carbide (SiC) paper then fine polished with diamond paste. To remove polishing residue, samples were sonicated in ethanol for 5 minutes. The samples later placed under UV for 45 min for sterilization.

Three samples from each composition for each time point were put inside separate wells in 24 well plates. HUVECs were used for the cell attachment studies. The cells were seeded directly on to the surface of the samples with the concentration of 20×10^3 cells/ 200 µl serum containing medium in each well. After the seeding, the plates were incubated in a humidified atmosphere with 5% CO₂ at 37°C for 30 min, 2h, 4h and 24h.

At the end of each time point, the samples were removed and stained for confocal imaging.

4.5.2 Confocal imaging

Media was removed from the cells and rinsed 2 times very gently with 300 μ I PBS. After removing the PBS solution, we applied 300 μ I of 4% paraformaldehyde (PFA) in PBS- to each sample and leave for 10-15 minutes at 23 °C. The cells were gently washed again with 300 μ I PBS. The cells were then permeabilized for 3 min with 0.2% Triton X-100 in PBS. Next, the cells were blocked in 300 μ I of 5% bovine serum albumin (BSA) in PBS for 15 min, and the cells were then rinsed twice with PBS. One hundred (100) μ I of DAPI (5 mg/mI stock, 1:5000 dilution to 1 μ g/mI) and/or phalloidin-AF555 solution (diluted 1:1000 in PBS- with 2%BSA) were then applied for 15 minutes at 23°C.

In subsequent steps, the samples were protected from light to preserve the fluorescent labels. The cells were then rinsed twice very gently again and finally, the samples were imaged using the Zeiss LSM 510 confocal system.

4.6 STATISTICAL ANALYSIS

All experiments were carried out in triplicate and are repeated minimum three times. Results are reported as the mean \pm standard deviation. Statistical differences between the groups were measured using a one-way ANOVA. Differences were considered significant when p values were found to be < 0.05. Hemolysis tests were repeated minimum three times with the blood collected from three different donors.

4.7 REFERENCES

- A. Oyane, H.M. Kim, T. Furuya, T. Kokubo, T. Miyazaki, T. Nakamura, Preparation and assessment of revised simulated body fluids, Journal of Biomedical Materials Research - Part A, 65 (2003) 188-195.
- 2. X. Gu, Y. Zheng, Y. Cheng, S. Zhong, T. Xi, In vitro corrosion and biocompatibility of binary magnesium alloys, Biomaterials, 30 (2009) 484-498.
- 3. X. Gu, Y. Zheng, S. Zhong, T. Xi, J. Wang, W. Wang, Corrosion of, and cellular responses to Mg-Zn-Ca bulk metallic glasses, Biomaterials, 31 (2010) 1093-1103.
- 4. H.X. Zhang, Q. Li, L.Q. Li, J.C. Zhou, S.Y. Wang, F. Liu, P. Zhang, In vitro studies of hydrothermally treated magnesium alloy in common simulated body fluid, Transactions of the IMF, 91 (2013) 141-149.
- 5. Abbate R, Favilla S, Boddi M, Costanzo G, Prisco D. Factors influencing platelet aggregation in the whole blood. AmJ Clin Pathol 1986; 86:91 –6.

Chapter 5: RESULTS and DISCUSSION

5.1 Material characterization

The alloys studied in this project were characterized for surface and microstructural properties. Atomic force microscopy was used for quantifying surface roughness; x-ray diffraction analysis was used for identifying the phases present in the alloys and scanning electron microscopy was used for observing the microstructures of the alloys. All alloy compositions are in weight % unless otherwise indicated.

5.1.1 Surface Characterization via Atomic Force Microscopy (AFM)

Determination of the surface roughness for the alloys at the nanoscale is important since it plays a crucial role in the functional performance of many devices. Defining the topography of the surface is also crucial for the alloys we developed that are to be potentially in biodegradable stents. Using AFM to observe the surface roughness offers a far exceeding resolution than other stylus and optical based methods.

We measured the surface roughness after three different polishing steps for each alloy compositions and the control materials, WE43 and SS316L. For each alloy, the surface roughness was found to decrease after each polishing step (Fig. 5.1.1.1). The biggest change in the roughness was observed for Mg-0.5Sr alloy. The smallest change was observed for SS316L. After SS316L the second smaller change was observed for WE43 alloy. The Zn containing alloys roughness was observed to reduce less than non-Zn containing alloys. The topography for each alloy and the controls have different salient features. Fig. 5.1.1.2 (a) shows that the SS136L alloy surface has various peaks as well as Mg-0.5Sr alloy (Fig. 5.1.1.2 (c)) and Fig. 5.1.1.2 (e) reveals that the surface of Mg-0.3Sr-0.3Ca-0.1Zn alloy has deep valleys implying a softer surface for this alloy. It can also imply that the increased surface area provides a better surface for adhesion. Furthermore, the appearance of the peaks on the surface varies for different alloys and for different polishing steps.

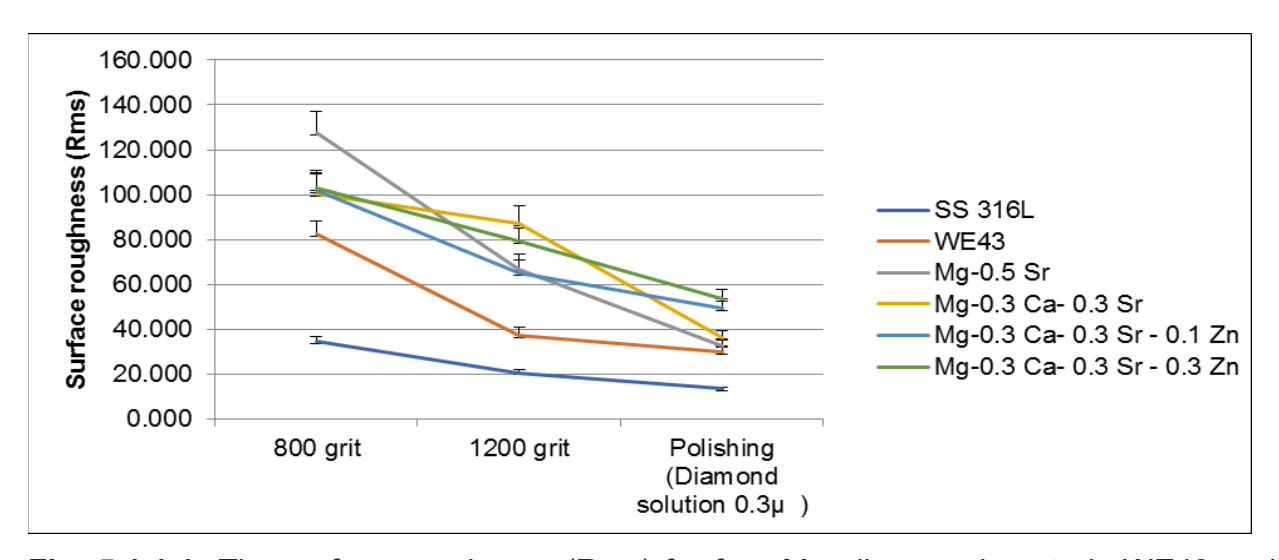


Fig. 5.1.1.1: The surface roughness (Rms) for four Mg alloys and controls WE43 and SS316L.

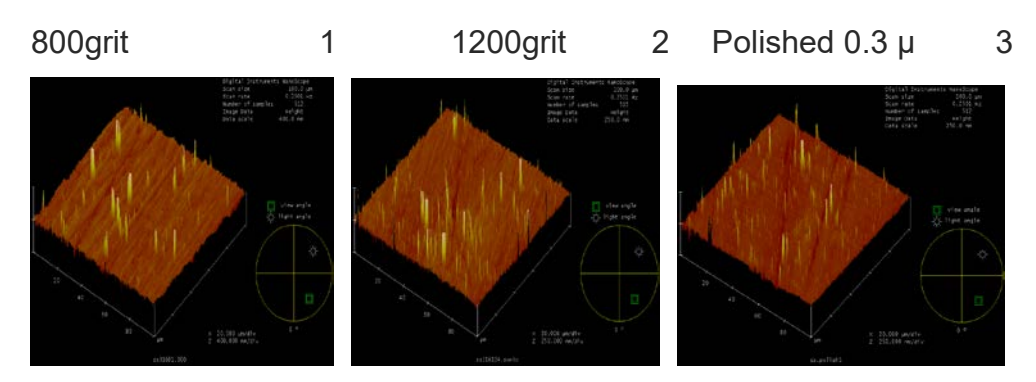


Fig. 5.1.1.1 (a): AFM pictures of SS 316L

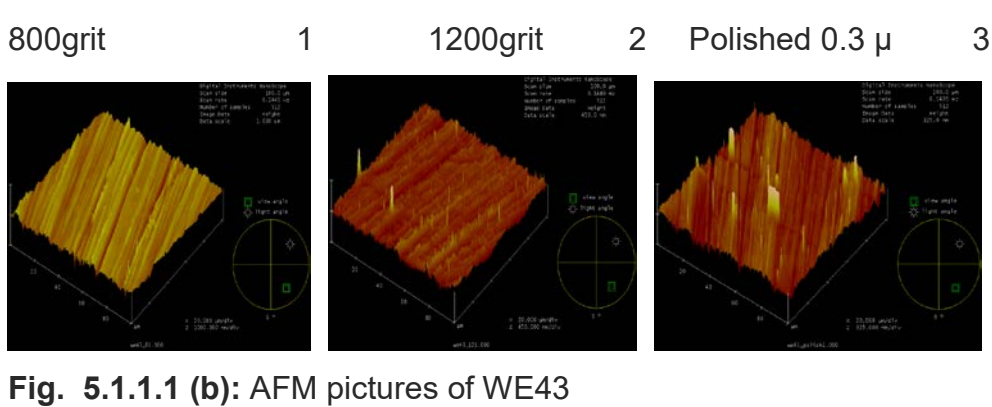


Fig. 5.1.1.1 (b): AFM pictures of WE43 800grit 1 1200grit 2 Polished 0.3 μ 3

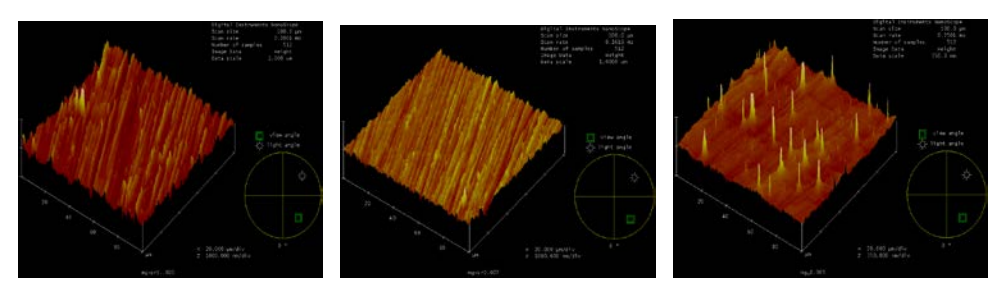


Fig. 5.1.1.1 (c): AFM pictures of Mg-0.5Sr

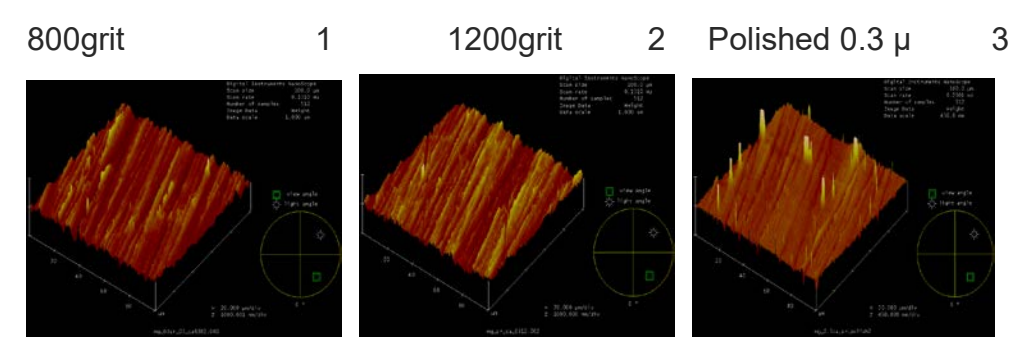


Fig. 5.1.1.1 (d): AFM pictures of Mg-0.3Sr-0.3Ca

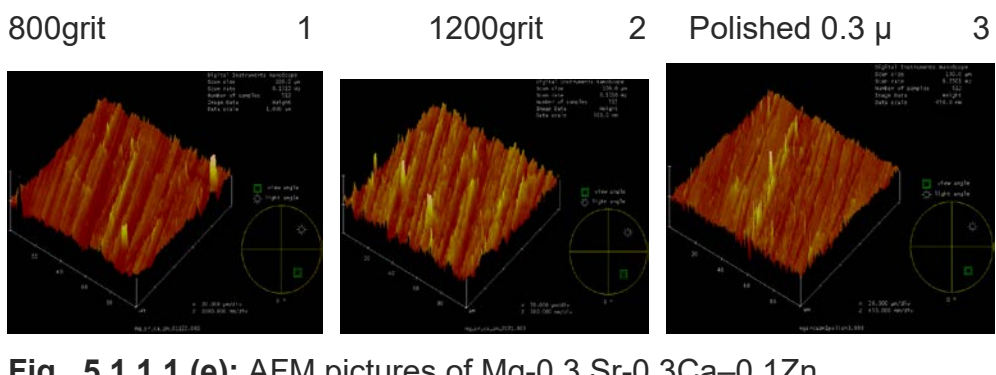


Fig. 5.1.1.1 (e): AFM pictures of Mg-0.3 Sr-0.3Ca-0.1Zn

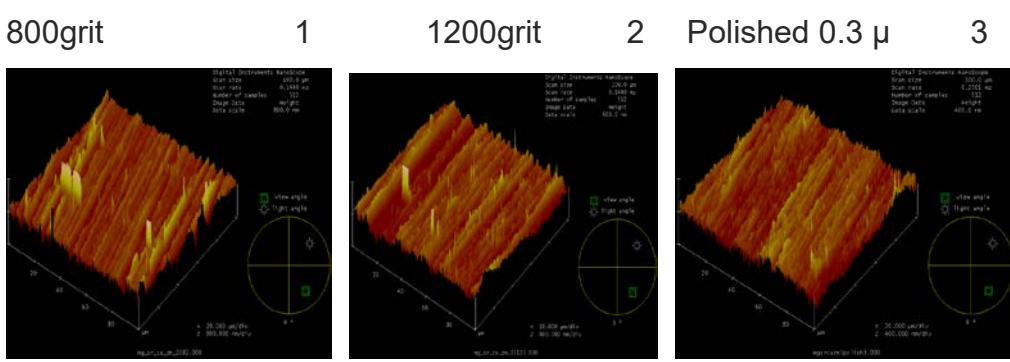


Fig. 5.1.1.1 (f): AFM pictures of Mg-0.3Sr-0.3Ca-0.3Zn

5.1.2 X-Ray Diffraction (XRD)

X-ray diffraction (XRD) analysis is a specific method that is used to determine the phases of an alloy based on crystallographic information. XRD analysis uses diffraction of X-rays from crystallographic planes in a crystalline phase to identify these phases by comparison with standard reference XRD patterns and measurements. Its limit is 5% and hence cannot determine phases that are present below this limit. The XRD spectra are given in Fig. 5.1.2.1. The XRD results were critically evaluated and can be summarized as follows:

- 1. Fig. 5.1.2.1 (a): Mg-0.5Sr alloy has the secondary phase of Sr_2Mg_{17} intermetallic phase in addition to the primary α -Mg matrix (primary phase).
- 2. Fig. 5.1.2.1 (b): The XRD analysis could only detect only the α -Mg matrix (primary phase) in the Mg-0.3Ca-0.3Sr alloy. This alloy is known to have Sr and Ca containing phases [1] in small quantities. Mandana et al [1] have found Mg₁₇Sr₂ or Mg₂Ca as well as nano-scale Sr-Ca non-equilibrium phases in the as cast alloy via transmission electron microscopy (TEM). Their absence in the XRD result can be explained by the fact that these phases are below the detection limit of XRD.
- 3. Fig. 5.1.2.1 (c): The XRD pattern for Mg-0.3Ca-0.3 Sr-0.1Zn alloy shows the presence of the SrMg intermetallic secondary phase and a phase designated as Mg0.972Zn0.028 which is the solid solution phase of Mg with some Zn, i.e. the primary α -Mg(Zn).
- 4. Fig. 5.1.2.1 (d): The XRD pattern for the Mg-0.3Ca-0.3Sr-0.3Zn alloy show only the presence of the primary α -Mg(Zn) designated by XRD as Mg0.972 Zn0.028 (see point 3 above). No secondary phase is detected likely due their low weight fraction.
- Fig. 5.1.2.1 (e): The XRD pattern for WE43 alloy shows two intermetallic phases rich in rare-earths designated as Ce4.726 Y4.920 Mg1.354- Mg43.98 (Cerium Magnesium Yttrium) and Mg25.3 Y3.7 (Magnesium Yttrium). As known, these phases correspond to the Mg41Nd5 and Mg24Y5 second phases present in WE43 commercial alloy [2].

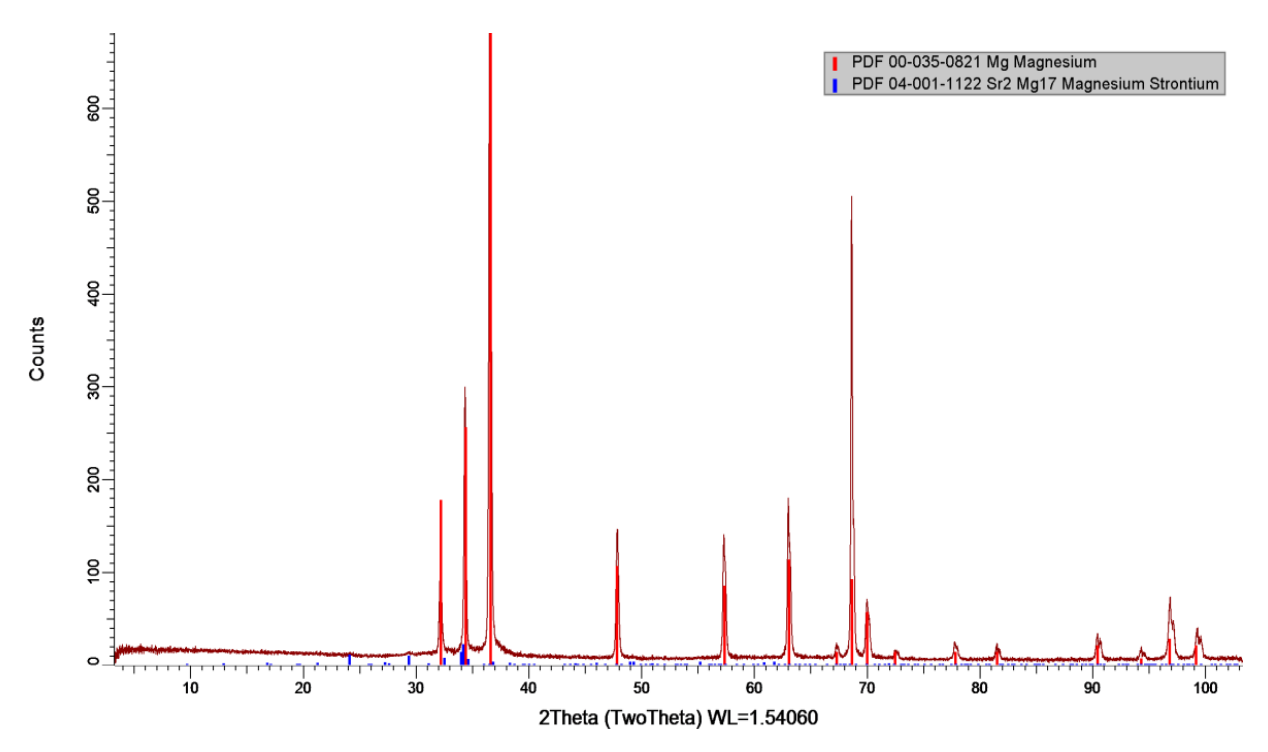


Fig. 5.1.2.1 (a): XRD patterns of Mg-0.5Sr

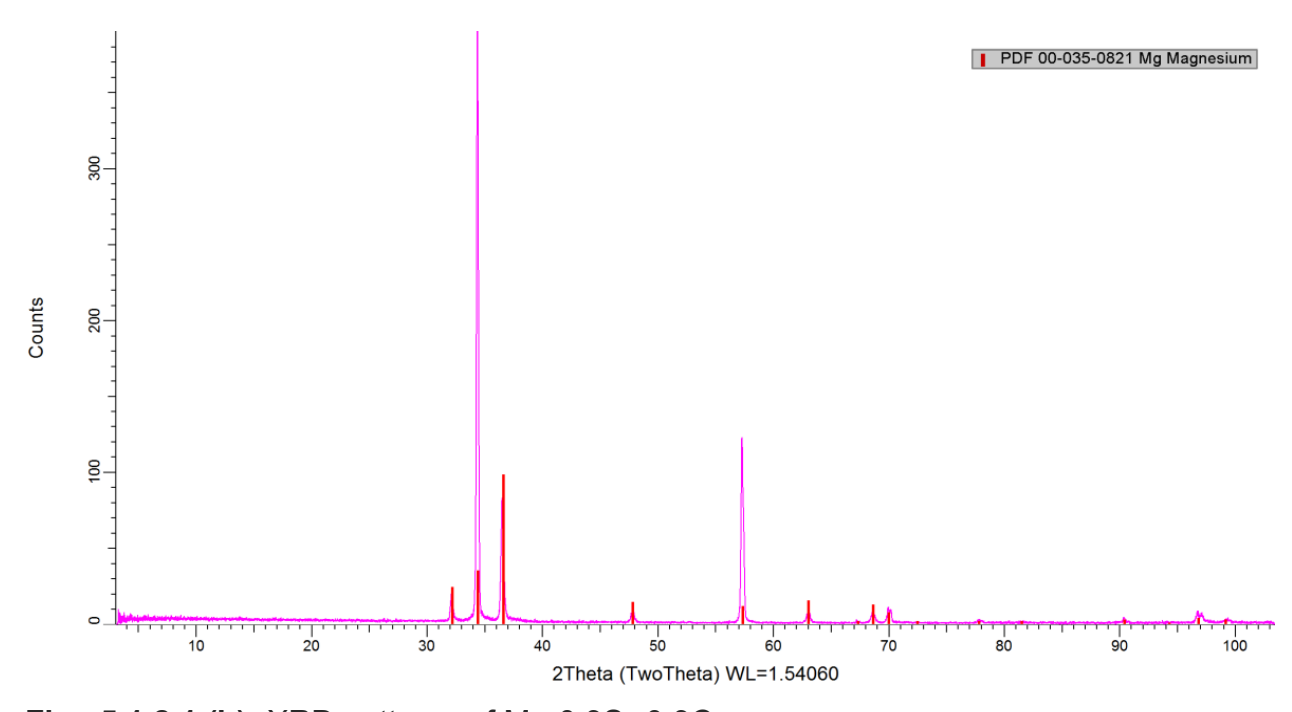


Fig. 5.1.2.1 (b): XRD patterns of Mg-0.3Sr-0.3Ca

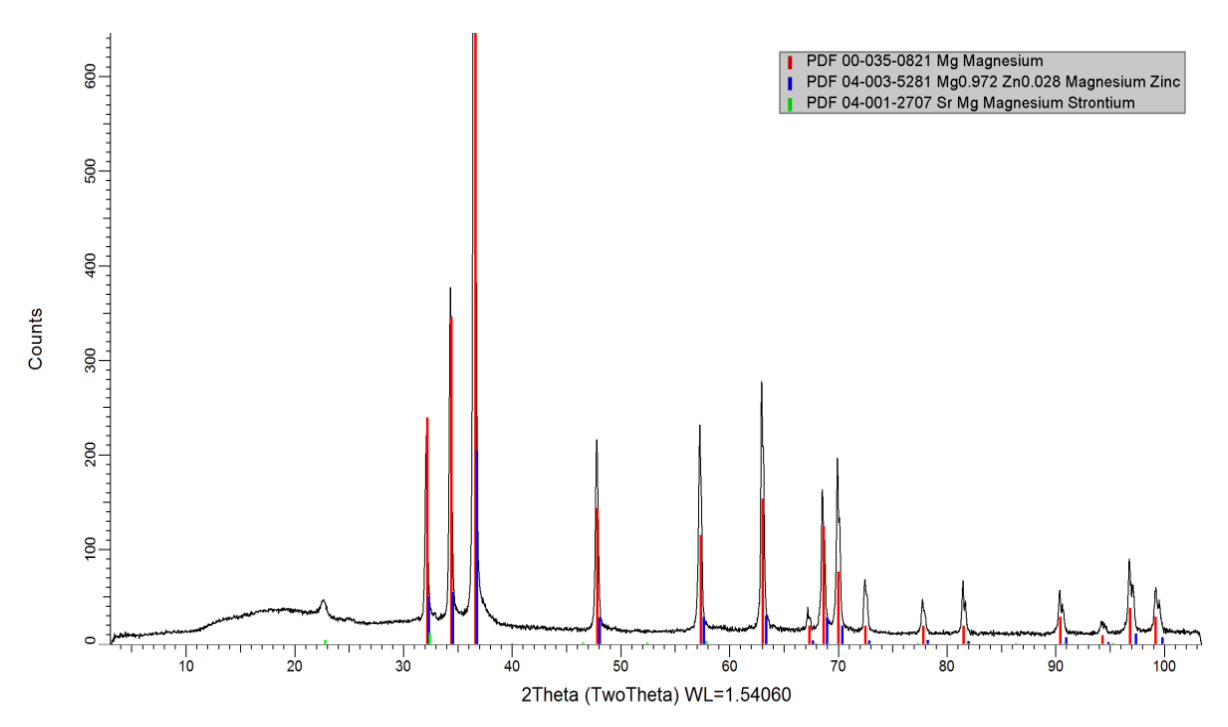


Fig. 5.1.2.1 (c): XRD patterns of Mg-0.3Sr-0.3Ca-0.1Zn

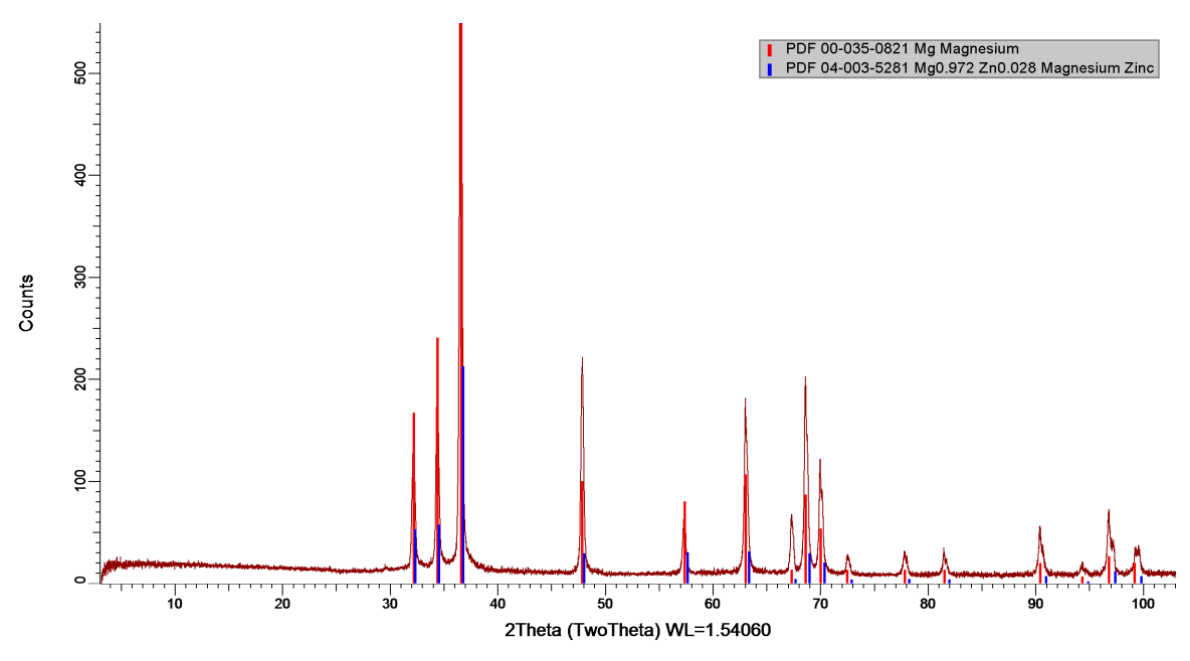


Fig. 5.1.2.1 (d): XRD patterns of Mg-0.3Sr-0.3Ca-0.3Zn

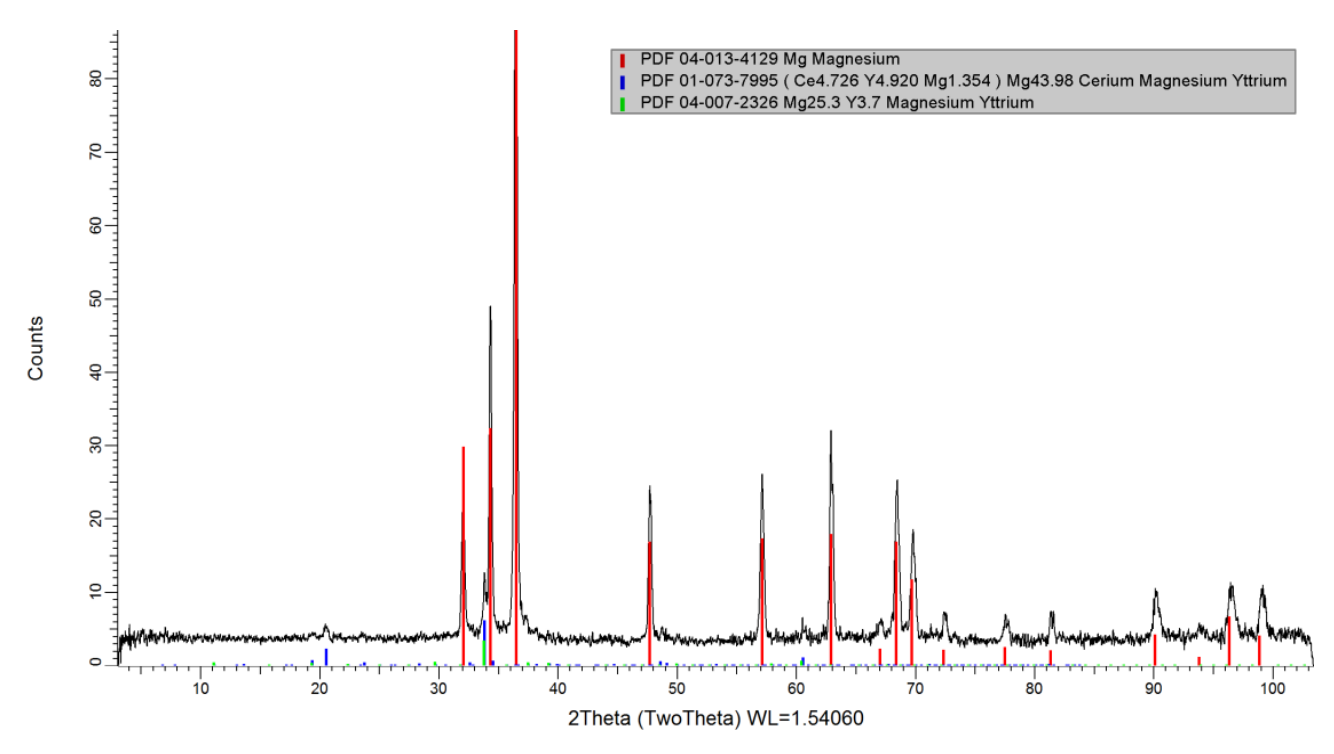


Fig. 5.1.2.1 (e): XRD patterns of WE43 commercial alloy.

5.1.3. Scanning Electron Microscopy (SEM) and Energy Dispersive Spectroscopy (EDS) analysis

SEM characterization was used to characterize the microstructure of the alloys in the surface layers. The chemical composition of microstructural phases was investigated using EDS point analysis. SEM images revealed a cast microstructure with dendritic α -Mg matrix and interdendritic intermetallic second phases containing Ca, Sr or Zn (Fig.5.1.3.1. (a)- (c), Fig.5.1.3.1. (b)- (c), Fig.5.1.3.1. (c)- (c), Fig.5.1.3.1. (d)- (c)). While the XRD spectrum of 5.1.2.1 (d) had shown only the presence of the primary matrix phase α -Mg(Zn) in the Mg-0.3Ca-0.3Sr-0.3Zn alloy, its SEM EDS in Fig. 5.1.3.1.9(d) reveals that alloy has second phases rich in Ca, Sr and Zn.

The images also show that the dendrite/grain size seemed to appear smaller for the Zn containing alloys compared to the other alloys. This is significant in that corrosion resistance of Mg alloys usually improve with the refinement of microstructural features such as grain size of dendrite size. The black dots on the Mg-0.5 Sr images are likely corrosion pits (Fig.5.1.3.1. (a)). Fig. 5.1.3.1 b also shows black dots on the ternary Mg-

0.3Ca-0.3Sr alloy which are more related to chunks of intermetallics that have detached from the surface due to the microgalvanic corrosion between the intermetallics and the matrix likely during sample preparation. The quaternary alloy Mg-0.3Ca-0.3Sr-0.1Zn and the WE43 alloy do not exhibit black dots on the surface which can suggest a lower surface corrosion and reactivity of these alloys.

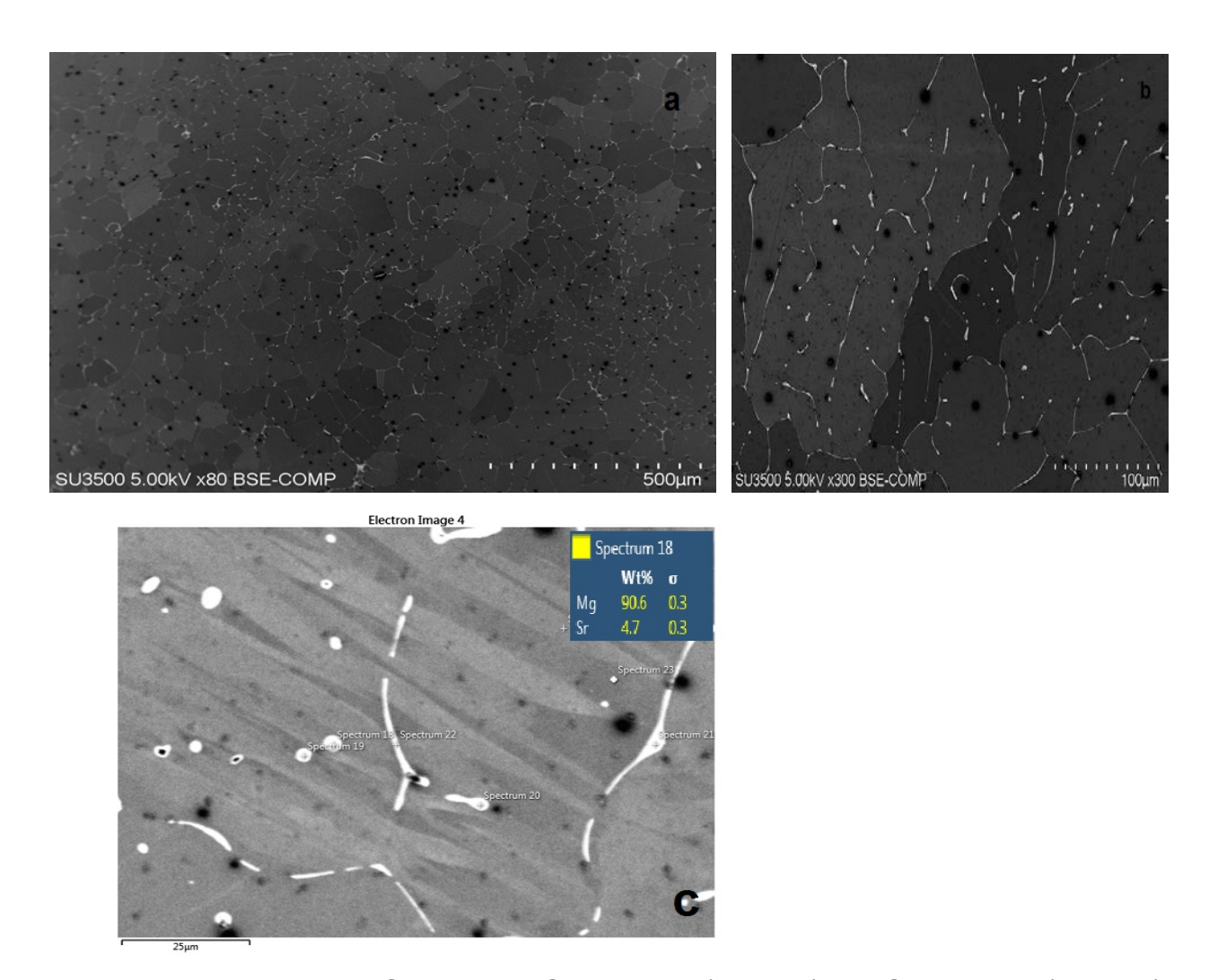


Fig. 5.1.3.1 (a): Mg - 0.5 Sr alloy; (a) SEM image (500 μ m), (b) SEM image (100 μ m), (c) EDS chemical point analysis results (10 μ m).

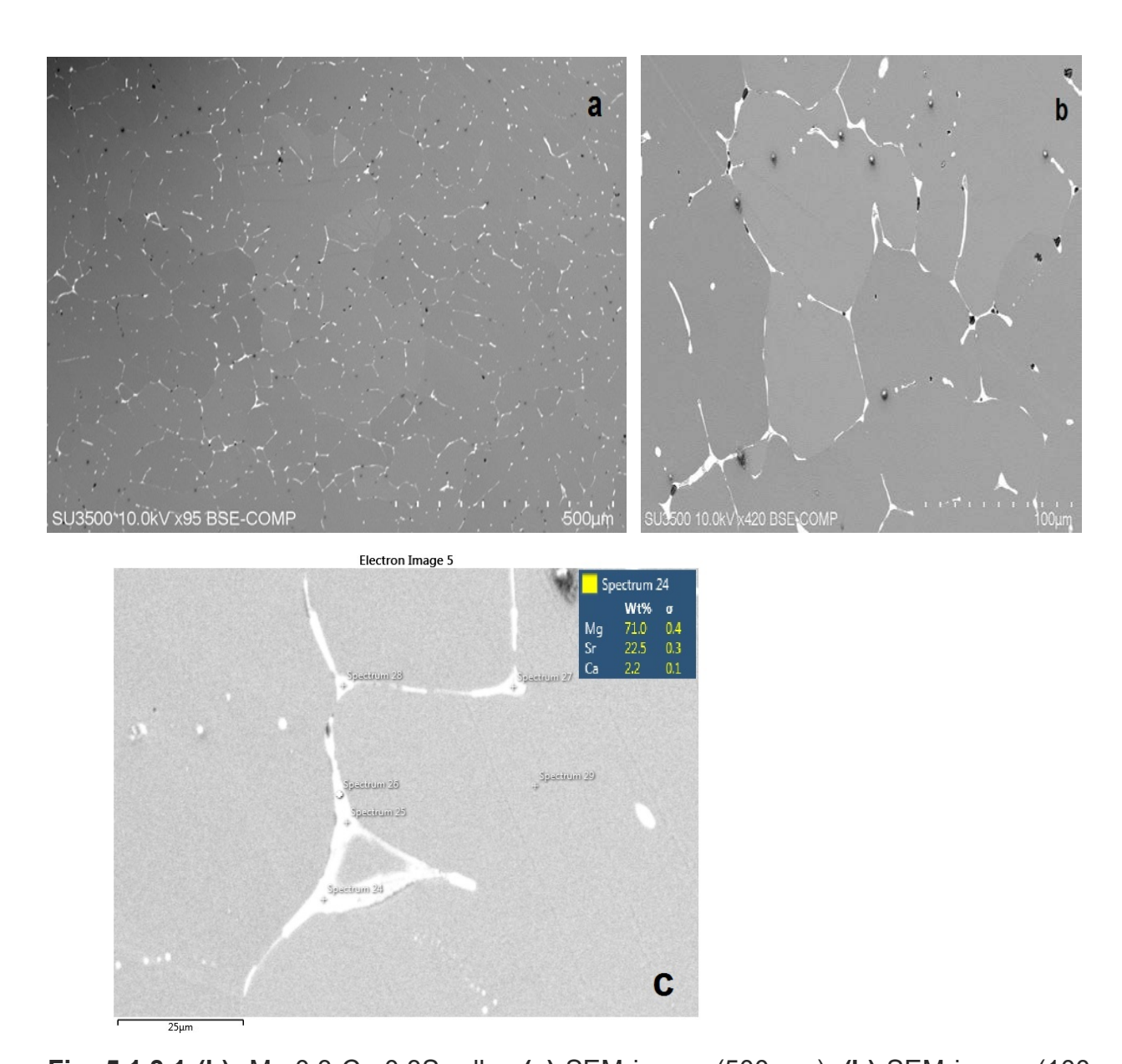


Fig. 5.1.3.1 (b): Mg-0.3-Ca-0.3Sr alloy (a) SEM image (500 μ m), (b) SEM image (100 μ m), (c) EDS chemical point analysis results (10 μ m).

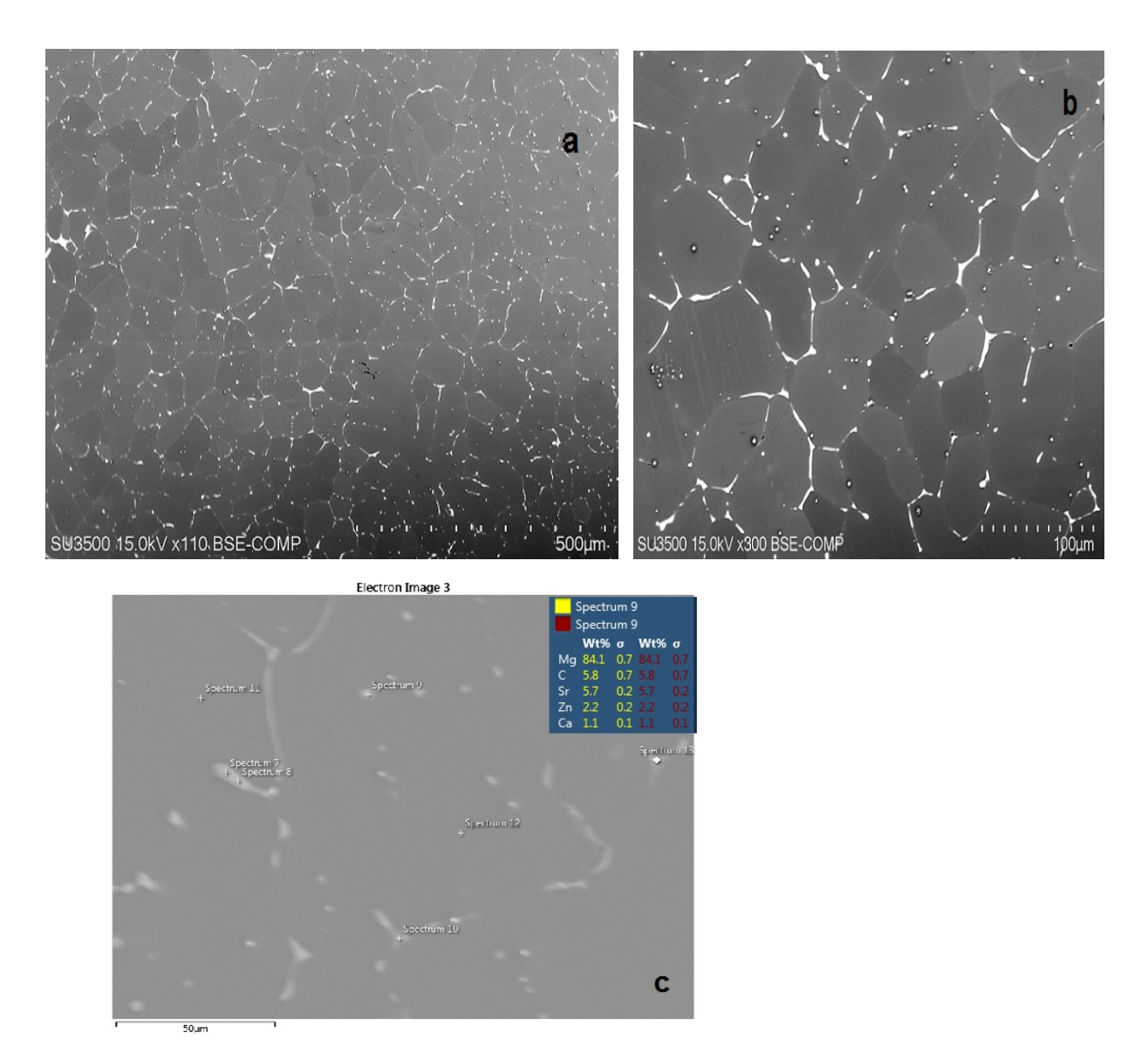


Fig. 5.1.3.1 (c): Mg- 0.3-Ca -0.3 Sr - 0.1 Zn alloy **(a)** SEM image (500 μ m), **(b)** SEM image (100 μ m), **(c)** EDS chemical point analysis results (10 μ m).

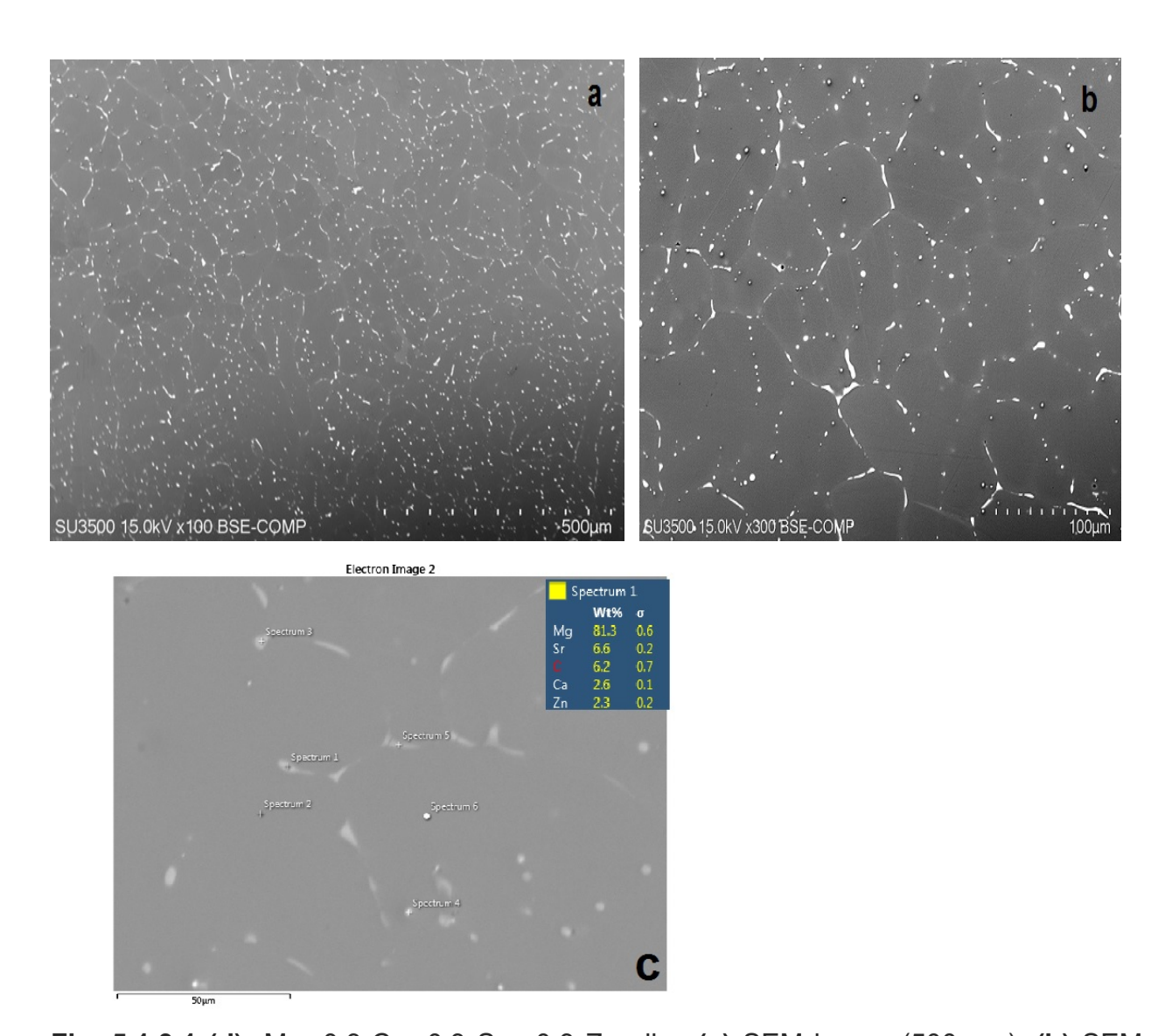


Fig. 5.1.3.1 (d): Mg- 0.3-Ca -0.3 Sr -0.3 Zn alloy (a) SEM image (500 μ m), (b) SEM image (100 μ m), (c) EDS chemical point analysis results (10 μ m).

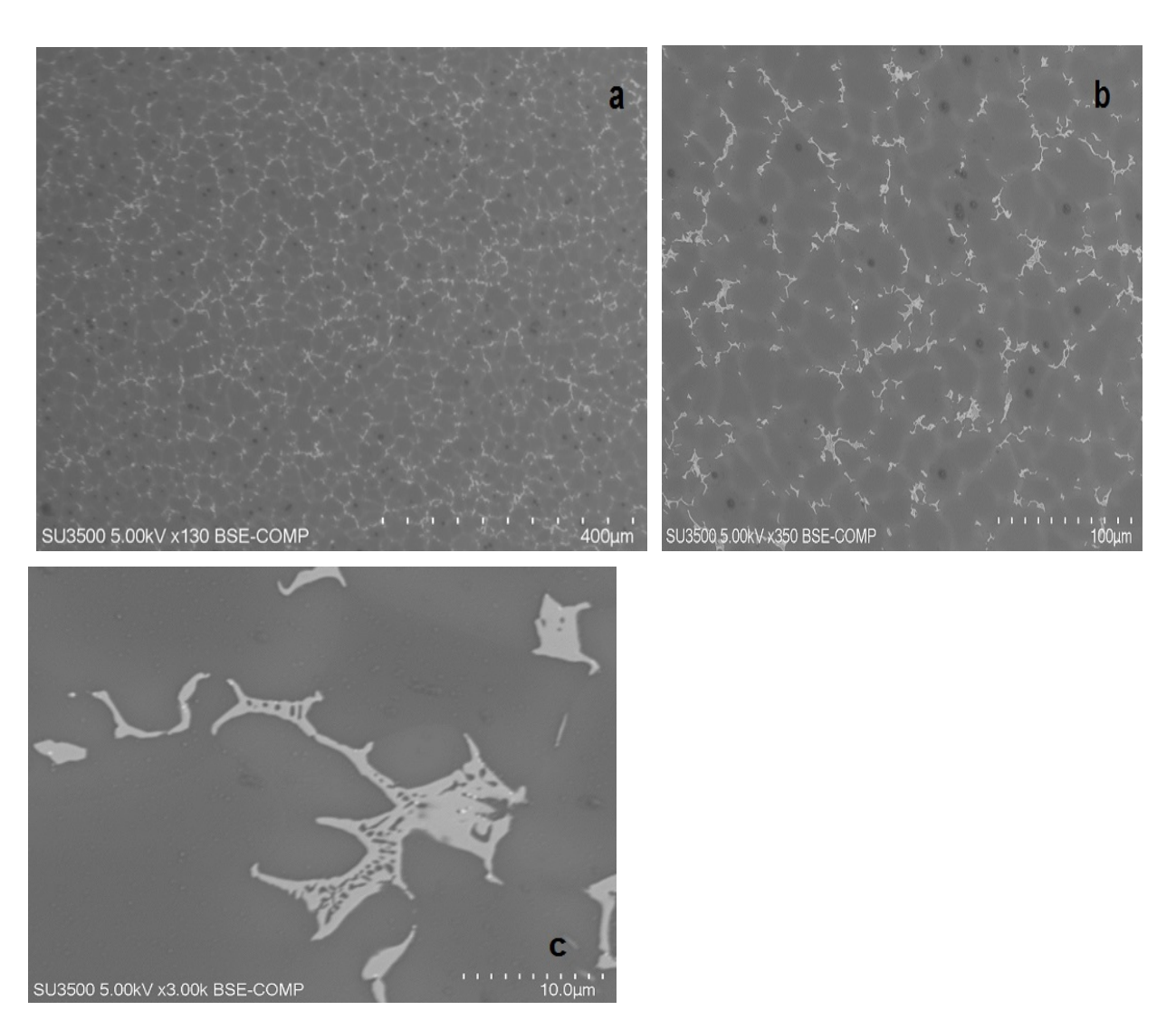


Fig. 5.1.3.1 (e): WE43 alloy (a) SEM image (400 μ m), (b) SEM image (100 μ m), (c) SEM image (10 μ m).

4.2 Corrosion rate

Corrosion rates were evaluated by using a static immersion test using m-SBF. We measured the hydrogen gas release and pH differences daily for five days. We also weighed the samples before the tests and at the end of the test after removing all the corrosion products for corrosion rate calculations by weight loss.

The highest corrosion rate in terms of weight loss was recorded for Mg-0.5 alloy. The second highest corrosion rate was Mg-0.3Ca-0.3 Sr alloy. The lowest corrosion rate was recorded for WE43 alloy. After that the second lowest was for Mg-0.3Ca-0.3Sr-0.1

Zn alloy. (Fig. 5.2.1. (a)). The ranking from the lowest to highest corrosion rate in terms of weight loss is;

WE43 < Mg-0.3Ca-0.3Sr-0.1Zn<Mg-0.3Ca-0.3Sr-0.3Zn<Mg-0.3Ca-0.3Sr<Mg-0.5Sr

The highest corrosion rate in terms of hydrogen evolution was recorded for Mg-0.3Ca-0.3 Sr alloy. The second highest corrosion rate was Mg-0.5 alloy. The lowest corrosion rate was recorded again for WE43 alloy. Following these the second lowest was for Mg-0.3Ca-0.3Sr-0.1 Zn alloy. (Fig. 5.2.1. (b)). The ranking from the lowest to highest corrosion rate in terms of hydrogen evolution is;

WE43 < Mg-0.3Ca-0.3Sr-0.1Zn<Mg-0.3Ca-0.3Sr-0.3Zn<Mg-0.5Sr<Mg-0.3Ca-0.3Sr

Fig.5.2.1(c) shows the pH variation during the duration of experiment. Because it was a static set-up and the SBF has not been changed throughout the experiment for 5 days, we observed an increase in pH for all the alloys every day. The highest pH values recorded was ~7.8 after the 5 days of immersion for Mg-0.5Sr and Mg-0.5Ca-0.5 Sr alloys. Throughout the experiment, the lowest increase in pH was recorded for WE43 alloy. At day five, the pH values for WE43 and Mg-0.3Sr-0.3Ca-0.1Zn and Mg-0.3Sr-0.3Ca-0.3Zn were very close. The pH values for these alloys were almost stabilized after the 3rd day and didn't increase much in the last 2 days of the experiment whereas the pH increase for WE43 alloy continued until the last day.

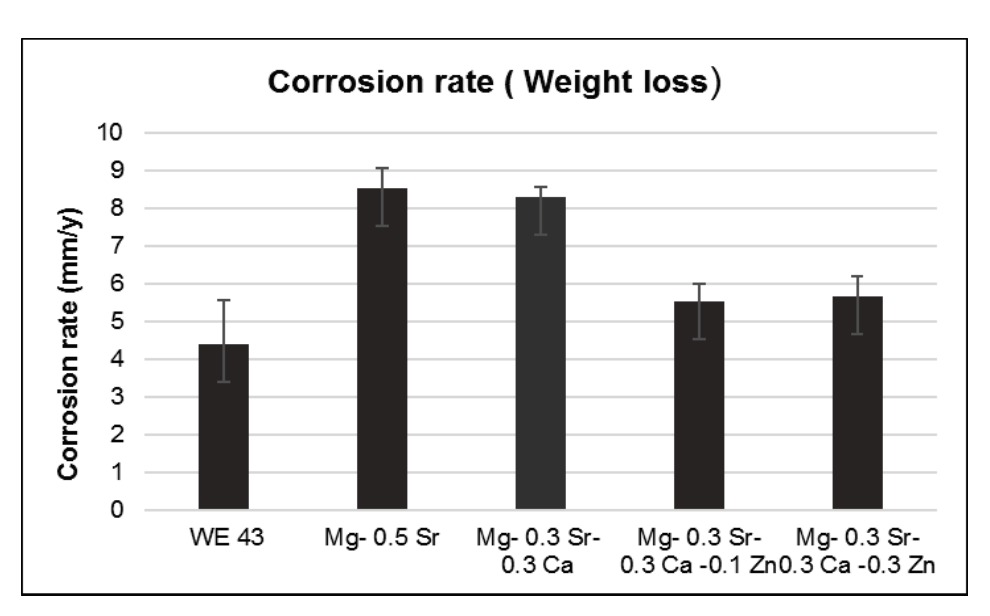


Figure 5.2.1 (a): The average corrosion rate (mm/year) in terms of weight loss after immersion in SBF at 37°C for five days.

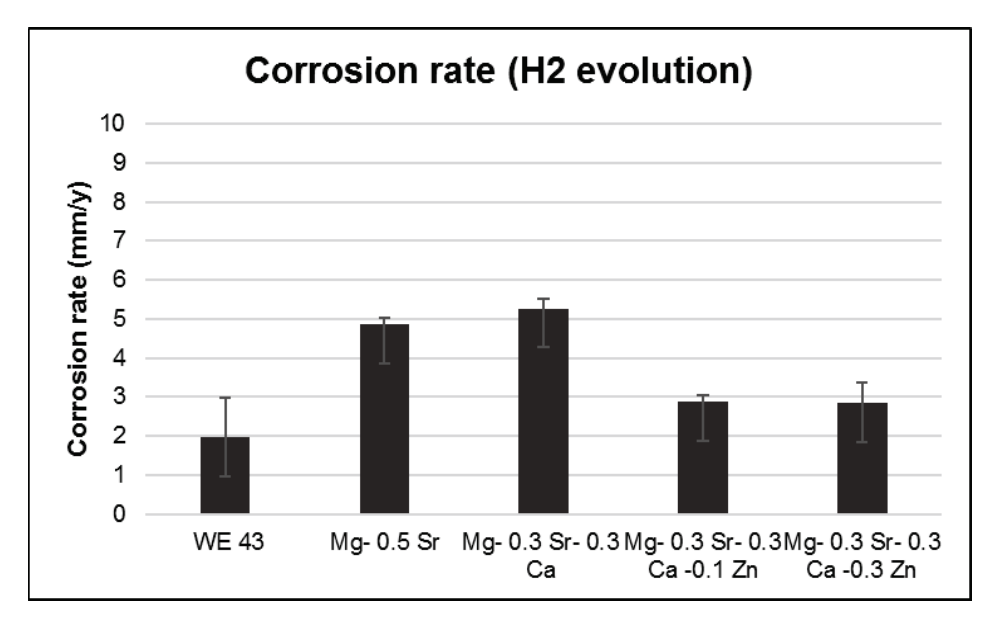


Figure 5.2.1 (b): The average corrosion rate (mm/year) in terms of hydrogen evolution after immersion in m-SBF at 37°C for five days.

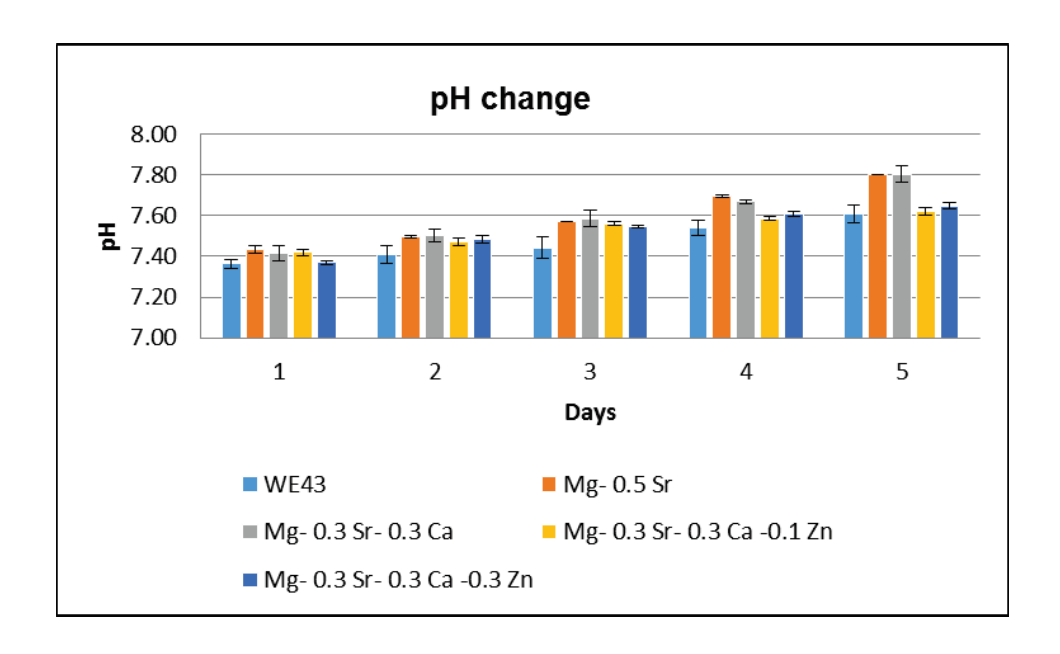


Figure 5.2.1 (c): The average pH change in m-SBF during the five days of static immersion experiments at 37°C.

5.3 Indirect Cytotoxicity Tests

5.3.1 MTT tests

While evaluating the results of the MTT test for HUVECs and MC3T3 cells, we used the cells without any extract but with just a serum with media as the positive control (Cells (+)). Our negative control was the cells with media without serum. When we compared the % viability with the cell control we measured for HUVECs, the day 1 results for WE43 was significantly lower than the rest of the alloys and control alloys. We can say that WE43 alloy has reduced viability of cells more than the other alloys.

The rest of our alloys the viability % was very close to the control cells (+) results. The initial toxicity of the alloys was not significant.

At day 4, we observed an increase in viability for WE43, Pure Mg, Mg-0.5 Sr and Mg-0.3Ca-0.3 Sr alloys as well as the reference Cells (+). The difference in % viability

between the alloys at day 4 was not significant. The highest increase in viability was measured for Mg-0.3Ca-0.3 Sr alloy.

At day 7, we observed a decrease in viability for all alloys and controls. The lowest viability was observed for pure magnesium and reference control cell (+). The difference between them was insignificant.

The day 1 results for MC3T3 showed that the highest viability was measured for pure magnesium. The lowest was for Mg-0.5 Sr alloy.

At day 4, we observed an increase in the viability for all the alloys as well as the cells (+). The highest value was measured for pure magnesium. The lowest was for Mg-0.3Ca-0.3Sr alloy. The difference in % viability between the alloys at day 4 was not significant.

At day 7, we observed a decrease in viability for control cells (+), for pure Mg and Mg-0.3Ca-0.3Sr-0.1Zn alloy. Although the variation between the viability results for day 4 and day7 were higher, the decrease is not significant. For the other alloys, the % viability increased at day 7.

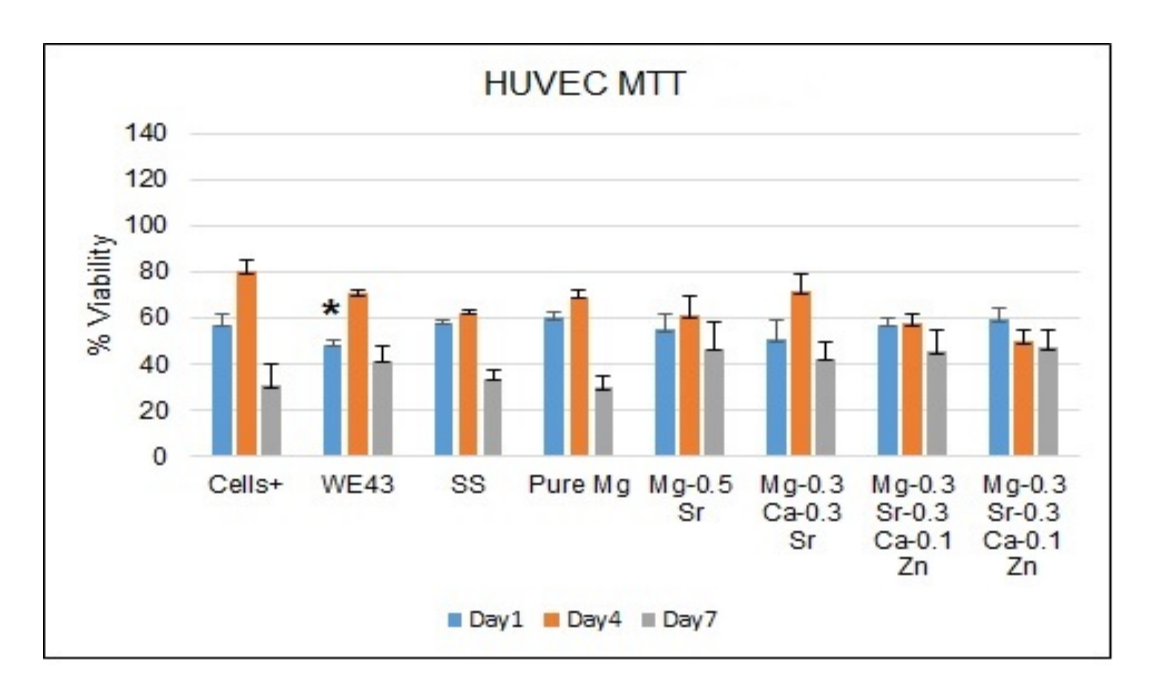


Fig. 5.3.1.1: The % viability for HUVECs after Day 1, Day 4 and Day 7. *The % viability rate for WE43 at day 1 was significantly higher than the other alloys (p<0.05)

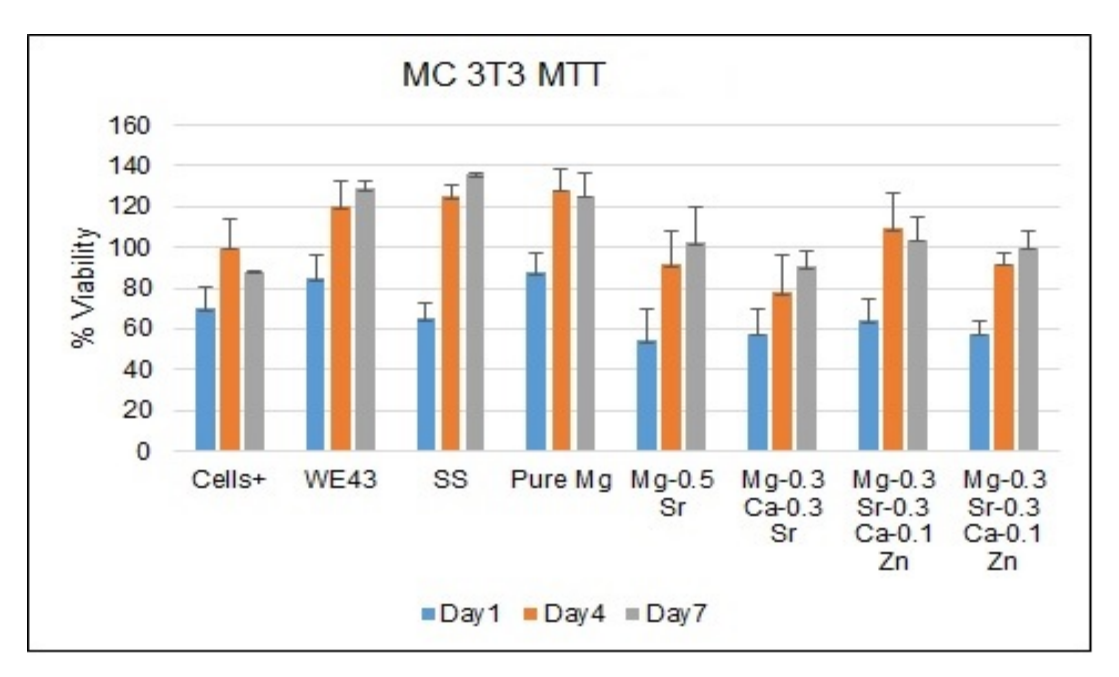


Fig. 5.3.1.2: The % viability for MC3T3 cells after Day 1, Day 4 and Day 7.

Overall for MC3T3 cells, the variation in results were recorded higher than the HUVECs. These different cell lines have different adaptability and also the media and the serum we used for the cell lines were different. Finally, we can say that we observed that the % viability for MC 3T3 cells were higher compared to the %viability of the HUVECs.

5.4 Blood compatibility

5.4.1 Hemolysis

The effect of the alloy samples on hemolysis of the blood was evaluated after three different exposure time; 30 min., 60 min., and 90 min. and for four different amount of samples; 1mg, 2.5 mg, 5 mg and 10 mg.

After 30 min. exposure to the samples, only higher-amount samples started to show hemolysis. The highest hemolysis rate was observed for WE43 control alloy (10 mg) sample. The second highest hemolysis was observed for Mg-0.3-Ca-0.3Sr-0.3Zn alloy (10mg). For control alloy, stainless steel 316L, the hemolysis rate was not affected with the increase of the sample amount. (Fig. 5.4.1.1).

After 60 min. exposure to the samples, we started to observe some increase in hemolysis for the alloys samples of 5mg. The highest hemolysis rate was observed for WE43 control alloy (5 mg) sample.

The 10 mg samples also showed higher percentages of hemolysis except the SS31L. The highest hemolysis rate was observed for Mg-0.3-Ca -0.3 Sr-0.1Zn alloy (10 mg) sample. For control alloy, stainless steel 316L, we observed that the hemolysis rate was not affected with the increase of the amount of the chips or with the increase in exposure time. (Fig. 5.4.1.2).

After 90 min. exposure, we started to observe increase in hemolysis for the alloy samples of 2.5mg. The highest hemolysis rate was observed for the WE43 control alloy (2.5 mg) sample. As for the 5 mg samples WE43 sample has again the highest hemolysis percentage. Both for WE43 2,5 mg sample and 5 mg sample, the increase in hemolysis rate was significantly higher than the other alloy compositions.

The highest hemolysis rate was observed for Mg- 0.3-Ca-0.3 Sr-0.1Zn control alloy (10 mg) sample. Yet the hemolysis rate was measured close to %100 for other alloys for 10 mg samples after 90 min. as well.

For control alloy, stainless steel 316L, we observed that the hemolysis rate has increased after the 90 min, exposure, yet the variation was also high for the other alloy samples (Fig. 5.4.1.3).

The increase in the pH was also measured for 90 min. exposure time. We observed the pH has increased above 9 for all the samples except stainless steel 316L. These results showed that the increase in hemolysis rate was independent of the increase in the pH. (Fig.5.4.1.4).

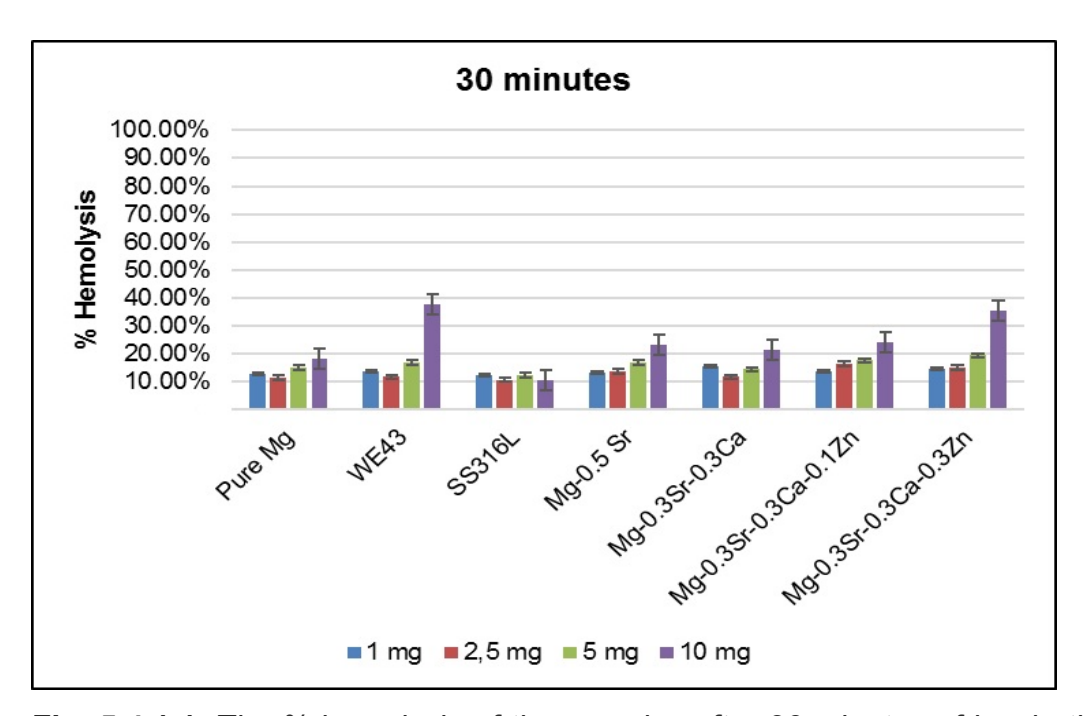


Fig. 5.4.1.1: The % hemolysis of the samples after 30 minutes of incubation in blood at 37°C.

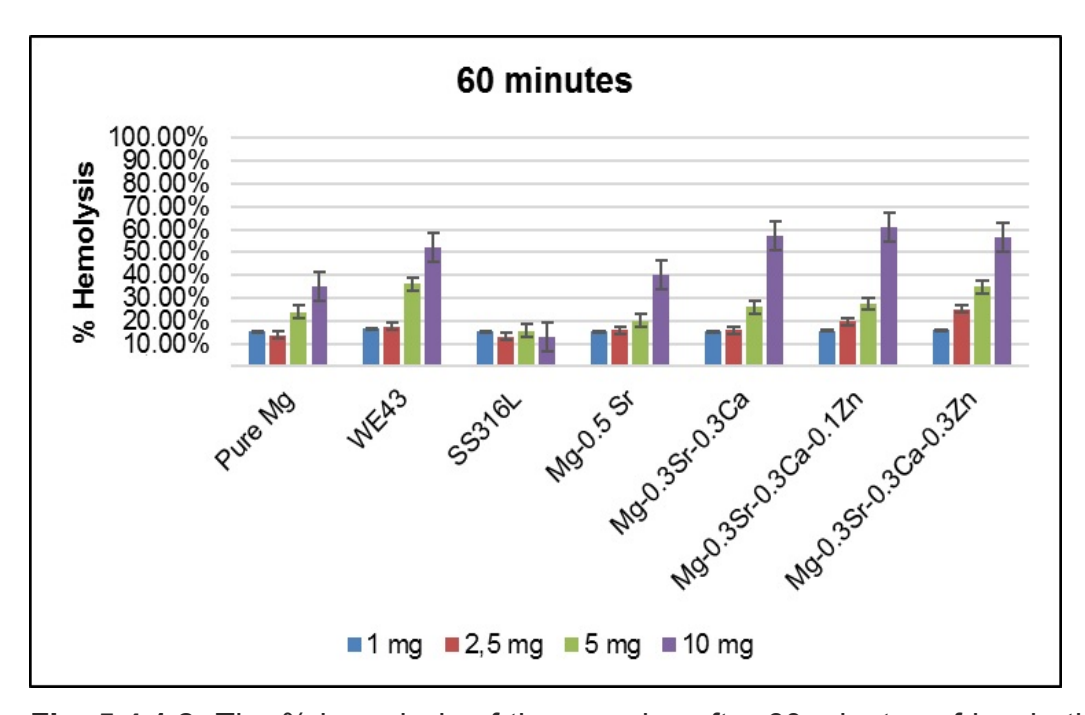


Fig. 5.4.1.2: The % hemolysis of the samples after 60 minutes of incubation in blood at 37°C.

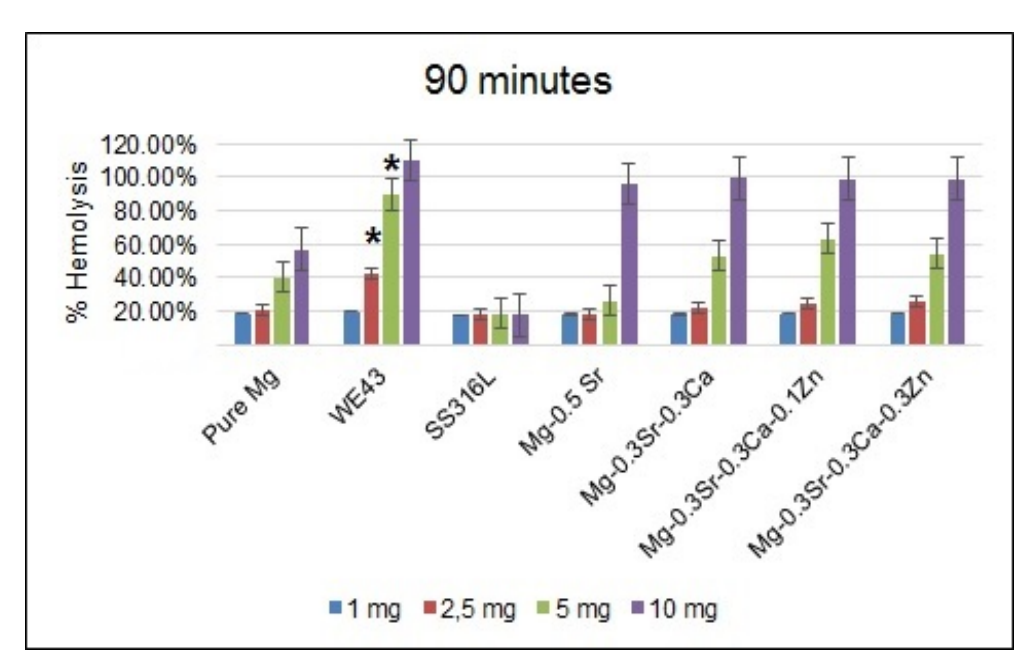


Fig. 5.4.1.3: The % hemolysis of the samples after 90 minutes of incubation in blood at 37°C. The hemolysis rate for WE43 2,5 mg and 5 mg samples were significantly higher than the other alloys (p<0.05).

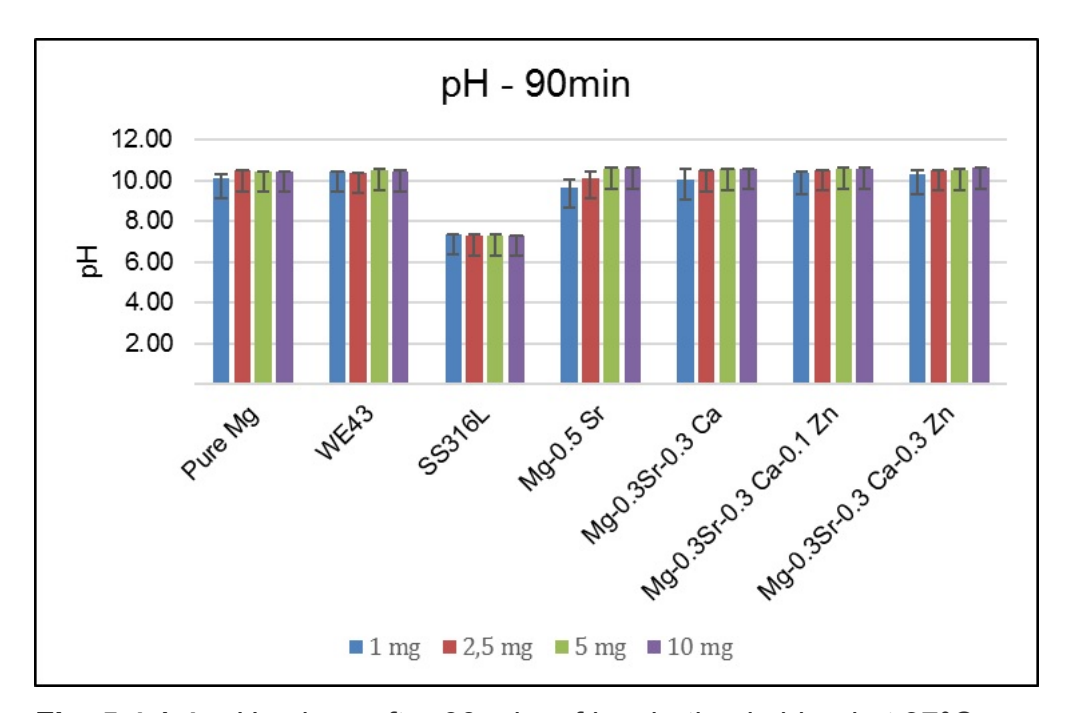


Fig. 5.4.1.4: pH values after 90 min. of incubation in blood at 37°C.

5.5 Results Summary

This study investigated the characteristics, corrosion rate and biocompatibility of four newly developed Mg-Sr based alloys. Main findings of this study briefly stated below;

- 1. The AFM analysis showed that the surface roughness decreased after each polishing step for each alloy. The biggest change in the roughness was observed for the Mg-0.5Sr alloy whereas the smallest change was observed for SS316L.
- 2. The SEM results showed that the Zn containing alloys appear to have smaller grain size.
- 3. SEM images revealed a cast microstructure with dendritic α -Mg matrix and interdendritic intermetallic second phases containing Ca, Sr or Zn.
- 4. The presence of the zinc in Zn-containing alloys improved their corrosion resistance.
- 5. The black dots appeared on the Mg-0.5 Sr during corrosion testing which are likely corrosion pits.
- At day 1 for HUVECs, WE43 % viability was significantly lower than the rest of the alloys and control alloys. We can say that WE43 alloy has reduced viability of cells more than the other alloys.
- 7. The rest of our alloys the viability % was very close to the control cells (+) results. The initial toxicity of the alloys was not significant.
- 8. At day 4, for HUVECs we measured the highest increase in viability for the Mg-0.3Ca-0.3Sr alloy.
- 9. At day 7, we observed a decrease in viability for all alloys and controls. The lowest viability was observed for pure magnesium and reference control cells (+). The difference between them was insignificant.
- 10. The day 1 results for MC3T3 showed that the highest viability was measured for pure magnesium where the lowest was for Mg-0.5 Sr alloy.
- 11. At day 4, for MC3T3 cells, we observed an increase in viability for all the alloys as well as the cells (+). The highest value was measured for pure magnesium. The lowest was for Mg-0.3Ca-0.3Sr alloy.
- 12. Overall for MC3T3 cells, the variation in results was higher than the HUVECs.

- 13. We observed that the % viability for MC 3T3 cells were higher compared to the HUVECs %viability.
- 14. Hemolysis studies showed that all our newly developed alloys caused less hemolysis compared to WE43 commercial alloy.
- 15. The hemolysis rate increased with the increase in concentration of the alloy material.
- 16. The increase in pH does not seem to have a considerable affect on hemolysis rate.

5.6 REFERENCES

- **1**. Bornapour M, M. Celikin, M. Pekguleryuz, "Thermal exposure effects on the in-vitro degradation and mechanical properties of Mg-Sr and Mg-Ca-Sr biodegradable implant alloys and the role of the microstructure", Mat. Sci. Eng. C, v. 46, 2015, pp.16-24
- **2.** Rzychoń T, Kiełbus A. Microstructure of WE43 casting magnesium alloy. Journal of Achievements in Materials and Manufacturing Engineering. Volume 21, Issue 1, March 2007, pp.31-34.

Chapter 6: DISCUSSION

Material Characterization

Understanding the material characteristics such as surface structure, corrosion or microstructure of our alloys was our main goal early in our study. Since the final aim is to develop a biocompatible, biodegradable cardiovascular stent material, we tried to understand these material characteristics and to relate them to the behaviour of our alloys in physiological environment.

Our initial step was characterizing the physical aspect of the surface. We know from the literature that majority of the stent problems such as acute thrombogenicity or delay in re-endothelization originates from surface related issues rather than the material itself [1]. The topography of the surface is believed to have a major role in stent performance because the smooth stent surface is believed to reduce platelet activation and aggregation, thus causes less thrombus formation and neointimal proliferation [1]. In a study which compares the effects of surface roughness on neointimal hyperplasia and clot formation showed that the electropolished, smoother surface stent has less effect on the clot formation or neointimal hyperplasia than untreated stents [1]. Another study that has investigated this question was a randomized double-blind study. The authors [2] looked at the relationship between stent-surface topography and outcome in patients undergoing implantation of stents with different type of surfaces. These results show that a rough stent surface does not increase late lumen loss after stent implantation when compared with smooth stent surface. The surface roughness investigated in this study had a minimum and maximum root mean square roughness values of 0.09 and 0.21 mm.

We observed in our study that the surface roughness of our control and new alloys were ranging between 0.02 and 0.13 mm before and after polishing steps. There are various kind of surface modification techniques such as roughening, patterning, chemical modification, and surface to modify the surface yet we can interpret from these results that, the roughness of our alloy surfaces would still be in the evaluation range even after the first polishing steps. We can also consider that the higher changes in the surface roughness as in Mg-0.5Sr alloy throughout the polishing steps, implies a softer surface

for this alloy. We can assume the surface roughness might influence corrosion rate as well. Yet, our study has not investigated these effects.

XRD detected well the primary phase and for certain alloys also the secondary intermetallic phases but failed to determine certain phases that are below its detection limit of 5wt%. Further analysis was carried out via SEM/EDS to characterize the phases and the microstructures of the alloys

The EDS analysis on the alloys showed that alloying elements such as Sr, Ca and Zn tend to accumulate around dendrite boundaries. We know from the literature that these alloying elements acts as a cathode since they are less active than magnesium that results in an increase in galvanic corrosion yet small dendrite size for magnesium alloys improves corrosion resistance since it results in a more homogeneous corrosion [5]. SEM analysis also showed that the presence of Zn in the alloys has an effect on reducing the dendrite size. Grain/dendrite size and the phase distribution are two factors that are known to influence the corrosion rates of magnesium alloys [3, 4]. Refining the dendrite size is expected to improve the corrosion resistance.

Controlling degradation rate of magnesium or its alloys is essential for their potential as clinically viable implants. The fast degradation of the material results in an early loss of mechanical properties which ultimately reduces its lifespan as an implant inside the body. We observed that after 5 days of immersion in m-SBF, the Zn containing alloys presented the lowest corrosion rate both in terms of weight loss and H₂ evolution after WE43 control alloy. The difference between the corrosion rates of these two alloys were very low.

In our static immersion test set-up, the SBF has not been changed throughout the experiment for 5 days hence we observed an increase in pH for all the alloys every day. The highest pH values recorded was for Mg-0.5Sr and Mg-0.5Ca-0.5Sr alloys. Minimum increase in pH was recorded for WE43 alloy throughout the experiment. The pH values for Mg-0.3Sr-0.3Ca-0.1Zn and Mg-0.3Sr-0.3Ca-0.3Zn alloys were almost stabilized after the 3rd day and didn't increase much in the last two days of the experiment whereas the pH increase for WE43 alloy continued until the last day. We

observed a correlation between the corrosion rate and pH; the higher the pH in the SBF, the higher the corrosion rate for the alloys.

While the slowest corrosion rate was measured for WE43 alloy through these experiments, the results of this study provided the evidence for the beneficial effects of Zn on corrosion resistance of the Mg alloy that could be a key factor to consider in order to improve the degradation requirements for next-generation biodegradable implants.

Bio-Compatibility

In direct cytotoxicity assays:

Indirect cytotoxicity assays showed that at day 1 for HUVECs, WE43 % viability was significantly lower than the rest of the alloys and control alloys. Bornapour et al [7] investigated the cytotoxicity for WE43 and Mg-0.5Sr. In that study, they observed the same trend in % viability between the WE43 and Mg-0.5 Sr alloy, except we found for the first day % viability was significantly lower for WE43 than other alloys.

We have not observed the same trend for MC3T3 cells. Overall, we observed for HUVECs, at the Day 4, the viability increased for all the samples and started to reduce at day 7.

For MC3T3 cells, at day 1, the highest viability was measured for pure magnesium and the lowest for the Mg-0.5 Sr alloy. At day 4, for MC3T3 cells, we observed an increase in viability for all the alloys.

Another observation was a higher variation in the results for MC3T3 cells than the HUVECs. There can be several factors which may explain the differences in the results for the different cell types;

(i) In our experiments, we observed that the % viability for MC 3T3 cells was higher compared to the HUVECs %viability. We know based on the experience of working in the laboratory with the different cell cultures that HUVECs are more sensitive cells compared to MC3T3 cells. HUVECs will not attach to the cell plate if it is not coated with gelatine solution, but the MC3T3 cells does not need a coating. We coated the cell plates with gelatine in our experiments for HUVECs. Yet when we consider the several washing steps we use during the MTT assay protocol, some of the cells may have been washed off because the attachments is not as strong for HUVECs as MC3T3 cells. This

is one of the reasons the comparison of the results for the same cell line is ultimately a better way to understand the response to the alloys than comparing the two cell lines with each other.

- (ii) Moreover, the differences between the results for HUVECs and MC3T3 cells can be correlated with the differences in the source of the cell culture types. MC3T3 cells are isolated from mouse (*Mus musculus*) and HUVECs are from human. Even apart from the cell origin, we were still expecting differences in the results because of the differences between the cell types, i.e., endothelial vs bone cells.
- (iii) Another factor to consider while evaluating the results is that after a certain percentage of surface coverage in the cell plate, the cells begin to die. It is considered to be %80 percent for HUVECs but higher for MC3T3 cells. The results we obtained from the assays for different cell types may be due to this difference. We observed that for MC3T3 cells, they continued to grow at the day 7, whereas the viability started to decrease for all of the HUVEC cells, for each alloy at day 7. That can be a result of high concentration in the cell plate. The increase in the concentration will trigger the cell death for HUVECs.
- (iv) One last point to consider is that we used %10 extracts in our experiments. This percentage was suggested by Bornapour et al. [7] where they were able to start observing the effects of alloy extracts on the viability of the cells at this concentration. That study was conducted using only HUVECs but our results we obtained from MC3T3 cell line suggest maybe higher concentrations can be used on MC3T3 cells, since the viability was found to be higher than HUVECs.

Hemacompatibility

When we think about a cardiovascular stent, the first contact of this implant material after implantation will be with blood. Therefore, it was necessary to evaluate the blood compatibility of these novel alloys.

The results showed that with the hemolysis rates increased with time for each alloy except for the SS316L control alloy. Also, the increase in the amount of the material, results in a direct increase in hemolysis. We observed that the pH has not affected the hemolysis rate.

We also observed that WE43 commercial alloy even for the smaller amounts was causing more hemolysis than our alloys with the increase in exposure time. The WE43 alloy has rare earth metals in its composition. The toxic effects of some of the rare-earth metals were summarised by Teak Rim et al. [6]. In one study, cerium, lanthanum, and neodymium were evaluated in an in vitro cytotoxicity assay using rat pulmonary alveolar M Φ . The results of this research showed that lanthanum chloride (LC50 = 52 μ M), cerium chloride (LC50 = 29 μ M), and neodymium oxide (LC50 = 101 μ M) exhibit significant cytotoxicity [6]. WE43 alloy has Y 4%, Nd 2.25%, 0.15% Zr, so one of these rare-earth metals might be the reason behind the high hemolysis rate that we observed in our experiments.

6.1 REFERENCES

- 1. De Scheerder I, Verbeken E, Van Humbeeck J. Metallic surface modification. Semin Interv Cardiol 1998; 3:139–144.
- Dibra A, Kastrati A, Mehilli J, Pache J, Von Oepen R. Influence of stent surface topography on the outcomes of patients undergoing coronary stenting: A randomized double-blind controlled trial. Catheterization and Cardiovascular Interventions, v65 n3 (July 2005): 374-380
- 3. Song G, A. Atrens, Corrosion mechanisms of magnesium alloys. Advanced Engineering Materials, 1999. 1(1): p. 11-33.
- 4. Deng Y, Z. Yin, K. Zhao, J. Duan, J. Hu, Z. He, Effects of Sc and Zr microalloying additions and aging time at 120°C on the corrosion behaviour of an Al–Zn–Mg alloy, Corrosion Science, 65 (2012) 288-298.
- 5. Witte F, N. Hort, C. Vogt, S. Cohen, K.U. Kainer, R. Willumeit, F. Feyerabend, Degradable biomaterials based on magnesium corrosion, Current Opinion in Solid State and Materials Science, 12 (2008) 63-72.
- 6. Kyung Taek Rim; Kwon Ho Koo; Jung Sun Park. Toxicological Evaluations of Rare Earths and Their Health Impacts to Workers: A Literature Review. Safety and health at work: SH@W, v4 n1 (2013년): 12-26.
- 7. Bornapour M, H Mahjoubi, H Vali, D Shum-Tim, M Cerruti, M Pekguleryuz Surface characterization, in vitro and in vivo biocompatibility of Mg-0.3 Sr-0.3 Ca for temporary cardiovascular implant. Materials Science and Engineering: C 67, 72-8.2016.

Chapter 7: CONTRIBUTIONS and FUTURE CONSIDERATIONS

In this research, we aimed to investigate the characteristics, bio-degradation and biocompatibility of four different Mg-Sr based alloys. The goal was to eventually take a step forward to developing a viable Mg implant alloy for human body. During the course of this study we were able to define some of the characteristics of these new alloys, namely, the microstructure, in vitro corrosion resistance and hemacompatibility. It was for the first time that a systematic in vitro study was carried out on a bio-degradable magnesium alloy that combines bio-degradation with bio-compatibility.

In order to have a complete picture of the potential of these four alloys further research can focus on the following areas;

- Our study only investigated the microstructure and the corrosion resistance for the alloys. The mechanical tests such as tensile tests, bending tests and impact tests would eventually need to be conducted on these alloys to achieve good design criteria.
- We observed in our experiments that the Zn containing alloys presented a better corrosion resistance compared to the other alloys. Regarding this information, we further recommend the investigation of corrosion rate for different Zn concentrations in the quaternary alloy structure. Based on the findings of our project, we can postulate that different Zn concentrations result in differing corrosion resistance and that Zn levels can be further optimized.
- In addition to the static immersion tests that we had performed in our study, we can further investigate the effects of changing the SBF daily on the corrosion rate of the alloys. A potential stent material would be exposed to a constant change of the blood when inserted inside the body. The removal of corrosion products and the corrosion layer constantly would have an effect on the corrosion rate. That kind of corrosion set up would enable us to better simulate the physiological conditions inside the body.

- High corrosion rate is always a problem that needs to be considered while planning an implant material. As well as trying different alloying techniques, one suggestion to address this issue would also be trying a different surface modification techniques or corrosion resistant coatings. Although our study did not consider surface modification, it is an active research field which would contribute to the solution of controlling the corrosion rate without a doubt.
- As we added in the appendix, we were able to start briefly to analyse the interaction between the cells and the surface of the alloys. Our observations in this area was limited. Therefore, further analysis trying different incubation times or maybe with different cell types would offer valuable information for understanding the interaction between cells and the alloy surface.
- We were able to evaluate the hemolysis effect of our alloys extensively during this research and we started the platelet aggregation studies briefly as well. Yet understanding the interaction of the alloys with the blood and platelets is crucial for a potential biodegradable material research. Nevertheless, further investigation is required on this aspect.
- Finally, one final proposition would be to conduct in-vivo studies to determine the behaviour and the effects of the alloys in the body. In-vivo experiments requires long time to plan and conduct, and also expensive, thus a master project was not long enough to enable us to involve this part of the research.

APPENDIX

A.1 Cell attachment

HUVECs were incubated with Mg alloys for 30 min, 2h and 4 h. and 24 hours. The earlier time points until 24h did not show any cell attachment. First cell attachment was observed at 24h and it proves that the cells are still viable and the alloy is not affecting the viability of the cells within the first 24 hours.

It can be postulated that due to the fast corrosion rate of Mg and the increase in the acidity around the alloy surface may have prevented the attachment of the cells to the surface in the first 24 hours. With increasing time, a corrosion layer forms on the surface of the metal and the presence of the corrosion layer may allow more suitable environment for cells to attach. For future studies, it is perhaps necessary to incubate the alloy samples 24 h ahead of the cell exposure. By doing so, the first 24h high corrosion environment can be avoided and the cell interaction could be observed more clearly. Furthermore, most stents are previously surface treated in order to optimize the early interaction with the tissue. Thus, pre-incubation of the samples before the cell exposure would ultimately provide more realistic results which could be correlated with the clinical application.

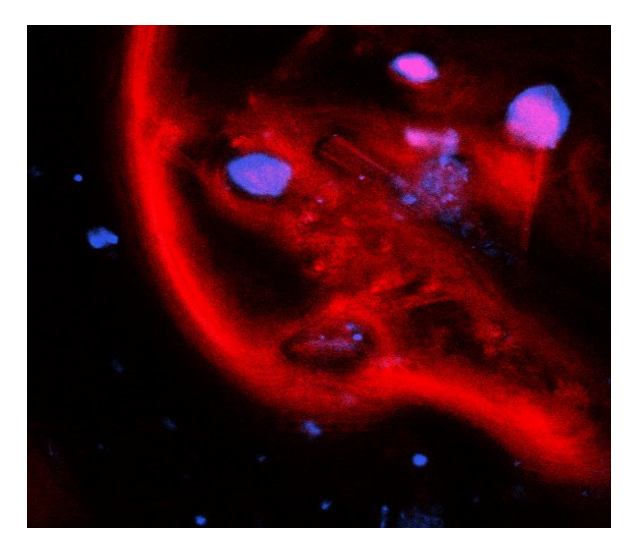


Figure A .1; The HUVECs confocal microscope image after 24h incubation on Mg- 0.3 Sr -0.3 Ca- 0.1 Zn alloy (DAPI (Blue- DNA (Nucleus)) & Phalloidin (Red) staining (Actin).

A.2 Platelet aggregation

In the platelet aggregation test, in the absence of an aggregating agent or agonist, the interactions between the platelets and the electrodes stabilize, and the impedance between the two electrodes becomes constant, producing a baseline. In the presence of an agonist, the platelets in the sample are activated and begin to aggregate and the baseline begins to shift, resulting in a slope which can be measured.

In our test, we used collagen as an aggregating agent which was our control. The results showed that after collagen, stainless steel alloy has the highest aggregation rate. All the other Mg alloys has lower aggregation rates which can be attributed of the presence of the magnesium ions in the sample. These results were in correspondence with literature, as it states, the presence of magnesium ions reduces platelet aggregation. We were not able to repeat the experiments enough to have a statistically sound data set, yet the trend shows that the reducing effect of the magnesium ions on the platelet aggregation.

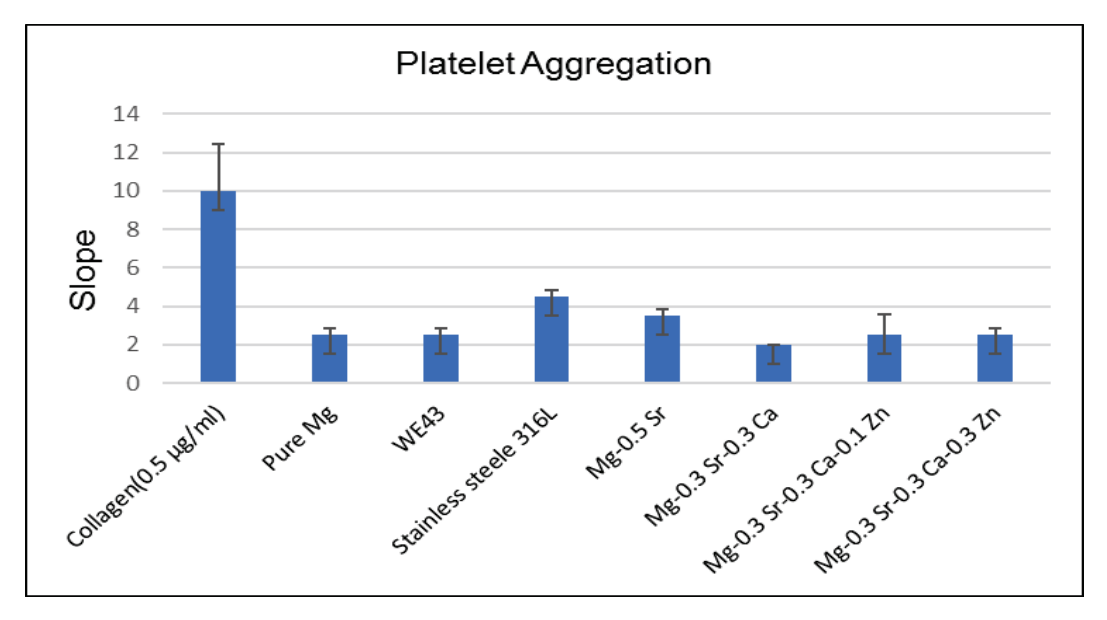


Fig. A. 2: The platelet aggregation results for three control materials (pure magnesium, Stainless steel SS316L and WE43) and four test compositions. 0.5 micrograms/ml of collagen was used as an aggregating reagent.